Forschungszentrum Karlsruhe
Technik und Umwelt

Wissenschaftliche Berichte
FZKA 5592

Summary Report of RAMONA Investigations into Passive Decay Heat Removal

H. Hoffmann, K. Marten, D. Weinberg, H. H. Frey, K. Rust, Y. Ieda, H. Kamide, H. Ohshima, H. Ohira

Institut für Angewandte Thermo- und Fluiddynamik
Projekt Nukleare Sicherheitsforschung

Juli 1995

FORSCHUNGSZENTRUM KARLSRUHE
Technik und Umwelt

Wissenschaftliche Berichte
FZKA 5592

SUMMARY REPORT OF RAMONA INVESTIGATIONS INTO PASSIVE DECAY HEAT REMOVAL

H. Hoffmann, K. Marten, D. Weinberg, H.H. Frey, K. Rust,
Y. Ieda*, H. Kamide*, H. Ohshima*, and H. Ohira*

Institut für Angewandte Thermo- und Fluiddynamik
Projekt Nukleare Sicherheitsforschung

* Power Reactor and Nuclear Fuel Development Corporation
O-arai Engineering Center, O-arai, Ibaraki-ken 311-13, Japan

Forschungszentrum Karlsruhe GmbH, Karlsruhe
1995

Forschungszentrum Karlsruhe GmbH
Postfach 3640, 76021 Karlsruhe

ISSN 0947-8620

SUMMARY REPORT OF RAMONA INVESTIGATIONS INTO PASSIVE DECAY HEAT REMOVAL

ABSTRACT

An important safety feature of an advanced sodium-cooled reactor (e.g. European Fast Reactor, EFR) is the passive decay heat removal. This passive concept is based on several direct reactor cooling systems operating independently from each other. Each of the systems consists of a sodium/sodium decay heat exchanger immersed in the primary vessel and connected via an intermediate sodium loop to a heat sink formed by a sodium/air heat exchanger installed in a stack with air inlet and outlet dampers. The decay heat is removed by natural convection on the sodium side and natural draft on the air side.

To demonstrate the coolability of the pool-type primary system by buoyancy-driven natural circulation, tests were performed under steady-state and transient conditions in facilities of different scale and detail. All these investigations serve to understand the physical processes and to verify computer codes used to transfer the results to reactor conditions.

RAMONA is the three-dimensional 1:20-scaled apparatus equipped with all active components. Water is used as simulant fluid for sodium. The maximum core power is 75 kW. The facility is equipped with about 250 thermocouples to register fluid temperatures. Velocities and mass flows are measured by Laser Doppler Anemometers and magneto-inductive flowmeters. Flow paths are visualized by tracers.

Nominal and non-nominal operating conditions were investigated. The main parameters studied in steady-state tests were the core power and the power distribution across the core, the geometry of the above-core structure, the design and number of decay heat exchangers in operation, the total interruption of the intermediate heat exchanger flow paths as well as the number of heat-transporting loops of the primary system. The transient investigations concentrate on the transition from forced to natural convection and the post-scram influence of the forementioned parameters on the primary system thermal hydraulics. The primary and secondary system pump coastdown, the decay heat exchanger start-up delay time and the number of decay heat exchangers in operation were additionally set as magnitudes of interest.

It could be demonstrated in the steady state tests that the onset of the decay heat exchanger operation stratifies the temperature distribution in the upper plenum with distinct large temperature gradients above the core. An impermeable above-core structure changes the temperature stratification in the upper plenum and reduces the temperature gradients. Operating only half of the available decay heat exchangers leads to an increased system temperature but does not alter the temperature distributions. The design of the decay heat exchangers can be optimized with respect to good mixing of cold and hot fluid to minimize the temperature gradients in the primary system. The coolability of the core could be demonstrated even when the flow through the IHXs is totally blocked. All these steady-state results could be well interpreted by the thermal hydraulic 3D code FLUTAN.

According to the RAMONA results obtained under transient conditions, the start of natural convection is mainly influenced by two effects, namely, the temperature increase on the IHX primary sides as a result of which the descending forces are reduced, and the startup of the DHXs which leads to a decrease of the buoyancy forces in the core. Hence, the thermal hydraulics of the primary system is influenced by the core power before and after scram and its radial distribution across the core, the primary pump coastdown, the IHX secondary-side flow reduction, the DHXs startup delay time, as well as the availability and the design of the DHXs.

The IHX secondary-side pump coastdown could determine the in-vessel thermal hydraulics during the total experiment duration.

The reduction in size from the four-loop arrangement of RAMONA-II to the three-loop model RAMONA-III decreases the amount of fluid in the primary system. The transition from forced to natural circulation depends on this magnitude. The studies of parameters identical to those used in RAMONA-II show, that all transient temperature courses behave similarly but reach steady-state conditions faster as the heat capacity is lower.

The comparison of numerically determined findings and measurements generally leads to encouraging agreements.

The conclusion of all these investigations is that the decay heat can be removed from the primary system by means of natural convection. Always flow paths develop, which ensure an effective cooling of all regions. This is even proved for extreme conditions, e.g. in case of delays of the decay heat exchanger startup, failures of several DHR chains, and a drop of the fluid level below the inlet windows of the IHXs and decay heat exchangers.

ZUSAMMENFASSENDER BERICHT ÜBER UNTERSUCHUNGEN DER PASSIVEN NACHWÄRMEABFUHR IN DER RAMONA ANLAGE

ZUSAMMENFASSUNG

Zusätzlich zur betriebsbestimmten Nachwärmeabfuhr (NWA) über die Natrium-Zwischenkreisläufe und den Wasser/Dampf-Kreislauf ist in einem flüssigmetallgekühlten Schnellen Reaktor (z.B. European Fast Reactor, EFR) ein gesondertes sicherheitstechnisches Nachwärmeabfuhrsystem installiert. Alle Systeme arbeiten so, daß die Nachwärme über Naturkonvektion vom Kern zu Wärmetauschern (Tauchkühlern) transportiert wird. Die Sekundärseite dieser Tauchkühler ist mit Luftwärmetauschern verbunden. Sie befinden sich in Kaminen und geben die Wärme über Naturzug an die Umgebung ab. Die Funktion eines solchen passiven Systems und der Nachweis seiner hohen Verfügbarkeit wurde durch Modellexperimente in der Anlage RAMONA (Maßstab 1:20) nachgewiesen. Als Modellfluid diente Wasser. Die maximal installierte Kernleistung betrug 75 kW. Zur Messung der Fluidtemperaturen wurden ca. 250 Thermoelemente in der Anlage montiert. Es wurden auch die Massendurchsätze gemessen und lokale Geschwindigkeitsverteilungen mit der Laser-Doppler -Anemometrie aufgenommen. Die Strömungspfade in den großräumigen Plena konnten durch Tracer sichtbar gemacht werden.

Es wurden betriebliche und nicht betriebliche Zustände des Reaktors in der Modell-Anlage RAMONA untersucht. In den stationären Versuchen wurden die Core-Leistung und deren radiale Verteilung variiert, die Geometrie des Instrumentierungsstopfens geändert, die Zahl und die Art der Nachwärmetauscher untersucht und die Auswirkung einer vollkommenen Blockierung der primären Strömungspfade in den Zwischenwärmetauschern ermittelt. Außerdem konnte das thermodynamische Geschehen eines 4-loop- und eines 3-loop-Systems in unterschiedlichen Modellen untersucht werden. Die transienten Untersuchungen beschäftigten sich mit dem Übergang vom nominellen Zwangskonvektions-Betrieb zum Nachwärmeabfuhr-Betrieb durch Naturkonvektion. Hier wurden die Parameter Core-Leistung, Auslaufcharakteristik der Sekundär-Kreisläufe der Zwischenwärmetauscher sowie der Einschaltzeitpunkt der Tauchkühler geändert und ihr Einfluß auf die Thermohydraulik des Primär-Systems festgehalten.

Als Ergebnisse der stationären Untersuchungen kann folgendes festgehalten werden: Der im Oberplenum installierte Tauchkühler verursacht eine starke Stra-

tifikation im Bereich seines Austrittsfensters und der Oberkante des Cores. Es kommt hier zu starken Temperaturgradienten. Ein offener Instrumentierungsstopfen reduziert den Temperaturgradienten im Oberplenum gegenüber einem geschlossenen Stopfen. Die Zahl der aktiven Tauchkühler beeinflußt das Temperaturniveau, aber nicht die Temperaturverteilung im Oberplenum. Durch eine geeignete Tauchkühler-Typen Auswahl können die Temperaturgradienten im Oberplenum optimiert werden. Auch bei totaler Blockade des Primärsystems in den Zwischenwärmetauschern ist die Kühlbarkeit des Kerns gewährleistet. Sämtliche stationären Versuche konnten mit dem 3D Thermohydraulik Rechenprogramm FLUTAN nachgerechnet und interpretiert werden, so daß für das Rechenprogramm ein hoher Grad der Verifikation erreicht werden konnte.

Die Ergebnisse der transienten Untersuchungen werden hauptsächlich durch zwei Vorgänge geprägt, nämlich durch den Temperatur-Anstieg nach Scram auf der Primärseite der Zwischenwärmetauscher (Reduktion der Abtriebskräfte) und den Einschaltzeitpunkt der Tauchkühler nach Scram (Reduktion der Auftriebskräfte). Beide Vorgänge vermindern im Naturkonvektionsbetrieb den Massendurchsatz im Kern. Der Einfluß der anderen Parameter auf die Thermohydraulik des Primärsystems wird ebenfalls systematisch dargestellt. So kann die Auslaufzeit des sekundären Massendurchsatzes der Zwischenwärmetauscher den Abkühlvorgang des Oberplenums ganz wesentlich beeinflussen. Aus der gesamten Kenntnis der transienten Übergangsphase von Zwangs- zu Naturkonvektion kann eine optimale Fahrweise von Primärpumpen, Sekundärkreisläufen der Zwischenwärmetauscher sowie Anfahrzeitpunkt der Tauchkühler entwickelt werden.

Die Untersuchungen zur 3-loop-Anlage mit dem geringeren Fluidvolumen gegenüber dem 4-loop-System ergaben, daß die transienten Massen- und Temperaturverläufe zwar ähnlich, aber schneller ablaufen und damit auch den stationären Zustand eher erreichen.

Auch für die transienten Vorgänge konnte das Rechenprogramm FLUTAN gute Übereinstimmung mit den wesentlichen experimentellen Ergebnissen erzielen.

Abschließend kann festgestellt werden, daß die Nachwärmeabfuhr aus dem Primärsystem durch Naturkonvektion sicher abgeführt werden kann. Es bilden sich immer kühlungseffektive Konvektionspfade, so daß selbst für außergewöhnliche Situationen wie verzögertes Einschalten der Tauchkühler, Ausfall von mehreren Tauchkühler-Kreisläufen oder das Absinken des Fluidspiegels im Primärsystem unter die Eintrittsfenster der Zwischenwärmetauscher die Kühlung des Primärsystems sichergestellt ist.

CONTENTS

1. INTRODUCTION

The reliable removal of decay heat after the shutdown of a nuclear reactor is an important safety criterion. For this reason, passive measures are the guiding principle for the design of the European Fast Reactor (EFR). The EFR is a sodium-cooled plant with a total thermal power of about 3,600 MW_{th}. The primary system is based on a pool-type configuration. The decay heat removal (DHR) concept comprises two diverse systems:

- Under nominal operating conditions, e.g., for a scheduled reactor shutdown, the decay heat is removed by intermediate heat exchangers (IHXs) and their cooling circuits via steam generators, water/steam systems, and condensers. The main components used for normal operation modes are sketched in Fig. 1a. In this system, the fluid is transported by primary pumps (PPs) in a forced convection mode. After a scram, the pumps are coasted down by controlling the electric power to values given as function of time. The PP coastdown characteristics determine the core mass flow rate and hence the core temperatures to meet the safety requirements.

- In unlikely cases of unavailability of the steam plant heat sink or a total loss-of-station service power, the decay heat will be removed by the safety graded system which operates entirely by natural convection. This passive DHR system, shown in Fig. 1b, is based on six direct reactor cooling (DRC) systems operating independently from each other. Each of them consists of a sodium/sodium decay heat exchanger (DHX) in the primary vessel connected via an intermediate sodium loop to a heat sink formed by a sodium/air heat exchanger (AHX) in a stack with air inlet and outlet dampers. The decay heat is removed by natural convection on the sodium side and natural draft on the air side [1], [2]. After scram the pumps run down and the mass flow rate of the core is reduced. The temperature differences in the core decrease right after scram and increase again until the buoyancy forces enable the fluid to be circulated by natural convection. After startup of the DHX circuits decay heat removal is ensured. To enforce this startup of the DHX circuits, the air flaps of the stack are opened automatically or mechanically. Except for this mechanical procedure, the safety related DHR system is entirely passive.

2. OBJECTIVE

It is the objective of the investigations to prove that the decay heat can be removed safely by means of natural convection without exceeding the maximum permissible load values specified for the respective structures [2, 3]. Thermohydraulics of the system is described by using one- and multidimensional codes. Computation using these codes is to be verified by experiments covering the most important physical effects. In general, the experiments are carried out on models, while reactor experiments serve to complete the results.

Numerous tests are performed on simplified model geometries and with water as simulant fluid for sodium to investigate thermohydraulics in detail. In the course of these experiments the measuring techniques available can be applied and the flow and temperature fields can be visualized. Thus, the physics of DHR can be studied and the computer codes can be validated with a reasonable expenditure.

The investigations focus on the thermohydraulics of the transition phase from nominal operation to decay heat removal, i.e. from forced to natural convection following a scram with a simultaneous loss of auxiliary power. Moreover, thermohydraulics in case of an entirely natural circulation (long-term effect) is of particular interest.

These investigations are part of a research program, which is realized in close cooperation with our French and British partners [4]. The tasks of this program are perfectly coordinated. In the following sections it shall be reported about the model investigations on natural circulation in the EFR primary system performed by KfK.

3. MODELS AND DESIGN

Performing model experiments, it must be assured that the gained results can be transferred to the reality. This is the case when the following is observed:

- geometrical similarity between model and reality
- similarity of the governing differential equations describing the velocity and temperature fields within the primary tank
- similarity of the boundary and starting conditions.

From these requirements, a model should represent the internal flow geometry of the reactor tank with all relevant components. From the governing thermo-hydraulic equations the dimensionless numbers Richardson (Ri), Peclet (Pe), and Reynolds (Re) can be deduced and they should be kept equal to those of the reactor. In addition, the relative pressure field induced by the tank internals DHX, core, IHX, pumps) should be similar to that of the reactor. A measure for this is the Euler (Eu) number. The following characteristics are of importance (Fig. 2):

- Reynolds number $Re = \dfrac{\text{inertia force}}{\text{friction force}} = \dfrac{u_o\, L_o}{\nu}$

- Richardson number $Ri = \dfrac{\text{buoyancy force}}{\text{inertia force}} = \dfrac{g\, \beta\, \Delta T_{UP} \cdot L_{UP}}{u_o^2}$

- Peclet number $Pe = \dfrac{\text{heat transfer by convection}}{\text{heat transfer by conduction}} = \dfrac{u_o\, L_o}{a}$

- Euler number $Eu^+ = \left(\dfrac{\text{pressure force}}{\text{inertia force}} \right)_{DHX} / \left(\dfrac{\text{pressure force}}{\text{inertia force}} \right)_c = \dfrac{\Delta p_{DHX}}{\Delta p_c} \cdot \dfrac{u_c^2}{u^2_{DHX}}$.

For similarity purposes the respective reactor (R) and model (M) characteristics have to match. This means that

$$\frac{Re_M}{Re_R} = Re^* = 1 \qquad \frac{Ri_M}{Ri_R} = Ri^* = 1 \qquad \frac{Pe_M}{Pe_R} = Pe^* = 1 \qquad \frac{Eu^+{}_M}{Eu^+{}_R} = Eu^* = 1 \ .$$

It is evident from the numbers above that a total similarity cannot be achieved. The Reynolds and Peclet numbers are proportional to u_o, while the Richardson and Euler numbers are inversely proportional to u_o^2. Here, the Euler number (Eu+) is used as a relative quantity. It denotes the ratio of the pressure drops between the immersion cooler and the core for the model and the reactor, respectively, and thus determines the main flow paths in the upper plenum.

When investigating pure natural convection the Ri*, Pe* and Eu* numbers are considered, while the Re number is allowed to deviate. From this the RAMONA-model scale of 1:20 can be calculated for a three-dimensional model similar to the reactor with water as the working fluid (Fig. 3). For investigations in the transition region from forced to natural convection, the Reynolds numbers of the model and the reactor have to agree. However, the deviation factor of the model scaled 1:20 is 10^{-3}. This factor is to be reduced by using the NEPTUN-model scaled 1:5 [5, 6].

Based on the aforementioned similarity considerations the models have to represent the internal flow geometry of the reactor tank. Hence they should contain a heated core, DHXs, IHSx, pumps, and an above core structure (ACS). The arrangement of these components should make possible a hot upper plenum and a cold lower plenum. All parts are constructed so that the circulation paths are easily observable, and velocities and temperatures are measureable.

The design of the experimental model proceeds as follows [15, 27]:

From the balance of friction, buoyancy and inertia forces:

$$\zeta \frac{\rho}{2} u^2 F - g \beta \Delta T \rho L F + \frac{\rho}{2} u^2 F = 0$$

and from the heat balance:

$$P = u \rho F \Delta T c.$$

the quantities

$$\Delta T = [\rho^2 (\zeta + 1) / 2g \beta L \rho^2 F2 c^2]^{1/3}.$$

for each component (core, DHX) are determined. Also the decisive Richardson number is calculated

$$Ri = g \beta \Delta T_{up} \cdot L_{up} / u_o^2.$$

The Richardson number is determined using the temperature decrease by heat rejection in the upper plenum ΔT_{up} and the core exit velocity u_o (Fig. 2). All these magnitudes are measureable values. Thermohydraulic similarity in the models is reached as mentioned before if the dimensionless numbers of reactor and models are identical.

For the SNR (sodium) and the 3D model scaled 1:20 (water), the calculated Richardson and Euler numbers together with experimental results as a function of heat input are shown in Fig. 4a. It is seen that the Richardson number decreases

with the heat input and that the Eu numbers are practically independent from this parameter. For the fuel elements with e.g. 4.5 or 3.16 bar pressure drop, the condition $Ri_M//Ri_R = 1$ is attained at the following powers:

Model: 6 - 10 kW Reactor: 75 - 125 MW

For these cases the model temperature differences for the core are > 10 K and for the DHX > 12 K.

In the following report the major results achieved with regard to DHR by natural convection shall be summarized. The results have been obtained by steady state and transient investigations on 3 different RAMONA models. The first two test facilities were actually initiated during the former German SNR-2 project. The third model is in geometrical similarity to the EFR. In spite of these features, the experiments cover the most important physical effects with regard to the cooling modes in the primary system and DRC system, give an insight into the relevant EFR phenomena, and provide a broad data basis for the development, improvement, and assessment of computer programs. Such qualified tools are necessary to make reliable predictions with respect to uniform and non-uniform cooling modes associated with the interactions of the core, the DHXs and the upper plenum (UP) of the vessel under highly different initial and boundary conditions. A second concern is to provide a possibility to transfer results gained from water test facilities of different scale to practical situations within the EFR primary vessel, the individual components, and the total DHR system.

4. RAMONA TEST FACILITIES

Three RAMONA models have been used. They are characterized in Table I and differ by the following features:

- RAMONA-I was built in similarity to the SNR-2. This is a four loop type reactor design with 4 PPs and 8 IHXs. Four DHXs are installed pairwise in angular positions of 180 deg. The maximum power of the RAMONA-I core was 30 kW. The core flow was registered by turbine type flow meters and 4 DHXs were installed pairwise in angular positions of 180°.
- RAMONA-II was also a four loop model with identical geometry as RAMONA-I. The maximum power of the core, however, was 75 kW. The core flow was registered by magneto-inductive flow meters. They showed a less sen-

sitivity against water impurities and hence revealed a higher measuring accuracy in comparison with the turbine type flow meters used in RAMONA-I.

- RAMONA-III finally was a 3 loop model, simulating the EFR geometry. Hence the vessel diameter was slightly reduced. The core power was 75 kW and magneto inductive flow meters were used. The model was equipped with 6 DHXs installed on both sides of each of the three primary pumps.

In the following the detailed description of RAMONA II is given. In general the RAMONA II description is also valid for RAMONA I and for RAMONA III design, the more as all components were used in the three RAMONA test facilities. The main differences between the three test facilities exist for the vessel dimensions, i.e. the diameter and height of the vessel.

The RAMONA-II model is made of plexiglass and provides easy access and simple exchangeability of components. Vertical and horizontal cross-sections of RAMONA II together with its main dimensions in millimeters are shown in Fig. 5. The vessel has an inner diameter of 1000 mm and a height of 600 mm. The volume is about 0.4 m^3 filled with demineralized and degassed water. The vessel contains the entire primary circuit. The primary system consists of a core, an upper (or hot) plenum (UP), a lower (or cold) plenum, a high pressure plenum (HPP), eight intermediate heat exchangers (IHX's) and four primary pumps (PP). In addition to these components, bundle-type or hybrid-type decay heat exchangers (DHX's) are installed in the upper plenum. In the center of the upper plenum there is an above-core structure (ACS). The core is surrounded by a water-filled cavity. In the lower part of the vessel a core support structure is placed which consists mainly of a plate fixed against the vessel. This plate supports the primary pumps and the feedlines to the high pressure plenum.

At the bottom end of the HPP, the reference or zero level is located in order to provide a common basis for the comparison of RAMONA and NEPTUN data as well as computations against measurements. A construction unit of bi-toroidal shape forms the intermediate plenum (IP) which separates the hot upper from the cold lower plenum. The upper contour of IP represents the so-called "redan". The IP is fixed at its outer periphery to the vessel and at its inner periphery to the core. Vertical shrouds of two different diameters penetrate the IP and serve for the installation of the PPs and IHXs, respectively. The lower part of the "redan" and the cylindrical structure of the core form the reactor typical cavity which represents the lower part of the upper plenum.

A lot of care was necessary to manufacture the components of the test facility and to assemble the RAMONA apparatus in order to avoid any undesired geometry induced asymmetrical effect during the course of the studies. In particular, accurate dimensions were required with respect to the horizontal alignment over the circumference of the upper HPP plate and the core at their top ends as well as of the ACS at its bottom end. Furthermore, attention was focused to the installation of the four PPs and the eight IHXs, and especially of the four DHXs with regard to an axially uniform level of their inlet and outlet windows within the vessel.

4.1 Core

The core with an outer diameter of 258 mm is designed for a maximum power of 75 kW. It consists of 8 annular flow channels formed by 8 heater rings and one heater rod. Fig. 6 shows the core construction. The heaters are made of $AlMg_3$ in which electric heater cables are embedded. Each heater consists of two parts. The lower part is the heated section of 130 mm length and the upper part represents an unheated section of 70 mm length. Each flow channel is formed by an annular geometry facing two heater rings with 2 mm gap width. The whole core is mounted on a grid plate and the gap widths are fixed by spacers. The heaters of the core are individually heatable to allow power gradients across the core. The heater power are controllable as function of time and the real power data are registered.

4.2 Above Core Structure

The cylindrical ACS with an outer diameter of 234 mm is centrically positioned in a vertical distance of 60 mm above the core. There are 3 different ACS configurations (Fig. 7)

- a cylindrical ACS with a horizontal bottom plate. this structure is made of plexiglass and no fluid enters the inner space of the ACS. This version is called "impermeable ACS".
- a cylindrical perforated ACS with a bottom plate. The perforated peripheral surface has a permeability of 13 % and the perforated bottom plate a permeability of 15 %. These perforations allow the fluid to pass through the ACS and this version is therefore called "permeable ACS".
- a cylindrical permeable ACS internally equipped with horizontal plates and vertical guide tubes which simulate the hydraulic behavior of the control

rod drivelines and core monitoring systems. The vertical guide tubes penetrate the permeable bottom plate. Their axial distance to the top end of the core is 7 mm. A perforated shell covers the peripheral surface of the ACS characterized by a permeability of 13 %. The bottom plate has a permeability of 15 %. An additional plate bolted between the bottom plate and the upper end of the core serves as lower guiding device of the protruding vertical tubes. By changing the peripheral surface with a totally closed shell, the fluid cannot enter the ACS and this version then also is a impermeable ACS (impermeable and permeable version are called "NEPTUN-type ACS").

4.3 Intermediate Heat Exchangers

In RAMONA II eight IHXs are installed. All IHXs are of identical design. This is a straight tube counter flow type heat exchanger. The design of the IHX is shown in Fig. 8. The bundle of 130 rods of 4 mm outer diameter is surrounded by a lucite shroud with inlet and outlet windows. The primary flow circulates on the shell side of the IHXs. The secondary side water flows down through the center tube (downcomer) and reaches the cold collector. Then the water flows up through the inside of the 130 stainless steel tubes in the hot collector. The active tube length is 405 mm. The cold inlet tube passes the hot collector. In this region it is isolated by an air gap. Two secondary cooling loops are available. Each is connected with 4 IHXs and consists of a pump, a flow-control valve, a flowmeter, a heater and a cooler connected to the cold water line with a cooling tower, Fig. 16. Inlet temperatures and flow rates of the secondary fluids are controllable as a function of time.

4.4 Primary Pump

The primary pump (PP) consists of an impeller (rotor) with 4 blades. The pump is driven by a speed controlled motor. The flow behind the pump is straightened by flow guides and a honeycomb grid (flow straightener). Fig. 9 shows the position of each pump with flow guides and flow meters installed next to it. The 4 pumps push the cold fluid from the lower plenum into the high-pressure plenum underneath the core. From there the fluid flows through the core into the upper plenum and via the IHX's back to the cold plenum. The pump speed is steered by a computer.

4.5 Decay Heat Exchangers

For the four DHX-loops, straight-tube bundle-type DHXs operating on the counter flow principle have been chosen. Fig. 10 indicates this DHX design. 54 vertically arranged tubes of 4 mm outer diameter are connected to a flow distributor at the lower end and to an annular collector at the upper end of the bundle. The bundle is installed in a shell with 12 slot-type upper inlet windows (109x8 mm) and 12 exit windows (20x8 mm). The primary upper plenum fluid enters through the inlet windows of the shell, travels down in counterflow to the secondary fluid and exits "bell-shaped"through the outlet windows.

The secondary-side coolant enters through a central tube of 16 mm diameter, travels down to the distributor and within the tube up to the collector. The collector is isolated from the inlet tube to minimize heat losses. From here, the water is fed to a secondary cooling circuit, see Fig. 16. In this circuit the mass flow rate and inlet and outlet temperatures are measured for a thermal balance of the heat removed from the primary vessel. The main reason is to fulfill the uniform boundary conditions for all DHXs being in operation. This concerns in particular the mass flow rate and the inlet temperature at the secondary side of the DHXs. The immersion depth of each DHX amounts to 265 mm. This means that the top edge of the inlet windows at the primary side exceeds the regular water level by approximately 23 mm.

5. INSTRUMENTATION AND DATA ACQUISITION

The temperatures are measured by about 250 thermocouples (NiCr-Ni, 0.5 mm diameter) installed in the model. Two groups of thermocouples can be distinguished; namely stationary measuring devices and those being installed on movable supporting systems. Stationary measuring devices are installed at various locations of interest within the core, the ACS, the PPs, the IHXs, the DHXs, and the plena. They are used during steady state and transient tests. Movable measuring devices allow measurements at nearly each position within the upper plenum. They are mainly used in steady state tests. The thermocouple arrangements in the upper, lower and high pressure plena are shown in Fig. 11, 12, 13 and 14, respectively. The thermocouple positions in the core are indicated in Fig. 15. All thermocouples are calibrated in the temperature range between 5 and 50 °C with an accuracy of $< \pm$ 0.1 K.

Velocities are measured by a 1D LDA-system in the hot plenum along an angular symmetrical section of 90 degree ($0 \leq \phi_{ang} \leq 90$). This section is formed by the outer radius of the above core structure ($r = 117$ mm) and the gap (60 mm) between the core outlet plane and the lower plane of the above core structure. The fiber optical Laser-Doppler-Anemometry is used. The probe head is immersed in water and positioned in the hot plenum of the RAMONA model. It is connected to an r,ϕ,z-traversing system, which allows probe movement along the selected flow regions.

Core flow rates are registered by eight flow meters installed in the feed lines between the primary pumps and the high pressure plenum, Fig. 9. They are magneto inductive flow meters. Each flow meter is calibrated in the range of mass flow rate between 10,0 and 200,0 g/sec with an accuracy of 2.0 % and below 10,0 g/s with an accuracy of less than 5 % deviation.

The data acquisition system is shown in Fig. 17. The thermocouple signals (mV) are registered by a mini-computer through a calibrated amplifier and converted to a temperature signal in °C. This conversion function was obtained from the calibration experiments. The mini-computer PDP-11 accumulates the data of the temperatures, flow rates and heater powers instantaneously. The sampling interval is changed several times in the range of 20 ms to 20000 ms during an experiment. The average of each 50 data samples is formed; the averaged data is recorded after each 50th sample. The recording starts 500 s before scram with a sampling interval of 200 ms. 10 s before scram this is changed to 20 ms. 100 s after scram it becomes 60 ms. 1000 s after scram it is changed to 200 ms, 4500 s after scram to 2000 ms, 4 h after scram to 20000 ms, and 20 h after scram back to 600 ms for the final steady-state measurement.

The data recorded and saved by the PDP-11 during the experiment are later transferred to a IBM M 3090 computer. There the data are analyzed and displayed graphically. The graphs shown in this report are laser-printer copies of such computer displays.

6. EXPERIMENTAL PROCEDURE

A typical experiment consists of a warm-up phase, a stationary phase, the scram and an after-scram phase. The warm-up phase and the stationary phase constitute the pre-scram-phase. During the entire experiment, important primary- and secondary-system flow rates and temperatures are registered by chart writers. This information is used in the pre-scram phase to adjust the model to standard steady-state temperature and flow conditions.

To reach these stationary conditions, the IHX's are in operation while the core is being heated during the warm-up phase. The DHX's are also operating, although at a very low flow level while the IHX's and the primary pumps run at full-operation power. This procedure assures the formation of the proper steady-state flow and temperature distributions. For the same purpose, additional externally positioned low-flow pumps are used during the warm-up phase to stir the fluid in the cold plenum and to circulate fluid into the cavity. These pumps are turned off at least 10 min before scram. After 2 h to 4 h of warm-up, stationary flow and temperature conditions are reached. During this stationary phase, the standard values shown in Table 2 persist.

Table 2 Power Densities (W/cm3) of the RAMONA Core Heater for Various Powers

Heater No.	1	2	3	4	5	6	7	8	9
Volume heated, cm^3	648	1131	972	812	693	494	334	175	26.1
P = 1 kW	0.02	0.0336	0.275	0.236	0.319	0.245	0.259	0.259	0.497
P=30kW	4.61	5.25	5.73	5.8	6.56	6.14	6.56	6.56	7.73
P=75kW	11.53	13.13	14.33	14.5	16.4	15.35	16.4	16.4	19.33

In the transient experiments the computer - controlling core-heater power, primary pumps, and secondary-side cooling - performs an automated reactor scram from 75 kW or 30 kW to a given decay heat power. The PDP-11 data collection sys-

tem is turned on 500 s before the scram and continues the data collection for 20 h, until the stationary after-scram conditions are reached. Even though the water surface of the model is insulated, a total of about 5% of the core power is given off to the environment of the reactor model. The after-scram total core power in general was 2 kW and 1 kW for a pre-scram power of 75 kW and 30 kW respectively.

In the steady state experiments the core power is set in the range of 1,0 kW $<$ P$<$ 8 kW and the heat removed only by the DHXs. The boundary conditions for the DHXs secondary side amount for the water flow rates to 35 g/s and decreased for the inlet temperature to 10 °C.

7. PARAMETERS OF THE INVESTIGATIONS

7.1 Investigations under Steady State Conditions

The main parameters which were varied include:

- Core power: The experiments were run in the power range of 1 kW$\leq$P$\leq$8 kW, which corresponds to reactor decay heat powers in the range of 25 MW$\leq$P$\leq$100 MW on the basis of the similarity principles.

- Power distributions across the core diameter: The core simulator consists of eight heater rings and one heater rod, which can be heated individually. The eight heaters are heated in such a way that, at an identical total power, the following radial power distributions result $X=X_{avg}/X_{max}$ = 1.0; 0.87; 0.65; 0.59.

- The ACS design: Impermeable and permeable ACSs are investigated as well as the scaled down NEPTUN-ACS (see Fig. 7).

- The axial position of the ACS: The axial position of the upper core structure was varied in the range of 20 mm $\leq \Delta Z \leq$ 60 mm . This was done by reducing the free flow area between core outlet and lower plate of the upper core structure. In this case the interaction zone between hot fluid from the core and cold fluid from the immersion coolers could be influenced.

- Operation conditions of the secondary loops of the DHXs: Experiments were carried out varying the inlet temperatures and the mass flow rates of the DHXs secondary loops. These investigations were carried out to reveal the influence of these characteristics on the primary DHXs mass flow rates and hence on the temperature distribution in the upper plenum.

- Type of DHXs: Bundle-type and hybrid-type DHXs were used. The goal of these tests was the selection of an optimum design with respect to good mixing behavior, cheap fabrication and easy installation in the upper plenum. Beside the bundle type DHX, described in chapter 4.5, the U-tube and hybrid-designs were used. Their main dimensions are indicated in Fig. 28.
  = The U-tube bundle-type DHX consists of 27 vertically arranged U-tubes. One end of each tube is connected to a flow distributor, the other end to a collector. Distributor and collector, two torus-shaped structures,

are positioned coaxial but isolated from each other in the upper DHX section. The secondary coolant enters the distributor, travels through the U-tubes and exits into the collector. The primary fluid enters the U-tube bundle mainly through the upper section of the bundle. It exits the bundle at the bottom in a "jet-like" stream, whose central axis coincides with the central axis of the U-tube bundle.

= The hybrid-type DHX consists of 28 U-tubes forming two annular rows. These U-tube rows cover the outer periphery of each IHX. The ends of the U-tubes are connected to annular distributors and collectors, respectively. The lower ends of the U-tubes are positioned near the lower edges of the IHXs inlet windows. The secondary fluid enters via the distributor to the inner row of tubes, travels downward and flows upward through the outer row of tubes to the collector. The primary fluid flows down the outer surfaces of the U-tubes. Partly it falls back in the upper plenum; partly it is suctioned by the IHXs inlet windows and goes to the lower plenum of the model.

= Various straight tube bundle type DHX designs as described in chapter 4.5 were also investigated, namely the DHX without and with a permeable shroud. The reason for these investigations was to avoid cold spots on the reactor vessel and along the walls of the intermediate plenum in the vicinity of the outlet windows of the DHXs.

Each of the straight-tube or U-tube DHX types is fed by identical mass-flow rates at identical inlet temperatures of the secondary coolant flow. Comparable conditions are chosen for every two of the hybrid-type DHXs. In addition all DHXs are installed in the upper plenum in such a way that their immersed heat transfer surfaces are identical. Hence the active surfaces of 4 straight-tube or 4 U-tube type DHXs are identical to those of 8 hybrid-type DHXs.

- The number of DHXs being in operation causing symmetrical and asymmetrical cooling mode respectively. An asymmetrical cooling mode is realized when two DHXs located side by side are turned off without any reduction in core power. Consequently, the power generated must be removed through the immersion coolers still in operation. However, as these are run at constant secondary mass flows with constant inlet temperatures, the systems temperature is bound to rise.

- Upper plenum - lower plenum flow paths (primary flow path): Experiments were carried out closing the flow paths between the upper plenum and the lower plenum. In these cases, no fluid reaches the HPP and the core must be cooled from the UP alone. In addition a very extreme operation condition was simulated, namely the fluid level decrease in the primary system due to a leakage of the primary tank. In this extreme case neither the inlet windows of the IHXs nor those of the DHXs are covered with fluid. Then both main flow paths from the upper to the lower plenum and within the DHXs are interrupted.

For all these cases, the temperature distributions are measured on horizontal and vertical traverses in the upper plenum. On the basis of these measurements the fields of isotherms can be determined. In certain cases, velocity distributions are measured on the core/upper plenum level. Generally, the flow paths are recorded visually and optically by means of tracers (color). All investigations are carried out under the same boundary conditions which allows comparisons to be made. If the boundary conditions are varied, then this will be noticed explicitly.

7.2 Investigations under Transient Conditions

The transient investigations using the RAMONA model serve to study thermohydraulics as a function of time after scram of a reactor with a simultaneous failure of the operational heat removal system. Under forced convection conditions the power supplied is first removed via the IHXs. Maximum nominal power is 75 kW. Numerous experiments were also carried out for a core power of 30 kW. This is the so called 40 % load case. After reactor scram and rundown of the pumps, decay heat removal takes place by means of the DHXs exclusively. Starting from the moment of scram the following transient functions are defined:

- power reduction of the core from 30 to 1 kW respectively 75 to 2 kW within a period of 1.5 s;
- reduction of the core flow rate of 840 g/s respectively 2100 g/s in accordance with a half time of the primary pump rundown characteristic of 10 s; the pumps are stopped at 130 s .

- reduction of the flow rate from 90 respectively 225 g/s to 0 g/s in each IHX secondary loop within a period of 15 s. The temperature is kept constant at a level of 23 °C.
- startup of the DHX secondary loops which is delayed by 240 s within a period of 160 s by increasing the mass flow rate from 0.5 to 6.4 g/s respectively to 16 g/s. The mean fluid temperature is 24 °C.

With the other conditions maintained constant, the following parameters are varied:

- power decrease from 30 kW or 75 kW to various DHR powers.
- halftime of the primary pump rundown characteristics
- outage time of the secondary IHX cooling system,
- startup delay time of the DHX's after shutdown,
- DHX-type (straight tube, U-tube, hybrid DHXs),
- complete failure of several DHX circuits.

For all these cases, the variations of thermohydraulics with time is determined in the model by means of power, temperature and flow rate measurements. Steady state thermohydraulic conditions are attained about 2 to 4 hours after the setting of the nominal experimental conditions. After scram the tests are usually run for a period of 4 hours and in many cases even up to 20 hours.

8. NUMERICAL SIMULATION OF THE EXPERIMENTS

The fully vectorized thermal-hydraulic computer code FLUTAN [7] is utilized for the numerical simulation of the RAMONA experiments. The FLUTAN computer code is a tool to analyze the combined fluid dynamics and heat transport for 3D, laminar and turbulent, steady-state and transient problems. The selection of either rectangular Cartesian or cylindrical coordinates is provided. The program includes physical models for volume porosity, surface permeability, surface heat flux, volumetric heat source, thermal interaction between the immersed structure and surrounding fluid, and turbulence. Two temperature-dependent fluid property packages are presently implemented, i.e., for water and sodium. Apart of the vectorization, an essential feature of FLUTAN is the self-optimizing algorithm CRESOR [8] for solving the Poisson equations for pressure, energy, and turbulence using a finite-difference numerical technique.

For the simulation of the RAMONA experiments, a 90° respective 180° sector is modeled by using a three-dimensional noding scheme with about 15,000 respective 20,000 volume cells. Figure 18 illustrates the nodalization of the test facility with r-ϕ and r-z cross-sections. The number of the chosen mesh cells depends on the degree of detail required to resolve the fluid field, the phenomena to be modeled, and practical restrictions such as computing time and computer storage limitations. To capture the dominant physical phenomena, the following approach is chosen:

For the multi-dimensional simulation of the core, an unequal mesh spacing is selected according to different requirements. In vertical direction, a different node length has to be provided to fit the axial regions of the heated core and the mixing range of cold and hot fluid above the core. In angular and radial direction, the positions of PPs, IHXs, and DHXs govern the nodalization. The core cells are described by porosities and permeabilities and by taking into account the space-dependent heat capacities of the heating elements in conformity with the actual radial power profile. Heat transfer and pressure drop in the core, IHXs and DHXs and feedlines to the core are based on pretests carried out with the original components [9, 10, 11, 12, 14, 15].

Typical steady state velocity and temperature fields computed for RAMONA under natural convection conditions with a decay heat power of 8 kW are indicated in Fig. 19. The graphs indicate the results for the core/upper plenum DHX cross-section as well as the results for the core/upper plenum IHX cross-section.

The velocity vectors plotted in Figs. 19a, indicate clockwise flow paths in the upper plenum. The vertically upward flowing water is heated up in the core channels. At the top end of the core, the warm flow is being deflected and mixed with the radial cold stream coming from the DHXs. Near the water surface, the warm fluid flows to the DHXs where it is cooled down. Cold fluid leaves the DHXs, sinks, and impinges on the intermediate bottom (redan). Another part of the warm fluid circulates via the IHX and the pump to the high pressure plenum and enters the core again.

These findings describe the two main flow paths in the primary system, namely flow path I and II. Flow path I is obtained under forced and natural convection conditions. Hot fluid from the upper plenum enters the intermediate heat exchangers where cooling takes place by forced convection only. Then, the fluid is

led to the lower plenum. By means of pumps it is fed back into the upper plenum via the core. In case of a failure of the pumps and safety related DHR operation fluid circulation results from the buoyancy forces of the core (natural convection). The flow path is identical to that of forced convection. Operation of the DHXs leads to flow path II. This flow path is limited to the upper plenum only. In this case, the hot upper plenum fluid is led into the DHXs for heat removal. The increase in density caused by cooling results in a downward flow. The cold fluid leaves the DHXs and enters the lowest region of the upper plenum, the cavity. By the cold fluid which is constantly fed into the cavity, the medium contained therein is pushed back over the edge of the core and mixes with the hot fluid coming from the core. Sometimes, the cold fluid penetrates radially and reaches the symmetry axis of the core.

The temperatures of the upper plenum vary accordingly. The computational results in Fig. 19b indicate that in the region from the lowest point of the cavity to the upper end of the core cold fluid with a homogeneous temperature is encountered. At this point a rapid increase in temperature can be noticed due to the isotherms squeezed together until the DHX outlet windows are reached. The horizontal character of the isotherms indicate a clear thermal stratification in the upper plenum. In the region above the DHXs outlet windows a hot fluid layer with a constant temperature is recorded.

Within the core region the isotherms are horizontally arranged because the core is heated homogeneously. The isotherms are registered only in the heated core region. Above the core the isotherms are again squeezed together and show a parabolic course. This is the mixing region of cold fluid coming from the DHX and hot fluid leaving the core.

9. RESULTS RAMONA-II

9.1 Investigations under Steady State Conditions

9.1.1 Characterization of the Basic Thermohydraulics in the Upper Plenum [13, 14]

These measurements were carried out under the condition that the heat is removed from the core only by operation of the DHXs. In this case the fluid motion is caused by both, the buoyancy forces of the core, and the downward flow within the DHXs s. Fig. 19a. The cold fluid leaves the DHXs, fills the cavity, flows over

the upper periphery of the core, and mixes with the hot fluid leaving the core. The UP temperatures vary accordingly.

When moving a thermocouple on a vertical traverse from the top to the bottom of the UP (Fig. 20a left side), a hot fluid layer with a constant temperature is recorded until the region with the cold DHX fluid is entered. This corresponds to the level of the DHX outlet windows. Here, a rapid decrease of the temperature can be noticed. In the region between the upper edge of the core and the bottom of the cavity, cold fluid with a homogeneous temperature is encountered. The results of FLUTAN computations are plotted for comparison. Satisfactory agreement between numerical and experimental data can be noticed.

The local flow events for the most interesting flow region formed by the upper core and lower ACS planes are indicated in Fig. 20b together with FLUTAN computations for two vertical traverses above the core. These are the horizontal velocity components measured by LDA technique. It can be seen that the fluid from the DHXs enters the above core space where it is mixed with the core fluid and rejected along the bottom of the ACS back into the upper plenum. A good agreement between numerical and experimental data can also be noticed for these measurements.

Detailed temperature field measurements are used for the representation of isotherm fields in the UP. In Fig. 21a the data of an experiment at 8 kW is compared with computation. The experimental results and the FLUTAN calculations reflect the horizontal character of the isotherms indicating the formation of a temperature stratification. The close spacing of the isotherms (intervals of 1 K) also points out that the entire temperature rise occurs in the region between top end of the core and outlet windows of the DHXs. The highest temperatures occur in and above the core, and they drop with increasing distance from the core center-line. At the DHX outlet windows a very inhomogeneous field of isotherms is registered resulting from cold fluid sinking to the redan. This leads to temperature differences on the redan walls. Fig. 21b indicates measurements and calculations for the DHX outlet region. Comparing the computed and measured results it can be seen that the temperature distributions in the UP are well represented by the calculations.

9.1.2 Results of the Parameter Studies

Thermohydraulics of the upper plenum which is characterized above is now effected by various parameters:

Core power [15, 16, 17]

The effect of core power on the upper plenum temperatures is shown in Fig. 22. In Fig. 22a two characteristic fields of isotherms for core powers of 3.6 and 8 kW are indicated. The horizontal development of the isotherms is clearly visible. The region of high temperature gradients is characterized by the close position of the isotherms. With increasing power temperature distribution in the upper plenum is not subject to noticeable changes. In contrast to this, a distinct change in the system temperature can be noticed.

In Fig. 22 a (bottom), the maximum upper plenum temperature is plotted versus the increase in power. As the experiments are carried out at an inlet temperature of the immersion cooler of 10 °C, the curve starts at this point and is proportional to $P^{1/3}$. The experimental values are well confirmed by computation. The influence of different core powers on the local velocity distribution is given in Fig. 22b. This figure shows as in Fig. 20b the horizontal velocities components measured by LDA technique for two vertical traverses above the core at radius 117 mm and 190 mm. The qualitative behavior for 1 kW and 2 kW core power is similar but is more pronounced for the case with 2 kW core power. The maximum outlet velocity of the space between core and lower ACS plate is 22 mm/s at 117 mm radius and the inlet velocity at 190 mm radius amounts to 11 mm/s. The higher backward velocity in the case of 2 kW core power indicates a stronger circulation flow in the UP induced by the DHX.

Radial power distribution [18, 19, 20]

The radial power distributions of $X=0.87$ and $X=0.66$ investigated simulate a core with a radial blanket or reflector (Fig. 23a). The values measured do not reveal any effect on the thermohydraulics of the upper plenum. Detailed measurement of the axial temperature behavior along the outer core flow channels (Fig. 23b), however, indicate thermosiphon effects for $X=0.66$. Starting from the core inlet continuously increasing temperatures are measured for $X=1.0$. In contrast to this, considerable temperature fluctuations occur in the unheated upper core

region for X=0.66. These fluctuations are caused by the cold fluid from the DHXs entering the upper core flow area from above. The small buoyancy forces resulting from the little heating of the outermost core flow channels do not suffice to overcome the cold downward flow. At X=0.66 the power of the outer flow channel is smaller by a factor of 6 compared to the X=1.0 case.

Geometry of the above core structure [17, 18, 21]

The geometry of the above core structure (ACS) influences both the flow paths as well as the regions where the hot fluid coming from the core mixes with the cold fluid coming from the DHXs. This is especially evident from the fields of isotherms evaluated from the measured temperature distributions. In Fig. 24, the influence of geometry is represented both for the impermeable (Fig. 24a) and for the permeable ACS (Fig. 24b). The permeable ACS allows the hot fluid to enter and pass it and to flow back into the upper plenum via the holes in the cylindrical ACS shell. Therefore, the isotherms extend over the total height of the upper plenum. The highest temperatures are measured on the model axis. For both the permeable and the impermeable ACS the results obtained by the computations using the FLUTAN code are in good agreement with the measured values.

Axial position of the above-core structure [16]

Temperature distributions were measured to clarify the thermohydraulics in the upper plenum for different axial ACS positions. Fig. 25 represents horizontal temperature profiles computed and measured 2 mm above the core for impermeable and permeable ACSs and for two axial ACS positions of $\Delta z = 20$ and $\Delta z = 60$ mm. The core power was subject to variations. It can be seen for for 8 kW heating power (see Figs. 25c and 25d) that with decreasing distance between core and impermeable ACS the registered minimum temperature increases drasticly, because no cold fluid enters the space between ACS and core outlet. Therefore the average temperatures above the core increase for the impermeable ACS and the temperature fluctuations (max./min. values) decrease to zero. Identical temperature profiles are measured in the flow area between core and ACS. In contrast for the permeable ACS the measured temperature profiles are similar for the discussed axial ACS positions. In this case the ACS position has practically no influence on the upper plenum thermohydraulics as mentioned before. There is a fairly good agreement between calculated and measured values. A reduction in the heating power with $\Delta z = 20$ mm has yielded decreases in the measured mean tempera-

ture above the core and a penetration of the fluctuation zone into the space between ACS and core. The calculated maximum temperatures above the core agree well with the measurements but deviations exist at the periphery of the cold cavity. Fig 26 indicates computed isotherm fields for $\Delta z = 60$ and 20 mm for the core power of 8 kW. The above discussed UP thermalhydraulics can well be argued.
Without structural components above the core the hot fluid rises plumelike into the upper plenum as demonstrated in 2D experiments [32]. The presence of a structure above the core influences this plumelike flow behavior.

Symmetric and asymmetric heat removal

Asymmetric heat removal refers to the fact that only 2 of 4 immersion coolers are being operated. Generally, this leads to an increase in the system temperatures with the core power being the same. In the asymmetrical decay heat removal case, especially the increase in the temperature level of about 11 K is observed. The temperature distributions in the upper plenum are not affected. However, temperature fluctuations are increased in the area of the immersion coolers in operation. In Fig. 27, the fields of isotherms are represented both for symmetric (operation of 4 DHXs) and asymmetric (operation of 2 DHXs) heat removal from the upper plenum. The core power is 3,6 kW.

The experimental findings are contrasted with the computed results. The horizontal form of the isotherms can be seen from the experiment and the calculation. This means that a stratified flow is present in the upper plenum. The close spacing of the isotherms also indicates that the entire temperature rise occurs chiefly between the levels of the core outlet and the outlet windows of the DHXs. The highest temperatures are determined above the core; they drop with increasing distance from the core axis. The isotherms of the experiments and the calculations in the cross section where the DHXs are operable ($\phi = 0°$) are more uneven than those in the region of the immersion coolers not in operation ($\phi = 90°$; 180°). From the comparison of the isotherms it can be concluded a small 3D-flow effect that can be observed only locally in the vicinity of the DHXs in operation.

Different decay heat exchangers [17, 22, 23]

The DHXs types studied (straight tube, U-tube, hybrid DHXs) are shown in Fig. 28 with the primary and secondary side flow behavior being indicated. The hybrid

DHXs are positioned around the inlet windows of the IHXs. The experiments are performed such that the heat transfer surfaces and the boundary conditions are the same for all DHX types. A more or less identical thermohydraulic behavior is exhibited by the straight tube and the U-tube, whereas the hybrid type DHX differs considerably as far as thermohydraulics is concerned. This is evident from the measurements of the fields of isotherms in Fig. 29. With the core powers being the same the temperature distributions of the upper plenum are measured for all DHX types. The highest upper plenum temperature of 31 °C is obtained for the straight tube type DHX. For both the straight tube and the U-tube DHXs temperature differences of about 7 K are recorded in the upper plenum. An upper plenum temperature of about 26 °C only is attained by the hybrid type DHX. Here, the temperature differences in the upper plenum amount to about 2 K only. This behavior of the hybrid type DHX must be attributed to the fact that a larger area of the upper plenum is covered by the heat rejecting surface. Hence, efficiency of the hybrid type IC is much higher than that of the other types as far as the thermohydraulic behavior is concerned.

When comparing the local temperatures and the fluctuations in the wall areas, all DHX types are found to exhibit similar temperature fluctuations that, however, refer to different positions in the upper plenum. Generally, these fluctuations can be affected and reduced by design modifications.

As an example for a design modification the straight tube DHXs generally equipped with outlet and inlet windows in the shroud were modified in the following matter, see Fig. 30.

- DHXs without shroud
- DHXs with perforated shrouds (140 bores of 2 mm diameter)

The DHX without shroud is a simplified design. In this way a better fluid mixing in the upper plenum may be reached. The perforated shroud allows the cooled fluid to enter the upper plenum along the perforated shroud length. Together with the small diameters of the bores an extended mixing zone of cold and hot fluid should be achievable.

Fig. 31 indicates the isothermal fields measured in the region of the outlet cross sections of the DHXs and Fig. 32 shows temperature distributions registered along vertical traverses on the periphery of the tank wall ($\phi = 0$, 6, 23.5 and 45°). The core power is 8 kW. Both measurements indicate that maximum temperature differences along the redan and the tank wall are reached for the DHX with win-

dow type shrouds ($\Delta T = 22K$) and minimum values for the DHX with perforated shroud ($\Delta T = 7$ K).

Fluid level in the primary tank [24, 25]

The main vessel of a sodium-cooled reactor is installed in a safety vessel to guarantee a sufficiently high sodium level in the primary system under the assumption of a break of the main vessel. This extreme situation was investigated in steady state experiments. The normal fluid level in the primary system was lowered in RAMONA from 580 mm to 460 mm. In this case, no fluid could either enter the IHXs inlet windows nor reach the inlet windows of the DHXs. Hence, no fluid could reach the core via the pump feedlines and the DHXs operation took place by suctioning of primary fluid via the upper half of the DHX outlet windows and feeding back the cold fluid via their lower half.

The experiments were conducted using a permeable ACS. The results of these measurements are shown in Fig. 33. Two cases are indicated for a power of 2 kW, namely with nominal and reduced liquid levels. The latter experiments were performed with DHXs equipped with shrouds and DHXs without shrouds.

As can be seen from the results in all cases a stratified temperature field is measured. The vertical temperature gradient extends along the whole UP. But the highest temperature gradient is still in the region between the top end of the core and the bottom end of the ACS.

The measured isotherms for the reduced fluid level show a remarkable rise of the system temperature level which amounts to 7 K compared to the nominal fluid level and steeper temperature gradients in the upper plenum. In the case where DHXs without shrouds are used the temperature level of the UP is reduced by 3 K compared with the results of the investigations using DHXs with shrouds. This is due to the fact that the hot UP fluid reaches the cool DHXs surfaces along the whole immersed DHX length.

In this case of blocked IHXs-PP-core flow paths which is named "blocked primary flow path" the core is cooled by cold fluid entering the flow gaps at the top level of the core. Flow recirculations (back flow) as well as large flow fluctuations can be registered. In general, a good coolability of the core is observed and the maxi-

mum temperatures of the upper plenum are registered along the centerline of the test facilities.

9.2 Investigations under Transient Conditions

9.2.1 Reference Conditions and Parameters

For comparison, one experiment was defined as the basic case simulating the thermohydraulic transient phenomena after a reactor scram from 40% nominal power. It was based on the results of a one-dimensional analysis for the SNR-2 performed with the system code DYANA [26]. This analysis was carried out for the postscram phase of certain safety-related reactor operating cases. The thermohydraulic performance for the RAMONA facility was determined from the reactor analysis using the similarity of Richardson, Peclet, and Euler numbers [6]. On this basis, the time functions of the model were calculated for the core power, the flow rate of the primary pumps, the secondary mass flow rates of the IHX, and the DHXs as well as the secondary inlet temperatures of both components. These reference variables are specified below as functions of time, and they are indicated in Fig. 34, together with their variations [28, 29, 30]:

- Unblocked primary flow path
- All DHXs are serviceable.
- The transient operation conditions are:
  - reduction of core power at scram from 30 to 1 kW within 1.5 s with a radial flat power distribution over the core.
  - reduction of the core flow rate from 840 g/s corresponding to the half-time of a primary pump coastdown of 10 s. The pumps were stopped at 130 s.
  - reduction of the mass flow rate per IHX secondary loop from 90 to 0 g/s within 15 s. The IHX secondary-side inlet temperature was kept constant at 23 °C.
  - DHXs startup, delayed by 240 s, of each of the four secondary loops of the DHXs within 160 s by a linear increase in the mass flow from 0.5 to 6.4 g/s. The mean secondary-side fluid temperature is decreased from 26 to 24 °C within 2160 s.

The parameters listed in Table II were subject to variations. The operational parameter variations are also represented in Fig. 34. The core power before scram simulate the 40 % (30 kW) and 100 % (75 kW) load case of the reactor. The core

power after scram varied between 0.6 and 4 kW. The half-time of the primary pump speed reduction ranged between 0 and 20 s and led to pump stops at 0 and 260 s after scram. The coastdown of the IHXs secondary-side flows was taken to be linear with pump stops at 15, 120, and 240 s, respectively. The 15 s-pump-stop was chosen to suppress the IHX coolability right after scram. An additional experiment was performed for comparison with the 240 s-pump-stop case using a residual flow rate of 50 g/s up to 1200 s after scram. This experiment simulates the expected natural circulation in the IHX secondary loops after the pump coastdown. The DHX startup delay time varied between 0 and 240 s. The 0 s-case represents the full operation of all DHXs before scram already. In this case they need not to be put in operation on demand and this case represents a totally passive DHR-system.

Table II
Experimental Parameters - transient - RAMONA I/II

Parameter	Variations
Core power before scram P_o(kW)	30 – 75
Core power (decay heat level), P(kW)	0.6; 1.0; 2.0; 4.0
Half-time of primary pump speed reduction, $t_{1/2}$	0; 10; 20
Linear coastdown time with secondary pump stop after scram, Δt (s)	15; 120; 240; 1200
DHX delay time after scram, Δt_{DHX}(s)	0; 240; 3000
Above core structure design	permeable impermeable
DHX design (Fig. 27)	straight tube U-tube hybrid
Radial power distribution across the core (X)	1.0; 0.87;0.65; 0.59
Number of DHXs in operation	- straight tube: 4; 2 - U-tube: 4; 6; 2; 3 - hybrid: 8; 4

The ACSs were chosen to be impermeable and permeable to alter the complexity of the flow patterns above the core. The design of the DHXs was varied with re-

spect to select a thermohydraulic optimum design. Most experiments were carried out with a flat radial power distribution across the core. They were completed by variing the radial power distribution up to very extreme values of X=0.59. (The power distribution is defined as average volumetric power density divided by maximum volumetric power density ($X = X_{avg}.X_{max.}$))To simulate very asymmetric DHR conditions and the unavailability of DHX circuits experiments were performed where only half of the available DHXs were put in operation.

Beside RAMONA I and II which are four loop models RAMONA III was used. This is a three loop model, similar to the EFR. The most interesting parameters were studied for comparison reason in this model. In most of the parameter variations, only one parameter was changed at a time while the other reference conditions were kept constant.

9.2.2 Results - Reference Operating Conditions [29]

In the following only the most decisive results will be described to study and reveal individual parameters influencing the primary system thermohydraulics. In this respect there are three main informations, namely the core mass flow which informs about the onset of natural convection, the temperature course of the core inlet and outlet and the vertical temperature distributions in the upper plenum. The graphs in general show the measurements as function of time over 4 h. All tests are run 20 h to reach steady state conditions.

The results of the reference case are plotted in Fig. 35. The core flow rate, core temperatures and the upper plenum temperatures measured on a typical traverse are represented for a period of up to 4 h after scram. The measuring positions of these results are indicated in the RAMONA sketch. It becomes evident that the core flow rate is reduced in a linear manner (half time of the pump rundown characteristic is 10 s) and reaches a minimum value after shutdown of the pump (s. Fig. 35a). Due to natural convection subsequent increase in the mass flow rate of the core takes place (up to about 300 s) until it drops again. This drop is attributed to the following facts:

- the IHXs are warmed up with hot fluid of the upper plenum temperature after the stop of the secondary side pumps at 15 s after scram. The cold flow of the IHXs producing descending forces is consumed subsequently.
- Starting with the DHX operation 240 s after scram the cold fluid filled up the cavity and generated a cold stratification layer above the core. The cold flu-

id layer results in a descending force being generated in the core channels. To compensate these forces exerted by IHXs and DHXs the core has to build up buoyancy forces as well by formation of a ΔT in the core, which maximum is seen after about 1800 s (Fig. 35b). As a consequence, the mass flow rate is reduced.

The core flow rate increases and stabilizes as soon as upper plenum fluid of mixed temperature reaches the IHX inlet windows at about 1800 s after scram. Subsequently, it is increased to a quasi-stationary value at about 2 h after scram. The core flow rates are measured in RAMONA II and III by magneto inductive flowmeters. For the RAMONA I the core mass flow rates have been recalculated by the enthalpy rate of the core. In Fig. 35aa) a comparison is shown of the core flow rate measured in RAMONA II and calculations for the identical experiments. Deviation from the experiments can be attributed to heat losses of the core to the UP by axial conductivity.

Thermal behavior of the upper plenum is reflected by the temperature variation given in Figs. 35c) and d). Immediately after scram cold fluid enters the lowest region of the upper plenum due to the reduction in core power and the still operating PPs. After the start of the DHX operation cooling is increased considerably in this region and after about 2 h a constant upper plenum temperature difference is obtained and the upper plenum temperature attains in a quasi-stationary value after a period of about 20 h only.

9.2.3 Results of the Parameter Studies

Increasing the core power before scram [31]

The reference case and all others experiments have been extended to the 100 % load case, which is identical to the nominal reactor operation. Then the core is heated with 75 kW and reduced after scram to 2 kW as decay heat removal power. For the onset of natural convection after scram, this means the steady state flow rate via the IHXs, two parameters are important:

1. the reduction of the core power level to the decay heat removal power of the core. In case of great decay heat power, the onset of natural convection will start earlier, compared to cases with very small decay heat power.
2. the primary mass flow rate before scram and during the pumps coastdown influences the dynamic fluid process in the upper plenum. Large mass flow

rates destroy the hot fluid layer in the upper plenum more than smaller ones.

Comparing the first parameter between the reference case with 30 kW and 75 kW core power, the ratio is practically the same, but the decay heat power is doubled in the 75 kW case. In the 75 kW case the influence of the second parameter is seen by a doubled primary mass flow rate.
Consequently the time for the onset of natural convection will be shorter for the 75 kW-case than for the 30 kW-case.
The results of the 100% load case (75-2 kW) are plotted together with 40 % load case (30-1 kW) in Fig. 36. In the 100 % load case it is visible that the core flow rate after scram is 50 % higher than in the 40 % load case. Also the core temperature drop right after scram is recovered faster as the buoyancy forces are higher than in the 40 % load case. The vertical temperature distributions in Fig. 36d) in the UP indicate that the fluid of mixed temperature reaches the IHXs inlet windows already 1200 s after scram due to the same reasons.

Core power after scram - decay heat level [20, 33]

The influence on the transition phase by different powers of decay heat is shown in Fig. 37. The measured core power behavior is indicated in Fig. 37a. It is obvious that the core power is reduced from 30 kW to 0.6, 1, 2, and 4 kW within 1.5 s and then kept constant during the experiment. For these parameter tests, the half time of the primary pump speed reduction is 10 s and all the pumps stop at 130 s after scram. Therefore, the core flow rate plotted in Fig. 37b drops considerably immediately after scram and shows a very steep gradient at the moment of the pump stop. The flow rates then rise again because of the onset of natural convection. This is caused by the increase in the core temperature differences (Fig. 37c). The buoyancy forces of the core increase with increasing core power. Therefore, the core flow rates and temperature differences are proportional to the core power. The measurements indicate a second minimum in the core flow rates. They occur the later and are the more intensive the lower the core power is (see Fig. 37b). This flow reduction is due to the high temperature fluid of the hot plenum entering the IHX and reducing its natural convection pressure head. It is mastered as soon as mixed fluid cooled by the DHX operation reaches the IHX windows, which takes longer when the core power is lower.

The temperatures at the inlet and outlet of the core are plotted in Fig. 37c as the mean values of all thermocouples. The outlet temperatures exhibit a decrease

just after scram and a rise with increasing time. The temperature decrease grows with reduced core power, while the temperature rise is increased with increasing core power. At high powers, the outlet temperatures are increased with time after scram. The higher the flow rate (power) is, the sooner is the onset of natural convection that reduces the increase of the core temperature rise and held it constant. An increasing temperature difference between the upper and the lower part of the upper plenum is registered right after scram (s. Fig. 37d). This temperature difference is strongly influenced by the start of DHX operation at 240 s. It results in the development of a temperature stratification in the hot plenum by the cold fluid delivered by the DHX. This stratification is fully developed at ~ 1000 s after scram for 4 kW - and at ~2 h for the 1 kW-case (Fig. 37e). The increase at high power or the decrease at low power of the overall systems' temperatures is due to the imbalance between the DHX power (inlet temperature and flow rates are kept constant) and the core power (Fig. 37d).

Primary pump coastdown [33]

The primary pumps control the core flow and, hence, the core temperatures. Three pump coastdown characteristics are investigated. The respective flow rate measurements are shown in Fig. 38a for the first 500 s after scram. They all start at scram time with the rated flow of 840 g/s. In the first case, the pumps are stopped at scram initiation ($t_{1/2}$ = 0 s). The other two cases differ by the half times of pump speed reduction, namely, $t_{1/2}$ = 10 s (pump stop 130 s after scram) and $t_{1/2}$ = 20 s (pump stop 260 s after scram) respectively. In all cases, the core power after scram is 1 kW. The onset of natural convection can be seen from the 500s plot. In the case of $t_{1/2}$ = 0 the flow rate is very large at the onset of natural convection and decreases continuously. For the two other cases at $t_{1/2}$ = 10 s and 20 s, the natural convection starts right after the pumps stop at 130 s and 260 s, respectively. For all three cases, more or less identical flow rates are measured 500 s after scram. The average core flow rates are shown for a time interval of 4 h. Minimum flow rates are registered at ~2000 s after scram. This is due to the development of temperature stratification in the hot plenum together with the reduction of the IHX natural-convection pressure head as mentioned earlier. As soon as the cooled mixed fluid of the upper plenum reaches the IHX windows, the core flow increases and the temperatures decrease (s. Fig. 38b).

The core temperatures are shown in Fig. 38b. A very quick and steep increase in the outlet temperature is detected in the $t_{1/2}$ = 0 s case. This temperature in-

crease results from the sharp decrease in the flow and the remaining large volume of heat stored because of the heat capacity of the core. Then, the outlet temperature decreases with time as a result of the onset of natural circulation. Up to ~350 s, the outlet temperatures of $t_{1/2} = 20$ s case are smaller than those of the $t_{1/2} = 10$ s case. The inlet temperatures of all cases are practically identical during this time. Hence, the lower outlet temperature of the $t_{1/2} = 20$ s case is due to the higher flow rate through the core.

The measured hot plenum temperature distributions in the upper part of the hot plenum during the first 500 s after scram do not exhibit any remarkable differences (Fig. 38c, 38d). Minor temperature stratification develops right after the scram, as the cold fluid passes the core and reduces the temperatures at the bottom of the cavity. This temperature drop is accelerated with increasing pump coastdown time. After ~1000 s, the influence of the half time of the pump speed reduction on the hot plenum temperatures is negligible.

IHX secondary side flow coastdown

The measured IHX secondary side flow rates are represented in Fig. 39a. It can be seen that the flow rate is reduced linearly and equals zero at 15, 120, 240 or 1200 s after scram. For these tests, the half time of the primary pump speed reduction is 10 s, and the immersion cooler operates as described for the reference case. Figure 39b represents the total core flow rates during 4h after scram. The core flow rates just after pump stop are increased with decreasing IHX secondary-flow coastdown. The reason for this is the fact that the longer coastdown prolongates the fluid cooling on the IHX primary side, which results in the higher natural circulation pressure head. Cases with a pump stop after 240 s and 1200 s, respectively show decreases in the flow rate just after 240 s. In both cases, the IHX secondary flow rates were reduced to zero and to a minimum of 50 g/s at 240 s, respectively. This means that the core flow rate decreases with the reduction of the IHX secondary side flow rate that initiates a temperature increase on the IHX primary side. After 240 s, the 1200 s stop case shows a core flow rate exceeding that of all other cases up to 1500 s. This is due to the still lower temperature on the IHX primary side resulting from the continuing low flow on the secondary side. The core flow rate decreases again at 1200 s due to the stop of the IHX secondary flow followed by a temperature increase on the IHX primary side. In all cases, the core flow rate increases again as soon as the mixed cooler fluid reaches the IHX inlet

windows. This results in a very effective increase in the natural circulation pressure head of the IHX flow path (Fig. 39b).

The core temperature history is shown in Fig. 39c: The inlet temperatures of the longer coastdown cases decrease faster because of the colder fluid from the IHX delivered via the lower plenum. The longer coastdown cases also show higher decreases in the outlet temperatures caused by the increased flow rates. The reduced outlet temperatures increase again after the stop of the IHX secondary-side flow, thereby decreasing the core flow rate. This is clearly seen in the 1200 s stop case at ~1200 s. The longer coastdown cases have lower peak temperatures at the core outlet due to the larger amount of heat transfered to the IHX secondary loops during the availability of the secondary flow path.

The hot plenum temperatures measured as a function of time are shown in Figs. 39d and 39e for the two extreme pump stop cases of 15 s and 1200 s . The longer coastdown case indicates a faster temperature decrease in the lower part of the hot plenum, whereas the temperature history of the upper part roughly correspond to that of the short coastdown case. This is due to the cooler core outlet fluid causing a very distinct temperature stratification within the first hour after scram. Nevertheless there exists a delay in the temperature decrease in the upper part of UP. In both cases the temperature stratification is fully developed at about 2 h after scram.

Decay heat exchanger startup delay time [33, 34, 35]

The measured DHX secondary side flow rates are represented in Fig. 40a for three of the five cases investigated .In the 0-s case the DHXs were already operating under the rated normal operation conditions before the scram. As far as the other cases are concerned, the flow rates were increased each at the start time of the DHX operation and reached identical values of the rated condition within 160 s.

The total core flow rates are shown in Fig. 40b. In all cases, the core flow is reduced right after scram as a result of the power loss. Afterward, the flow rate recovers within a few seconds and decreases to a minimum value again in the following 2000 s. This is due to the hot fluid entering the IHX windows and reducing the natural circulation pressure head. The cold fluid from the DHXs creates a temperature stratification in the hot plenum. The 3000 s case shows the smallest flow rate reduction compared to the other cases. In this case the DHXs are not in op-

eration. Hence, the flow rate reduction is only due to the heat up phase of the IHX reducing its natural circulation pressure head. After the start of the DHX operation, the flow rate of the 3000 s case decreases slightly up to ~1.3 h and then increases again. This second core flow reduction results from the cold fluid from the DHXs, forming a cold fluid layer above the core. This reduces the buoyancy forces of the core and stratifies the hot plenum.

The core temperature behavior is shown in Fig. 40c. For the first 500 s, the inlet and outlet temperatures are identical. They start to deviate from each other at ~1500 s. It can be noticed that the outlet peak temperature of the 3000 s case only slightly exceeds those of the other cases. This is due to the large heat capacity of the plenum. In this case the outlet and the inlet peak temperatures are higher and are reached later compared with the other cases. This is caused by the time delay in the DHX operation, as a result of which the low temperature fluid is supplied to the plenum later.

The formation of the thermal stratification in the hot plenum is shown in Figs.40d and 40e for the two DHX startup delay times of 240 s and 3000s, respectively. The most impressive thermohydraulic behavior between the 240s-case and 3000s-case in Fig. 40d is the delay of the stratification layer of the 3000 s-case. Up to this time the temperatur in UP is held constant, only in the lower part of the UP (cavity) cold fluid is observed coming from the cold chock of the core. After 3000 s in the cavity exists a temperature of only 41 °C, in the 240 s-case the cavity is cooled down on 37 °C, see Fig. 40e.

The temperature of the UP is cooled down continuously for the 240 s-case. This cooling behavior starts for 3000 s-case after this delay time and after 4 h it exists only a small temperature difference.

Above core structure design [32, 34]

Two different designs of the ACS are examined in the transient experiments to reveal their influence on the thermohydraulic behavior of the upper plenum and the primary system, namely the impermeable and permeable ACS. Transient experiments have been performed with these ACS design. The IHX secondary pump coast down time was linear, the pumps stop set at 240 s.

The core mass flow rates, the inlet and outlet temperatures of the core as well as the temperature history in the UP are sketched in Fig. 41. As can be seen by comparison there is no remarkable difference to be detected except near the model axis, Fig. 41d. This Figure shows the vertical temperature distribution (HT1.1) immediately above the core at a distance of 12 mm from the cylindrical ACS wall (Fig. 11). As can be seen, in the initial condition before the scram, temperature differences between the permeable and the imperable ACS type already exist in the region between core outlet level and ACS bottom. This is due to the fact that the hot fluid from the core flows into the hot plenum mainly through the ACS in the case of the permeable type. Nevertheless similar distributions are observed in the time range from the scram to 3000 s. The lowest temperature at the height of 255 mm at 240 s is caused by cold fluid which is accumulated in the cavity during the flow coastdown (cold shock) and spills over interacting with the hot fluid from the core. With increasing time for the impermeable ACS, the temperature gradient in the upper section above the ACS bottom level becomes fairly uniform. By contrast, the permeable ACS reveals increasing temperatures all along the upper plenum height. Besides, the impermeable type shows the temperature peak near the ACS bottom level at steady state conditions (20 h). This means that the hot fluid from the core goes into the hot plenum directly lead by the impermeable bottom plate of the ACS. It interacts with the cold fluid from the DHX mainly in the region between the core outlet and the ACS bottom levels. This results in an inhomogeneous temperature field across the mixing region.

Decay heat exchanger design [34, 36, 37]

This chapter describes a series of transient experiments performed in RAMONA under the reference operation conditions compared with the same case but with a 3000 s delay in the start of the DHXs. The ACS is permeable. The object of these experiments is to demonstrate the thermohydraulic behavior of the following different DHX types in the transition region from forced to natural circulation (see Fig. 28):

- Straight-tube bundle-type with shell (S-tube-type)
- U-tube bundle-type without shell (U-tube-type)
- U-tube hybrid-type without shell (hybrid-type)

The variations with time of the thermohydraulic conditions in the model are shown in Figs. 42 to 44. Each of these figures indicate the core flow rates, core

temperatures, and a typical course of the vertical hot plenum temperature distribution for the long term behavior up to 4 h after the scram. In addition, the development of the vertical hot plenum temperatures are shown for discrete time intervals after the scram. All graphs on the left hand side represent the results for a delay of 240 s between scram and DHX operation start and all graphs on the right side indicate the results for a start delay of 3000 s. The results distinguish from those indicated in Fig. 40 by the insertion of a permeable ACS.

Straight-tube bundle type DHX (Fig. 42): The core flow rates indicate a strong drop immediately after the scram. (Fig. 42a) This drop is registered for all investigations reported here. It is due to the fact that the half time of the primary pump speed reduction is only 10 s with a stop of all pumps at 130 s. Since the DHXs start to operate at 240 s after scram, they cannot influence this first flow reduction. Right after the pumps stop, the core flow rates rise again because of the onset of natural convection caused by the increase of core temperature differences (Fig. 42b). Thereafter a second minimum in core flow reduction is registered which is brought about by two effects; namely the IHX heat up by the entering hot UP fluid and the start of the DHXs operation delivering cold fluid in the UP. During this low core flow interval the temperatures within the core increase up to the maximum. The highest core temperatures start to decrease as soon as the natural convection flow increases.

This behavior is reflected in the stratification of the upper plenum (Fig. 42c). It is visible in the vertical temperature plots for different time intervals of the transient (42d). At the start of the transient a uniform vertical temperature distribution is registered. This distribution changes as soon as cold fluid reaches the cavity and it can be seen that the lower part of the upper plenum gets colder and colder. There are practically no large temperature reductions up to 0.25 h after the scram in the upper section of the plenum. Thereafter mainly the temperatures in the upper section of the plenum are reduced. These effects exhibit the diminution of the overall system temperatures. Finally, a temperature stratification is formed reaching the steady state status about 20 h after the scram.

The influence of the 3000 s delay of the start of the DHX operation is also visualized in Fig. 42 (right). After the first strong drop of the core flow immediately after scram small second and third flow reductions are registered. Both are due to the heat up processes of the IHX's and the start of the operation of the DHXs. In the cases shown both processes are separated and it can be deduced that the IHXs

heat up phase lasts about 0.25 h and the flow reduction because of the DHX operation about 0.5 h. These processes are reflected by the registered core temperatures as well (Fig. 42b). The maximum core outlet temperatures are influenced only to a minor degree by the delayed start of the DHX operation. This small amount of core outlet temperature is due to the heat capacity of the in-vessel coolant.

The course of the upper plenum temperature distribution shows only a small stratification, lasting until the operation of the DHX is started (Fig. 42c). These small temperature differences are produced right after scram. At that moment the power is reduced within 1,5 s. During the pump coast down, which takes 130 s, the coolant temperature differences in the core collapse (Fig. 42b). The resulting cold core fluid spills in the cavity where it is mixed with the masses of hot fluid present in the cavity. This behavior is reflected in the vertical temperature plots (Fig. 42d) for the time interval up to 500 s. This small temperature decrease can be observed also in the $\Delta t_{IC} = 240$ s case as well. However, the graphs shown here exhibit this small temperature decrease separated from the DHXs operation and held the temperature and its gradient constant up to 3000 s. The start of the DHXs lead to remarkable temperature reductions in the cavity. A temperature stratification with a distinct temperature gradient at the upper core edge is formed successively. This stratification finally reaches steady state after about 20 h.

U-tube bundle-type DHX: For this type of immersion cooler in the transient tests for 240 s and 3000 s delayed start of the DHXs practically the same thermodynamics behavior (Fig. 43) can be registered for the U-tube type DHX as for the straight-tube DHX. The course of the core flow rate and the temperatures of the core do not differ much from the data plotted in Fig. 42, respectively. Only in the course of the temperatures in the lower part of the upper plenum (Figs. 43c, 43d) a difference is visible. Here temperatures are registered which are roughly 2 K lower. This temperature difference is still present 20 h after scram as a comparison of the vertical temperature profiles shows. This behavior is due to the "jet like" outlet flow behavior, feeding less mixed, very cold fluid to the cavity.

Hybrid-type DHX: The registered core flow rates, core temperatures and upper plenum temperatures are shown in Fig. 44. The core mass flow rate (Fig. 44a) reaches a first minimum at the pump stop time. After the recovering of the flow rate a second but small core flow reduction is detected. In this case it is only due

to the heat up phase of the IHXs, since the hybrid-type DHXs show a very good mixing of cold and hot fluid. This observation can be deduced from the measured uniform vertical temperature distributions (Fig. 44d). The differences to the bundle type DHXs are evident. The good mixing is caused by the large area that is covered by the heat-transfer surfaces in the upper plenum, as well as by the direct contact between each individual U-tube and the hot upper-plenum fluid. This is a specific feature of the hybrid-type DHXs. It could be demonstrated by temperature field measurements in preceding steady state tests (Fig. 29) that the cold fluid falling down into the upper plenum mixes entirely with the hot fluid within a few tube diameters below the lowest end of the DHX. The IHX inlet windows are fed with the well mixed upper plenum fluid immediately after the start of the DHX operations. In addition, portions of cold fluid from the DHX enter the IHX windows directly. As a result the second core flow reduction, which is caused by the heat up of the IHX's, is small. The cold IHX fluid continues to travel down and through the core. This results in maximum core temperatures that are 1 K lower than the ones measured for the bundle-type DHXs (Fig. 43b).

These features of the hybrid-type DHX taken together result in an only small vertical temperature stratification in the upper plenum. Practically uniform temperature distributions are registered from the lowest to the highest point of the upper plenum. The continuous coolability of the overall system is clearly indicated by the vertical temperature measurements for the different time intervals. Steady state conditions are reached at about 20 h after scram.

These observations stay practically unchanged when the start of the operation of the DHXs is delayed by 3000 s. The core flow course features only a small instability at the 3000 s (0.83 h) time point. Its influence on the maximum core temperatures is small. The measured vertical temperature distributions are identical with the ones measured for the bundle-type DHX as long as the DHXs are not working. With the start of the operation at 3000 s, the upper plenum is uniformly cooled, reaching steady state conditions about 20 h after scram. The steady state temperatures in the upper plenum indicate practically the mean temperature of the upper plenum also for the bundle type DHXs, but do not reveal the distinct temperature gradients near the upper edge of the core outlet.

Radial power distribution across the core [38, 39]

So far, all experiments have been performed with a radially flat heater power distribution across the core. It was therefore necessary to investigate also the transition from forced to natural circulation in RAMONA with a reactor-like cosin-shaped radial heater-power distribution. A series of experiments with increasingly cosin-shaped radial power distributions was done to make sure that there was no counter flow or flow stagnation inside the core, even under extreme conditions. The power distribution is defined as average volumetric power density divided by maximum volumetric power density ($\chi = \chi_{avg.}/\chi_{max}$). Fig. 45 represents different radial power distributions of the reactor design and the way how they were realized by varying the core power density in the model. Here the results are reported only for impermeable and permeable ACS geometries, and for IHX-run-down times of 240 s and 15 s. The most extreme radial power distributions of $\chi = 1.0$ and $\chi = 0.59$ are compared with each other. Both χ-values could only be reached by a reduction of the total core power from 30 kW to 21 kW, because of limitations of the capacity of the central core-heating element.

The data are presented in five graphs in Fig. 46 for better understanding. Graph a and b show the core flow rates over a time range of 4 h. This core flow rate is a calculated value using the measured core power and enthalpy rise of the core. Graph c, d and e, f depict the temperature courses of the outermost (channel 1) see Fig. 6 and the forth of eight core flow channels at four angular positions ($\phi = 45°$, 135°, 225°, 315°) of this core channel. Graph g and i show the course of the UP temperatures measured at various heights ranging from the lowest to the highest point of the UP. Graph i and j indicate hot plenum temperature profiles measured at various after scram times. All experiments had a total power of 21 kW before scram and of 1 kW after scram. In each individual experiment, the power distributions were kept the same before and after scram.

Fig. 46 represents the results of the experiment characterized as follows: $P = 21$ kW; $\tau_{IHX} = 240$ s; ACS impermeable; $\chi = 1.0$ and 0.59. In both cases the known thermohydraulic behavior of preceding transient experiments is reflected, namely:

- the decrease of the core flow to a minimum and its increase to a steady state value

- the reduction of the core temperature difference due to the after-scram PP coast down with pump stop at 130 s and the installation of a constant temperature difference in all core channels
- the onset of a stratified temperature field in the UP with the start of the DHXs operation with a distinct temperature gradient in the region between core and DHXs outlet.

In these cases the system temperatures before scram is 6 K lower compared to the 30 kW-case (see Fig. 35). The temperatures 20 h after scram are the same since the operation conditions are the same in both cases and the power of decay heat.

Varying the radial power distribution to $\chi=0.59$ a similar thermohydraulic behavior is registered in the UP with one exception, namely the temperature increase in the outer core channels is lower compared to that of the central channels. This is demonstrated by Fig. 46d and Fig. 46f. All core flow channels have identical pressure-loss coefficients. Hence the mass flow rate per unit flow area is the same in each channel. Therefore, the temperature increase of the fluid is only a function of the specific volumetric power of the heater rings. For $\chi=0.59$, the power of the two outermost heater rings of the core is only 10% of that of the inner heater rings. Therefore, only a small coolant temperature rise is registered in the outermost flow channel before scram. After scram, this temperature difference increases without reaching the values of the inner flow channels. But for the 4th channel the temperature rise before scram in the $\chi = 0.59$ case is higher than in the $\chi=1.0$ case. The reason is the local higher volumetric power with $\chi= 0.59$, see also fig. 45b). The upper plenum temperature distributions are similar for all two cases. This temperature behavior is absolutely different from that displayed by configurations with permeable ACS, as described below. The reason is the good mixing of cold and hot fluid in the space above the core when the ACS is impermeable.

Fig. 47 indicates the results for a permeable ACS. All other parameters were kept identical. These data reveal a very strong influence of the radial core power distribution on the system thermohydraulics. Unlike the graphs for $\chi=1.0$ with both impermeable (Fig. 46) and permeable ACS (Fig. 47) the results for $\chi=0.59$ display salient upper plenum temperature distributions. For $\chi=1.0$ a fairly uniform temperature distribution is registered for pre-scram conditions. This is totally changed for $\chi= 0.59$, because the permeable ACS can be passed directly by the hot fluid. The cold fluid from the outermost flow channels does not mix with the

hot flow from the central core channels (unlike the impermeable-ACS case). The cold fluid fills the upper plenum up to the IHX-entrance windows. Above these windows a fluid layer is found with temperatures that are 3 K higher (Fig. 47 j). These temperature differences are equalized by 4000 s after scram, and from that time on, uniform temperatures are registered in the upper part of the plenum. In contrast, the temperature in the cavity decreases because the DHX operation starts 240 s after scram. The typical temperature stratification with the known steep temperature gradient near the top end cross section of the core, is developed successively.

The influence of the radial core power distribution can be deduced from the graphs: Driven by natural circulation, the core mass-flow rate develops after the pump stop the faster the higher the χ-value. For $\chi = 1.0$, only a few ten seconds are necessary to install a very coolant-effective natural-circulation flow. With decreasing χ-value, i.e. increasing radial core power distributions, the core mass-flow courses are successively more and more strongly influenced. This is because the power of the outer core heater rings is reduced continuously. As a result, more and more colder fluid reaches the upper plenum and leads to the build up of a distinct temperature stratification at the IHX's entrance windows, even already under pre-scram conditions. The cold core fluid is clearly indicated by the core outlet temperatures of channel 1 (Fig. 47d) in comparison to those of channel 4 (Fig. 47f), and by the non-uniformity of the vertical temperature distributions in the upper plenum (Fig. 47j)) for pre-scram conditions.
After scram, the DHX operation starts, and successively the initially high temperatures of the upper part of the hot plenum are reduced. Thereby, the characteristic temperature profile with a cold cavity and a uniformly hot plenum above the core-outlet cross section is formed. All temperature profiles after 20 h of operation of the primary system are the same in all cases, since the boundary conditions are the same as well.
Fig. 48 shows the influence of the radial core power distribution for an IHX-run-down time of only $\tau_{ZWT} = 15$ s compared to the forementioned cases with $\tau_{ZWT} = 240$ s. The main information taken from the various graphs represented is that the core mass flow decreases following the pump coast down curve and reaches its minimum value at the time were all pumps stop (130 s). This is in contrast to the $\tau_{ZWT} = 240$ s case, where the prolonged cooling of the IHX's over 240 s feed large amounts of cold fluid via the core into the upper plenum (Figs. 46 and 47). These effects explain the differences in the time-dependent core flow rate curves.

Symmetric and asymmetric heat removal [35, 40]

A highly asymmetrical decay heat removal occurs under the condition that only two out of four pairwise installed DHXs can be put in operation. To address this operational case, transient tests have been carried out for the following operation conditions:

- reduction of core power from 75 to 2 kW within 1.5 s
- half time of a primary pump coast down: 10 s
- mass flow rate reduction of the IHXs secondary loop within 240 s
- start of the DHXs operation 240 s after scram
- DHX-type: straight tubes

Figure 49 compares the results of the measurements with 4 and 2 DHXs in operation. It can be seen that after scram the core mass flow rates during operating 2 DHXs (Fig. 49a) are identical to the measurements recorded during nominal operation conditions with 4 DHXs being in operation. This is also true for the temperatures measured at the core inlet and outlet side during the first 30 minutes after scram (Fig. 49b). With increasing time, however, the inlet and outlet temperatures increase slightly to steady state values reached at equilibrium conditions, i.e. when the removed decay heat is identical to the heat input.

The formation of the upper plenum temperature stratification is seen from Figs. 49c and d. Comparing these results one with another it can readily be seen that similar temperature profiles are registered within the first 1000 s after scram for 2 and 4 DHXs in operation. But as soon as the two DHXs are in full operation, mainly the temperatures of the upper plenum differ from the symmetric load case. This is due to the fact that the heat transferring surfaces are only half as large as in the case of a symmetrical cooling mode. The temperature level of the system decreases up to a time of about 4000 s and increases slightly thereafter reaching steady state about 20 h after the scram. For the symmetric and non-symmetric load cases, the steady state temperature levels differ by 5 K.

These investigations were supplemented by additional parameter tests but with a core power reduction at scram from 30 to 1 kW. In this case three experimental series were performed with the three DHX designs under consideration, namely the straight-tube and U-tube bundle type and the hybrid type DHXs (Fig. 28). Non-symmetric heat removal is achieved by operating only two adjacent bundle type DHXs or 4 adjoining hybrid-type coolers. All these experiments are carried

out with an impermeable above core structure. The straight-tube bundle type DHX (Fig. 50) shows practically a similar thermohydraulic behavior as the U-tube bundle type DHX. Therefore, the U-tube DHX investigations are not reported here. The comparison of the main results with the forementioned ones (Fig. 49) shows a similar thermohydraulic behavior of the primary system. The main difference is the lower temperature level in this case due to the lower core power before and after scram.

A decisive influence on the primary system thermohydraulics however is exerted by the DHX type. This is demonstrated in Fig. 51 for the hybrid-type DHXs. The differences to the bundle type DHXs (Fig. 50) are evident. The core mass flow rate is continuously reduced and reaches a minimum value. The lower part of the upper plenum is fed with cold fluid by the IHXs within the first 400 s after the scram. By contrast to the bundle-type DHXs, the hybrid-type shows a very good mixing of cold and hot fluid. This could be demonstrated by temperature field measurements in preceding steady state tests (Fig. 29). The cold fluid falling down into the upper plenum mixes entirely with the hot fluid within a few tube diameters below the lowest end of the DHX. Therefore, the registered temperature stratification at 500 s after scram (Fig. 51d) which results in the long time reduction of the IHXs secondary pump coastdown of 240 s will be changed to an uniform vertical temperature distribution at 2000 s.

The IHX inlet windows are fed with the well mixed upper plenum fluid immediately after the start of the DHX operations. In addition, portions of cold fluid from the DHX enter the IHX windows directly. As a result, the core flow increases right after the heat-up of the IHXs. The IHX fluid continues to travel down and through the core. This results in maximum core temperatures that are 1 K lower than those measured for the bundle-type DHXs (Figs. 51b and 50b). These features of the hybrid-type DHX taken together result in small vertical temperature stratification in the upper plenum (Fig. 51c).

For the non-symmetric load case (only four of eight hybrid-type DHXs are in operation), identical temperature courses are recorded within the first 400 s after scram as for the symmetric case. At 400 s the full operation of only 4 DHXs does not influence the core mass flow. The core temperatures and the upper plenum temperatures increase slightly with time and reach steady state values at about 20 h after scram. In comparison to the symmetric load case, the system temperature level is increased by 4 K.

9.2.4 Numerical Simulation of a Transient Experiment [41, 42, 43]

From the multitude of RAMONA tests performed, a close-to-reality experiment was selected for computation. This experiment represents the transient thermohydraulic behavior starting from reactor shutdown. The power was reduced from 30 kW to 1 kW. Reactor specific boundary conditions were chosen. The ACS shell was permeable and the PPs and IHXs secondary pumps came to a stand-still after 130 s and 15 s, respectively. The experimental results are indicated in Fig. 52.

For the computation, a symmetric 90° section of RAMONA is considered. About 15,000 cells are used. The input data for the computations using the FLUTAN code take into account all components as well as their time dependent boundary conditions during the experiment. The calculation starts from a steady state and covers a period of 3,600 s. The stationary state developing after a long term (about 20 h) between the constant decay heat of the core and heat removal of the DHXs results from a separate calculation.

In Fig. 52 the computed results (on the right side) are compared with the measurements (left side). The mass flow rates calculated as well as the temperatures on the inlet and outlet side of the core exhibit the same characteristic behavior and are in good quantitative agreement with the experiments. The time-dependent UP temperatures at the highest and lowest measuring points as well as the vertical UP temperature distributions from the cavity to the top of the plenum clearly reflect the effect of the cold mass flow coming from the DHXs into the cavity and the slow filling of the UP with fluid of mixing temperature. After 20 h, the axial temperature distribution in the region of the lower ACS edge exhibits a thermal stratification with a temperature difference of about 3 K. This behavior is simulated well by the computations.

The results using the FLUTAN code were obtained by careful modeling of the RAMONA test and an enhancement of the code. The computation time required exceeds the real time by a factor of 400. Efforts are being made to reduce the cpu time.

The model tests serve in addition to compare out-of-pile with inpile experiments [44]. This is the case for the PHENIX-COLTEMP 4 reactor test. Figure 53 shows the vertical temperature distribution measured in PHENIX at different time intervals

after the primary pump stop extended over 40 minutes at a constant reactor power of 5.8 MW, starting from isothermal conditions. A comparable RAMONA experiment is characterized by primary pump stops extended over 120 minutes at a core power of 1 kW, starting from isothermal conditions. It can be deduced from the graphs that the physics in the RAMONA test section does not differ remarkably from the PHENIX experiment. Both tests were simulated by the 2D code ATTICA [3]. In addition, results for the RAMONA simulation with the 3D code FLUTAN are indicated. The diagram shows that the comparison of the computed and experimental results is satisfactory.

10. RESULTS - RAMONA-III

RAMONA I and RAMONA II are four loop models (Table I). The model diameter is 1 m and the fluid volume about 0.4 m^3. The heat under nominal operation condition is removed by 8 IHXs. The flow in the primary system is circulated by 4 pumps. In RAMONA III only 6 IHXs and 3 PPs are used and the model diameter is only 850 mm. Hence the fluid volume is about 0.3 m^3. In addition RAMONA III is equipped with 6 straight tube type DHXs instead of 4 DHXs as in RAMONA I and II. Vertical and horizontal cross sections of RAMONA III are shown in Fig. 54 together with the main dimensions in millimeters.

To study the thermohydraulics under steady state and transient operation conditions and to compare with results if RAMONA I and II a series of experiments has been carried out with RAMONA III. The variables of these experiments were set in close approximation to those of RAMONA II. The instrumentation, the data acquisition and the test procedures are identical to RAMONA I and II.

10.1 Parameters and Results under Steady-State Conditions

The number of parameters for these investigations was restricted to the variations of the decay heat power of the core (1 kW; 2 kW) and the design of the above core structure (permeable, impermeable). The influences of all other parameters on the steady state primary system thermohydraulics are comparable to the RAMONA-II-results. Additional informations can be found in the transient experiments which include the parameters core power before scram and the asymmetric decay heat removal with only 3 out of 6 DHXs in operation.

The influence of the core power on the upper plenum temperature distributions is indicated in Fig. 55 for the impermeable ACS and in Fig. 56 for the permeable ACS. The DHXs secondary side inlet temperature was 24 °C. Both figures show the isothermal plots (interval of 0.5 K) measured with movable thermocouple rakes for two circumferential positions. The first one is the 16.5 deg. position identical to a cross section formed by the model axes and the DHX-position, the other is the 60 deg. position which is the cross section without DHX (Fig. 54). From the plots it can be seen that for an impermeable and permeable ACS the temperature increases with the power the impermeable ACS produces a stratified temperature profile with horizontal arrangement of the isotherms in the region between upper end of the core and lower edge of the outlet windows of the DHXs. By contrast the permeable ACS shows a field of isotherms extended over the whole volume of the UP. The vertical temperature gradient is therefore reduced and the max. temperatures are found on the model axis. This behavior is similar to RAMONA II with the exception that the isotherms measured in RAMONA II seem to be more concentrated in the region between core and DHXs outlet. This can be seen from the comparison with Fig. 33a showing measurements in RAMONA II for identical boundary conditions.

10.2 Parameters of the Transient Investigations

The variables of the transient investigations were similar to the reference conditions (RAMONA I, II) and were set as follows:

- The primary system via DHX and pressure plenum is unblocked.
- All DHXs are serviceable
- The transient operation conditions are:
  - reduction of core power at scram from 30 to 1 kW within 1.5 s with a radial flat power profile
  - reduction of the core flow rate from 840 g/s corresponding to the half-time of a primary pump coastdown of 10 s. The pumps were stopped at 130 s.
  - reduction of the mass flow rate per IHX secondary loop from 120 to 0 g/s within 15 s.
  - DHXs startup, delayed by 240 s, of each of the six secondary loops of the DHXs within 160 s by a linear increase in the mass flow rate from 0.4 to 4.3 g/s.

The decisive parameters influencing the primary system thermalhydraulics, listed in Table IV, were subject to variations. All investigations were performed with straight tube-type DHXs.

Table IV
Experimental Parameters - transient - RAMONA III

Parameter	Variation
Core power before scram P(kW)	30; 75
Core power after scram (decay heat level) P(kW)	1; 2
Half-time of primary pump Speed reduction, $t_{1/2}$	10
Linear coastdown time with secondary side pump Stop after scram Δt, s	15; 240
DHX delay time after scram, Δt_{DHX}, s	240, 3000
ACS design	impermeable, permeable
Number of DHXs in operation	6; 3

10.3 Results of the Studies under Reference Operation Conditions

The comparison is made between the results of RAMONA II and RAMONA III for the reference conditions. These conditions are comparable as the power reduction, the secondary side parameters of IHXs and DHXs as well as the pump speed reduction were identical. The heat transfer surfaces of the DHXs were also the same in both models. This however is not the case for the IHXs heat transfer surfaces. As the RAMONA II - IHXs are used in RAMONA III the heat transfer surface of the RAMONA-III-IHXs is reduced to 75 % of that of RAMONA II. This must be taken into account when the results are intercompared. The commentaries concentrate on the differences with respect to the 4-loop design as the general thermohydraulic behavior does not change from the physical point of view.

Fig. 57 compares the results of the experiments on the transition from forced to natural circulation for reference operation conditions of RAMONA II and III for a time span of 4 h after scram. The core flow increase after IHX loss of natural

convection pressure head is faster by a factor 0,5 for RAMONA III than for RAMONA II.The core outlet and inlet temperature courses differ from each other. In RAMONA III a higher temperature level is registered before scram. This is due to the reduced number of IHXs in operation compared to RAMONA II. As the secondary side operation conditions and the core power were kept identical the temperature differences between the secondary side and the primary side of the IHXs has to increase to balance the heat transport (Fig. 57b). The maxima of the core temperatures are reached at earlier time in RAMONA-III. This is due to the smaller water volume in the tank resulting in higher circulation velocities within the primary system. Therefore the gradient of the temperature reduction of the UP is higher. The temperature distributions in the UP are comparable. In RAMONA III the vertical temperature gradient extends along a higher plenum length and is less pronounced with respect to the measurements in RAMONA II. This is due to a higher cold fluid layer and less fluid volume in the UP of RAMONA III.

10.4 Results of the Parameter Variations

The influence of the core power before scram can be taken from Fig. 58. In comparison to the results shown in Fig. 57 the core mass flow rate is higher as well as the temperature level after scram. The overall thermohydraulics indicates that a faster temperature decrease is registered due to the smaller tank volume (see Fig. 35). The steady state temperature distribution reached about 20 h after scram is identical to RAMONA II. This was already demonstrated with the measured isothermal fields (Figs. 55 and 56).

The coastdown time of the IHXs secondary side pumps was varied from 15 to 240 s. This influence is demonstrated in Fig. 59. The salient feature in comparison to the results for $\tau_{IHX} = 15$ s (Fig. 58) is the strong core mass flow reduction which decreases with the IHXs secondary side flow rate and increases again as soon as mixed cooler fluid reaches the IHXs inlet windows. By contrast to the 4 loop results the cold fluid delivered during the first 500 s fills a larger portion of the UP volume of RAMONA III. This is the reason for the fast and steep temperature reduction in the core (Fig. 59b) and in the UP (Fig. 59c). This large amount of cold fluid in the UP exerts a downward buoyance force in the core. Therefore the core builts up higher buoyancy forces and therefore the temperature difference increases. The onset of the DHXs operation delivers additional masses of cold fluid leading to an additional temperature drop in the highest part of the UP well to

be seen in Fig. 59d in the height of the IHXs inlet windows. This high column of cold water above the core enters the core outlet locally, in general in all rings and provokes a thermosiphon effect well to be seen from Fig. 59b. About 900 s after scram a small temperature reduction of the core outlet temperature is registered. Within a few hundred maximum up to 1000 seconds this effect disappears and the continuous cooling of the UP start.

This thermosiphon effect is intensified when the DHXs heat transfer surface is increased. This was done by lowering the DHXs s. Fig. 60. In this case the distance between core upper edge and lower edge of DHXs was changed from 87.5 to 41 mm keeping the fluid level in the primary tank constant. The result is a faster cooling of the primary tank fluid and a more pronounced thermosiphoning (Fig. 60b) even registered at the core inlet side.

The ACS design was used in its permeable and impermeable versions. Its influence on the primary system thermohydraulics can be seen by comparing the results indicated in Fig. 59 (impermeable) and Fig. 61 (permeable). There is only one remarkable feature and that is the slight change of the temperature distribution in the UP. The impermeable ACS allows the hot core flow to pass through. Therefore, the UP temperatures increase slightly with increasing UP height. By contrast this temperature is constant for an impermeable ACS.

The delay in the start of the DHXs was investigated also with RAMONA-III for a delay time of 3000 s after scram and for $\tau_{IHX} = 15$ s and 240 s with impermeable and permeable ACSs. The results of these investigations are indicated in Figs. 62 and 63. As can be seen from Fig. 62 for a $\tau_{IHX} = 15$ s the mass flow rate indicates the onset of the DHX operations as a small depression in flow rate at 3000 s. The max. core temperatures increase slightly within the DHXs outage time by about 3 K. This is also the case for the UP temperatures. The cold fluid delivered during the 15 s operation of the IHXs first decreases the UP temperatures. Then they increase again by 2 K as no cooling of the primary system takes place. The IHXs are out of operation and the DHXs not yet operable. With the DHXs start the system temperatures however begin to decrease, reaching steady-state conditions about 20 h after scram. The influence of the ACS design is practically only to be seen in the vertical temperature distributions of the UP as demonstrated on the right hand side graph of Fig. 62d.

The longer delivery of cold fluid from the IHXs due to the prolonged operation of the IHXs secondary loops (τ_{IHX} = 240 s) results in a continuous reduction of the core flow (Fig. 63a). It leads to the ramp-type fluid temperature decrease in the core inlet and outlet (Fig. 63b) as well as in the UP (Figs. 63c and 63d). By contrast to the nominal DHX operation case no thermosiphon effect can be registered in the core outlet temperature measurements. The start of the DHXs operation results in a small flow reduction (Fig. 63a). During the outage time of the DHXs the cold fluid above the core delivered by the IHXs during the 240 s operation is mixed with the hotter fluid in the highest region of the UP as can be seen from the vertical temperature distributions in the UP (Figs. 63c and 63d). Additionally a warm up effect is registered of the UP temperature during the period up to 3000 s. With the onset of the DHX operation the temperatures of the UP are continuously reduced. The influence of the ACS design in this case is also of minor importance.

An asymmetrical decay heat removal was investigated by operating only 3 out of 6 DHXs. The results for τ_{IHX} = 15 s and 240 s are indicated in Fig. 64. As can be seen for τ_{IHX} = 15 s the core flow rate is not influenced by these operational conditions (compare Figs. 64a and 58a resp. 59a). The core and UP temperatures, however, increase slightly to reach steady-state values about 20 h after scram. At that time the system temperatures are 15 K higher in comparison to the symmetrical DHR operation. It is to be remarked that the core outlet temperatures show a thermosyphon effect about 900 s after scram that disappears again at the time point of 1800 s after scram.

11. SUMMARY AND CONCLUSIONS

Experimental investigations on natural convection for steady state situation as well as on the transition from forced to natural convection of the primary system of a fast reactor model have been carried out, using the three-dimensional RAMONA facilities scaled 1:20 with water as simulant fluid. The RAMONA model simulates reactor conditions in the Ri, Pe and Eu number ranges of interest.

The steady-state natural convection of the primary system is considerably influenced by the core power and its radial distribution, the geometry and axial position of the ACS, the availability and design of the DHXs as well as by the fluid level in the primary tank.

- The overall system temperature is increased with rising core power. The higher core power results in high core outlet temperatures together with high flow rates.

- The radial power distributions influence the temperature distributions over the core cross-section; at X = 0.59, major gradients in the outer core zone are registered.

- The permeable upper core structure influences the flow and temperature distributions in the upper plenum. The permeable upper core structure produces lower gradients in the region between core outlet and lower edge of the ACS and, thus, a changed temperature stratification compared to the impermeable ACS.

- Asymmetric heat removal (only half of the available DHXs in operation) results in a temperature increase in the system, but not in changes in the general temperature distribution.

- Bundle-type DHXs produce cold fluid that falls into the lowest part of the upper plenum and stratifies the temperature distribution of the plenum. This stratification leads to remarkable temperature differences with distinct temperature gradients. The hybrid-type DHXs mix cold and hot fluid very effectively. Therefore, no temperature stratification exist in the upper plenum and its coolability is very uniform.

- A reduced fluid level in the primary system due to leakage into the safety tank guarantees the coolability of the core even when the coolant cannot enter the inlet windows of IHXs and DHXs. In this case a perforated shroud of the DHXs or DHXs without shroud improves the coolability of the primary system.

- With the pressure drop and heat transfer relations of the reactor components being known, the experimental results of these steady-state studies can be simulated well by the FLUTAN code. These relations have been determined for the model components in separate studies.

According to the RAMONA results obtained under transient conditions, the start of natural convection is mainly influenced by two effects, namely, the temperature increase on the IHX primary sides as a result of which the descending forces are reduced, and the startup of the DHXs which leads to a decrease of the buoy-

ancy forces in the core. Hence, the thermal hydraulics of the primary system is influenced by the core power before and after scram and its radial distribution across the core, the primary pump coastdown, the IHX secondary-side flow reduction, the DHXs startup delay time, as well as by the availability and the design of the DHXs.

- The upper plenum is stratified by the cold fluid fed by the IHXs and DHXs after scram. This temperature stratification is maintained by bundle-type DHXs as they produce cold fluid that falls into the lowest part of the upper plenum.

- Increasing the power increases the system temperatures. Large radial power gradients give rise to large temperature gradients in the UP already before scram. The system temperatures are systematically reduced as soon as cooled mixed fluid of the hot plenum, resulting from the DHX operation, reaches the IHX inlet windows and causes an increase in the core flow rate.

- The primary pump coastdown curve influences the reactor thermohydraulics only during the first few hundred seconds after scram. With the pumps being stopped simultaneously, the core outlet temperatures are increased remarkably during the first 100 s. For the long-term temperature history, no remarkable influence of the pump coastdown curve on the hot plenum thermohydraulics was observed.

- The IHX secondary-side coastdown determines the in-vessel thermohydraulics during the total duration of an experiment. The faster the pumps are stopped, the higher are the core and plenum temperatures. In cases where natural circulation can be established in the secondary loops, the core temperatures are reduced significantly, and the hot plenum temperature differences are increased remarkably.

- The delayed start of the DHX operation influences the core mass flow only when bundle-type DHXs are used. This delay separates the two effects which influence the core mass flow, namely the heatup of the IHXs as well as the formation of the stratification. The lowest core flow rates are measured when both effects appear at the same time. Significant delays of the start of the DHXs lead to slight increases in the core outlet temperatures only.

- Asymmetric load conditions (only half of the available IHXs in operation) influence the transient temperature and mass flow courses only to a minor extent. These conditions, however, increase remarkably the final steady-state temperature level of the system.

- The reduction in size from the four-loop arrangement of RAMONA II to the three-loop model RAMONA III decreases the total mass of the fluid in the primary system. The transition from forced to natural circulation depends on this magnitude. All transient temperature courses are faster and reach steady-state conditions earlier as the heat capacities are lower.

- The FLUTAN code used for simulation of transient experiments has to meet high requirements due to the different circuits and the complex geometry of the primary system. By careful modelling of all heat exchanging components, all relevant flow paths are determined. The comparison of numerically determined findings and measurements generally leads to encouraging agreements. Development and validation of the computer code are advanced, but have not yet been completed. Determination of local and transient processes is very time-consuming and still remains to be improved.

The following conclusions can be drawn:

- It is obvious from the investigations performed in the test facilities that the decay heat can be removed from the primary system by means of natural convection. Always flow paths develop, which ensure an effective cooling of all regions.

- This statement can be transferred to the EFR, as thermohydraulically similar natural convection experiments have been carried out in the models.

- Decay heat removal even works under extreme conditions, e.g. in case of delays of the DHX startup, failures of several DHR chains, and a drop of the fluid level below the inlet windows of the IHXs and DHXs.

- Further optimization of the FLUTAN program is required in terms of calculation of turbulent flows and reduction of the required computation time.

12. NOMENCLATURE

a	thermal diffusivity $= \lambda/\rho c_p$
c	specific heat
Eu	Euler number
F	flow area
g	gravitational acceleration
L	length
m	mass flow
Pe	Peclet number
Δp	pressure drop
P	power
r	radius
Re	Reynolds number
Ri	Richardson number
t	temperature
Δt	temperature difference
u	velocity
z	height
β	expansion coefficient
v	viscosity
ζ	loss coefficient
ρ	density
ϕ	angular position
τ	time
$\Delta\tau$	time difference
χ	normalized power distribution

Abbreviations and Subscripts

ACS	Above core structure
AHX	Sodium/air heat exchanger
AVG	Average
DHR	Decay heat removal
DHX	Decay heat exchanger
DRC	Direct reactor cooling
EFR	European fast reactor
HPP	High pressure plenum
IHX	Intermediate heat exchanger
IP	Intermediate plenum
LDA	Laser Doppler anemometer
LOSSP	Loss-of-station service power
LP	Lower or cold plenum
M	Model
Max	Maximum
Min	Minimum
R	Reactor
SNR	Sodium cooled fast reactor
t	total
TC	Thermocouple
UP	Upper or hot plenum
2D	Two-dimensional
3D	Three-dimensional

13. REFERENCES

[1] Düweke, M., Friedrich, H.J., Hofmann, F., Valentin, B., and Webster, R.: The Direct Reactor Cooling System of EFR, Overview and R&D Activities, 1990 Internat. Fast Reactor Safety Meeting, Snowbird, UT, U.S.A., August 1990, Vol. II, pp. 309-318.

[2] Gyr, W., Friederl, G., Friedrich, H.J., Pamme, H., Firth, G., and Lauret, P.: EFR Decay Heat Removal System, Design and Safety Studies, 1990 Intewrnat. Fast Reactor Safety Meeting, Snowbird, UT, U.S.A., August 1990, Vol. III, pp. 543-552.

[3] Essig, C., Düweke, M., Ruland, V., Ertel, V., and Kiera, M.: "Consistent thermal hydraulic approach of EFR decay heat removal by natural convection", Proc. of the 5th Internat. Topical Meeting on Nuclear Reactor Thermal Hydraulics (NURETH-5), Salt Lake City, UT, U.S.A., 1992, Vol. I, pp. 135-142.

[4] Hoffmann, H., Sardain, P., and Webster, R.: "The European R+D program on natural convection decay heat removal for the EFR", Proc. of the Internat. Conf. on Fast Reactors and Related Fuel Cycles, FR'91, Kyoto, Japan, 1991, Vol. II, pp. 13.5/1-5/9.

[5] Weinberg, D., Hoffmann, H., Hain, H., Hofmann, F., Dueweke, M., Experimental and theoretical program to study the natural convection decay heat removal system of the SNR-2. Science and Technology of Fast Reactor Safety: Proc. of an Internat. Conf. St. Peter Port, Guernsey, GB, May 12-16, 1986, Vol. 1, pp. 289-294.

[6] Weinberg, D., Suckow, D., Müller, U., and Hoffmann, H.: unpublished internal report, August 1990.

[7] Borgwaldt, H., Baumann, W., and Willerding, G.: FLUTAN Input Specification, KfK 5010, Kernforschungszentrum Karlsruhe, May 1992.

[8] Borgwaldt, H.: CRESOR, - A Robust Vectorized Poisson Solver Implemented in the Thermal-hydraulic Code COMMIX-2(V) -, First Internat. Conference on Supercomputing in Nuclear Applications, Mito City, Japan, March 1990, pp. 346-351.

[9] Marten, K.: unpublished internal report, August 1986.

[10] Tschöke, H.: unpublished internal report, October 1986.

[11] Fath, M. und Tschöke, H.: unpublished internal report, September 1991.

[12] Hoffmann, H., Weinberg, D., Baumann, W., Hain, K., Leiling, W., Marten, K., Ohira, H., Schnetgöke, G., Thomauske, K.: Scaled model studies of decay heat removal by natural convection for the European Fast Reactor. Courtaud, M. (ed.), Proc. of the 6th Intern. Topical Meeting on Nuclear Reactor Thermal Hydraulics (NURETH-6), Grenoble, France, October 5 - 8, 1993, Vol. 1, pp. 54 - 62.

[13] Marten, K., Hoffmann, H., Tschöke, H.: 3D-Untersuchungen zur SNR-2 Nachwärmeabfuhr unter Naturkonvektion im 1:20-Modell RAMONA. Jahrestagung Kerntechnik '87. Karlsruhe, 2. - 4. Juni 1984, pp. 157 - 160, Karlsruhe.

[14] Weinberg, D., Hoffmann, H., Ieda, Y., Marten, K., Tschöke, H. Frey, H.H., Dres, K.: Experimental and theoretical program to study the natural convection decay heat removal system of the SNR-2. Experimental results of the 1:20-scaled model RAMONA and verification calculations with COMMIX-1B, 6th Intern. Specialists' Meeting on Liquid Metal Thermal Hydraulics, O'arai, Japan, August 1 - 3, 1988.

[15] Hoffmann, H., Marten, K., Weinberg, D., Ieda, Y., Frey, H.H.: Investigations of inherent decay heat removal performances in LMFBRs, Proc. of the Intern. Meeting on the Safety of Next Generation Power Reactors, Seatle, WA, May 1 - 5, 1988, pp. 830 - 837.

[16] Hoffmann, H., Ieda, Y., Weinberg, D., Marten, K., Frey, H.H., Tschöke, H., Dres, K.: Investigations on decay heat removal by natural circulation in LMFBRs, Proc. of the 4th Intern. Topical Meeting on Nuclear Reactor Thermal Hydraulics (NURETH-4), Karlsruhe, Germany, 1989, Vol. 1, pp. 384 - 391.

[17] Hoffmann, H., Marten, K., Weinberg, D., Ieda, Y.: Investigations on natural circulation in reactor models and shut down heat removal systems for LMFBRs, 5th Proc. of Nuclear Thermal Hydraulics: 1989 Winter Meeting of

the American Nuclear Society, San Francisco, CA, November 26 - 30, 1989, pp. 446 - 454.

[18] Weinberg, D., Marten, K., Ieda, Y., Hoffmann, H., Frey, H.H.: Investigations into LMFBR decay heat removal by natural convection under nominal and non-nominal conditions, Winter Annual Meeting of the American Society of Mechanical Engineers, Chicago, IL, November 28 - December 2, 1988, HTD-Vol. 104, Collected Papers in Heat Transfer, pp. 193 - 200.

[19] Marten, K., Ieda, Y., Hoffmann, H., Schnetgöke, U.: Modelluntersuchungen zur SNR-2 Nachwärmeabfuhr unter Naturkonvektion. Einfluß der Kernleistung und deren Verteilung auf die Thermohydraulik im Oberplenum. Jahrestagung Kerntechnik '88, Travemünde, May 17 - 19, 1988, pp. 125 - 128, Travemünde.

[20] Hoffmann, H., Marten, K., Weinberg, D., Kamide, H.: Thermohydraulic model experiments on the transition from forced to natural circulation for pool-type fast reactors, Nuclear Technology, 99, 1992, pp. 374 - 385.

[21] Hoffmann, H., Marten, K., Weinberg, D., Kamide, H.: Investigations of an inherent decay heat removal system for LMFBRs, European Nuclear Conf. (ENC '90), Lyon, France, Sept. 23 - 28, 1990, Vol. II, pp. 789 - 793.

[22] Hoffmann, H., Marten, K., Schnetgöke, U., Bickert, R.: Naturkonvektionsversuche mit verschieden gestalteten Tauchkühlern und ihr Einfluß auf die Wandtemperaturverteilung im Oberplenum des SNR-2/EFR. Jahrestagung Kerntechnik '89. Düsseldorf, May 9 - 11, 1989, pp. 121 - 124.

[23] Hoffmann, H.: Modelluntersuchungen zum Naturumlauf im Primärsystem des EFR, Jahrestagung Kerntechnik '91, Bonn, May 14 - 16, 1991, Fachsitzung "Naturumlaufprobleme zur passiven Nachwärmeabfuhr bei fortschrittlichen Reaktoren", pp. 18 - 46.

[24] Hoffmann, H., Rust, K., Weinberg, D.: Studies on EFR safety-graded decay heat removal concept - Results of model experiments and code simulations, Intern. Topical Meeting on Sodium-cooled Fast Reactor Safety, Obninsk, GUS, Oct. 3 - 7, 1994, Obninsk, Vol. 4, pp. 6/86-6/98.

[25] Hoffmann, H., Wilhelm, D., Weinberg, D.: Untersuchungen zur passiven Nachwärmeabfuhr für schnelle Reaktoren, KfK-5326 (May 1994), pp. 33 - 73.

[26] Ertel, V., Reinders, R.: Development and Application of the Thermohydraulic System Code DYANA/ATICA", Proc. Science and Technology of Fast Reactor Safety, BNES, London, UK, May 1986, Vol. 2, pp. 191.

[27] Weinberg, D., Suckow, D., Müller, U., Hoffmann, H.: The transferability to reactor conditions of thermo-hydraulics model investigations of decay heat removal. Proc. of the 1990 Intern. Fast Reactor Safety Meeting, Snowbird, UT, August 12 - 16, 1990, Vol. II, pp. 341 - 350.

[28] Marten, K., Kamide, H., Hoffmann, H., Weinberg, D.: Thermohydraulische Modelluntersuchungen zum Übergang von Zwangs- auf Naturkonvektion in der Nachscramphase eines Schnellen Reaktors. Jahrestagung Kerntechnik '90, Nürnberg, May 15 - 17, 1990, pp. 77 - 80.

[29] Hoffmann, H., Marten, K., Kamide, H., Weinberg, D.: Thermohydraulic model studies of the transition from forced to natural convection in the post-scram phase of a fast reactor. Proc. of the 1990 Intern. Fast Reactor Safety Meeting, Snowbird, UT, August 12 - 16, 1990, Vol. III, pp. 523 - 531.

[30] Hoffmann, H., Marten, K., Weinberg, D., Kamide, H.: Thermohydraulic model experiments and calculations on the transition from forced to natural circulation for pool-type fast reactors. 6th Proc. of Nuclear Thermal Hydraulics: Winter Meeting of the American Nuclear Society, Washington D.C., November 11 - 16, 1990, pp. 143 - 151.

[31] Hoffmann, H., Hain, K., Marten, K., Ohira, H., Rust, K., Weinberg, D.: The status of thermal-hydraulic studies on the decay heat removal by natural convection using RAMONA and NEPTUN models. Proc. of the 4th Intern. Topical Meeting on Nuclear Thermal Hydraulics, Operations and Safety, Taipei, RC, April 3 - 6, 1994, Vol. 1, pp. 22-A/1-A/8, Taipei.

[32] Hoffmann, H., Marten, K., Weinberg, D., Kamide, H.: Thermohydraulic model experiments on the transition from forced to natural circulation for pool-type fast reactors. Nuclear Technology, 99 (1992), pp. 374 - 385.

[33] Kamide, H., Hoffmann, H., Weinberg, D.: Investigations of natural circulation in pool-type reactors with 1:20 scale model RAMONA. Proc. of the Annual Meeting of the Atomic Energy Society of Japan, Higashiosake, J, March 28 - 30, 1991, pp. 158.

[34] Hoffmann, H., Marten, K., Ohshima, H., Weinberg, D.: Investigations on natural convection with the 3 D-model RAMONA. Influence of the configuration of the immersion coolers on the upper plenum thermohydraulics and core mass flows. 7 th Proc. of Nuclear Thermal Hydraulics: 1991 Winter Meeting of the American Nuclear Society, San Francisco, CA, November 10 - 14, 1991, pp. 212 - 220.

[35] Hoffmann, H., Hain, K., Hayafune, H., Marten, K., Rust, K., Weinberg, D.: 1994, Experimental studies on passive decay heat removal by natural convection under nominal and non-nominal operation conditions", '94 ASME Winter Annual Meeting, Chicago, IL, U.S.A.

[36] Marten, K., Ohshima, H., Hoffmann, H.: Transiente Modelluntersuchungen zum Einfluß unterschiedlicher Tauchkühler auf die Thermohydraulik im Oberplenum des EFR. Jahrestagung Kerntechnik '92. Karlsruhe, May 5 - 7, 1992, pp. 65 - 68.

[37] Oshima, H., Hoffmann, H., Weinberg, D.: Investigations on natural circulation in fast reactors - Influence of the configuration of the immersion coolers on the upper plenum thermohydraulics, 1992, Meeting of the Atomic Energy Society of Japan, Nagoya, J, October 20, 1992, Nagoya.

[38] Schmidt, P., Böttger, F., Marten, K., and Hoffmann, H.: unpublished internal report, January 1991.

[39] Weinberg, D., Hoffmann, H., Ohira, H. Schnetgöke, G.: The status of studies using RAMONA and NEPTUN models on decay heat removal by natural convection for the European fast reactor. IAEA-IWGFR Specialists' Meeting on Evaluation of Decay Heat Removal by Natural Convection in Fast Reactors, O 'arai, J, February 22 - 25, 1993, pp. 51 - 57.

[40] Hoffmann, H., Kamide, H., Marten, K., Ohshima, H., Weinberg, D.: Investigations on the transition from forced to natural convection for the pool type European fast reactor in the 3-D RAMONA model. Intern. Conf. on Fast Reactors and Related Fuel Cycles (FR '91), Kyoto, J, Oct. 28 - Nov. 1, 1991, Proc. Vol. III, pp. 3.14/1-14/10.

[41] Weinberg, D., Frey, H.H.: Vergleich von transienten 3D-Rechnungen mit RAMONA Modell-Experimenten, Jahrestagung Kerntechnik '92, Karlsruhe, May 5 - 7, 1992, pp. 85 - 88.

[42] Weinberg, D., Frey, H.H., Tschöke, H.: A three-dimensional transient calculation for the reactor model RAMONA using the COMIX-2 (V) code. Küsters, H. (ed.), Proc. of the Joint Intern. Conf. on Mathematical Methods and Supercomputing in Nuclear Applications (M u. C + SNA '93), Karlsruhe April 19 - 23, 1993, Vol. 1, pp. 292 - 303.

[43] Weinberg, D., Hoffmann, H., Rust, K: Experimental investigations and numerical simulations of three-dimensional temperature and velocity fields in the transition region from laminar forced to natural convection, 10th Intern. Heat Transfer Conf., Brighton, GB, Aug. 14 - 18, 1994, Vol. 5, pp. 585 - 590.

[44] Hoffmann, H., Weinberg, D.: Investigations on natural convection decay heat removal for the EFR using various model geometries, Proc. of the Internat. Conf. on Design and Safety of Advanced Nuclear Power Plants, Tokyo, Japan, Oct. 25 - 29, 1992, Vol. III, pp. 26.2/1-2/7.

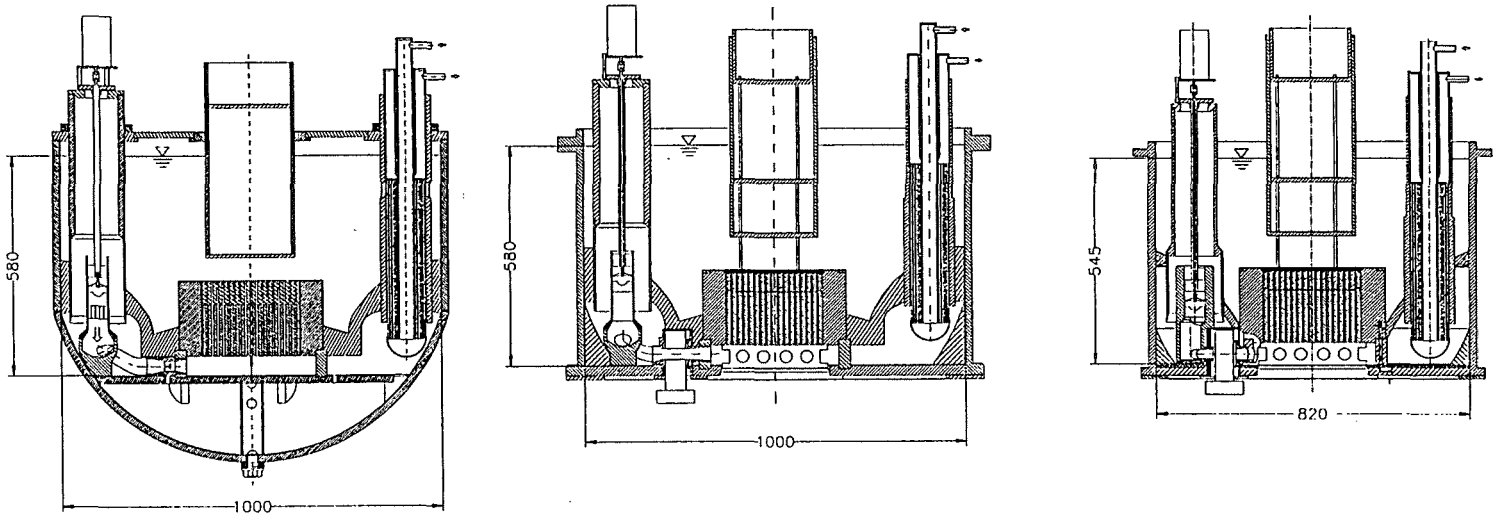

	RAMONA-I	RAMONA-II	RAMONA-III
Reactor simulated	SNR-2; SPX	SNR-2-SPX	EFR
Secondary heat transport systems	4	4	3
Number of primary system components	4 PPs; 8 IHXs; 4 DHXs	4 PPs; 8 IHXs; 4 DHXs	3 PPs; 6 IHXs; 6 DHXs
Dimensions in mm ($\varnothing$ x z_{water})	1000 x 580	1000 x 580	820 x 545
Max. core power, kW	30	75	75
Power supply	above	below	below
Flow meters	8 turbine type FM	8 magnetoinductive FM	6 magnetoinductive FM

Table 1: Main characteristics of the different RAMONA test facilities

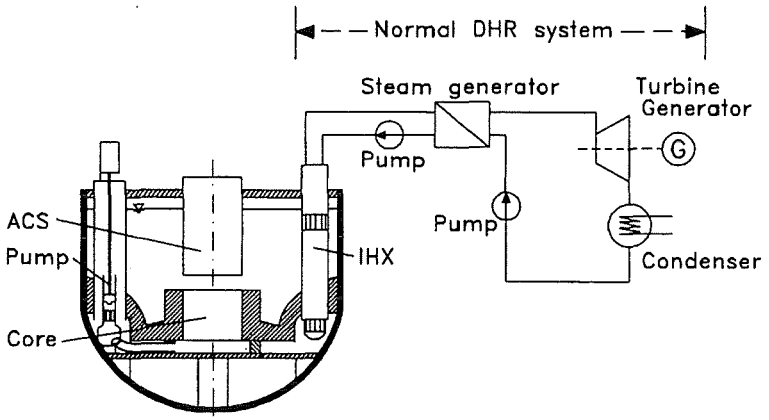

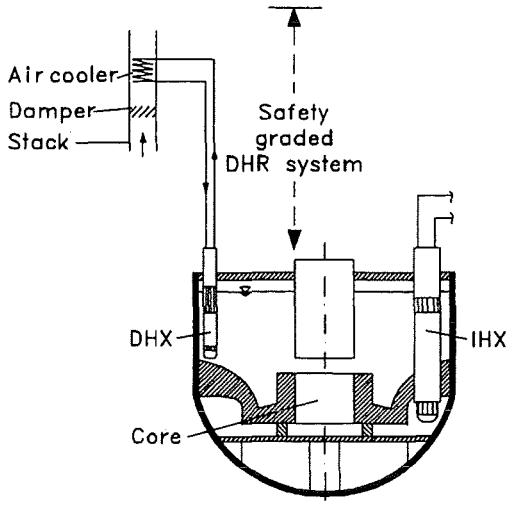

Fig. 1 Normal and safety-graded decay heat removal systems

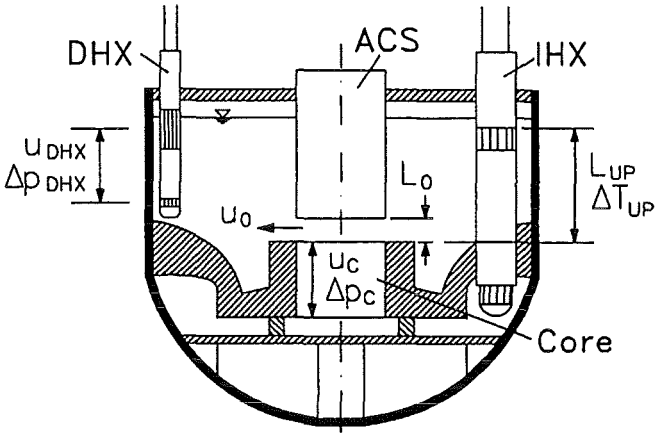

$$Ri = g \cdot \beta \, \Delta T_{UP} \cdot L_{UP} / U_o^2$$

$$Re = U_o \cdot L_o / \nu$$

$$Pe = U_o \cdot L_o / a$$

$$Eu^+ = \Delta p_{DHX} \, U_c^2 / \Delta p_c \, U_{DHX}^2$$

Fig. 2 Definition of the characteristic numbers

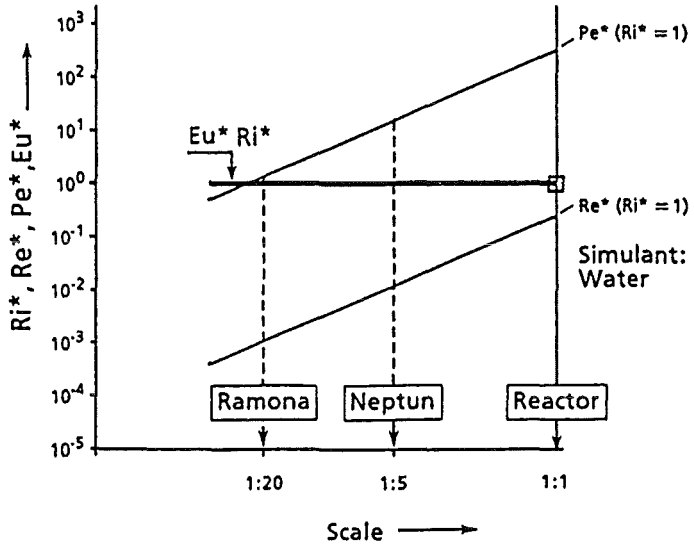

Fig. 3 Characteristic numbers as a function of the model scale

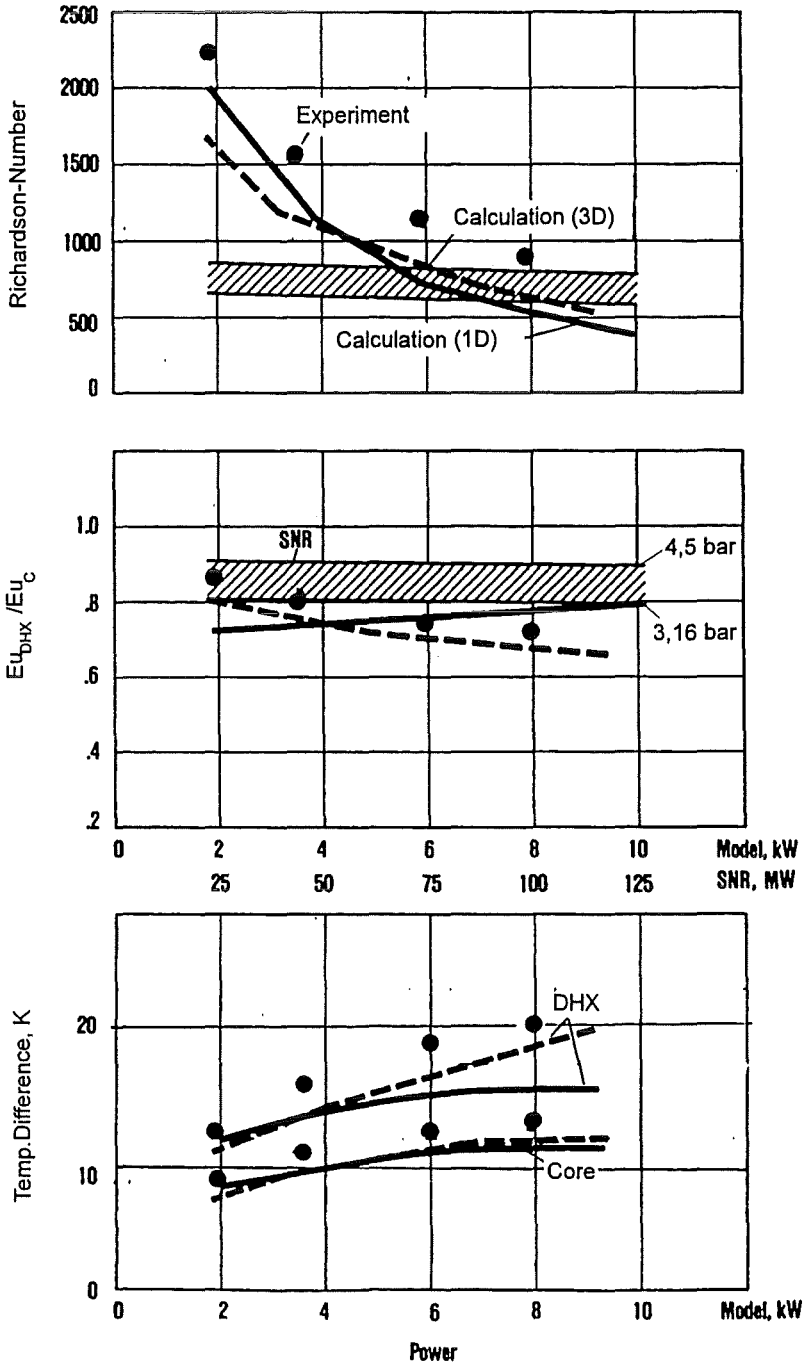

Fig. 4 Comparison of computed and measured model and reactor characteristics

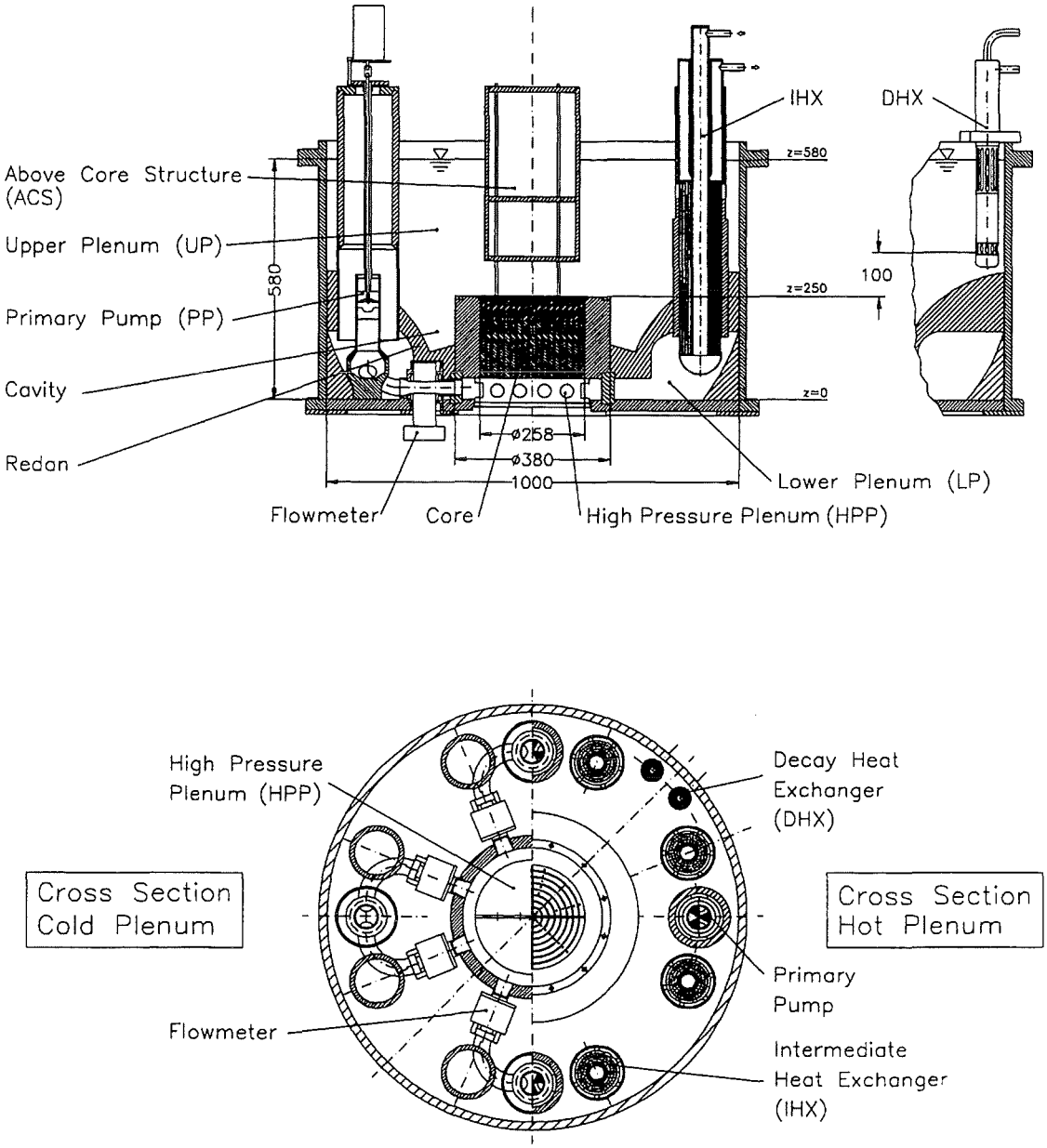

Fig. 5 Vertical and horizontal cross-sections of the RAMONA test facility (dimensions in millimeters)

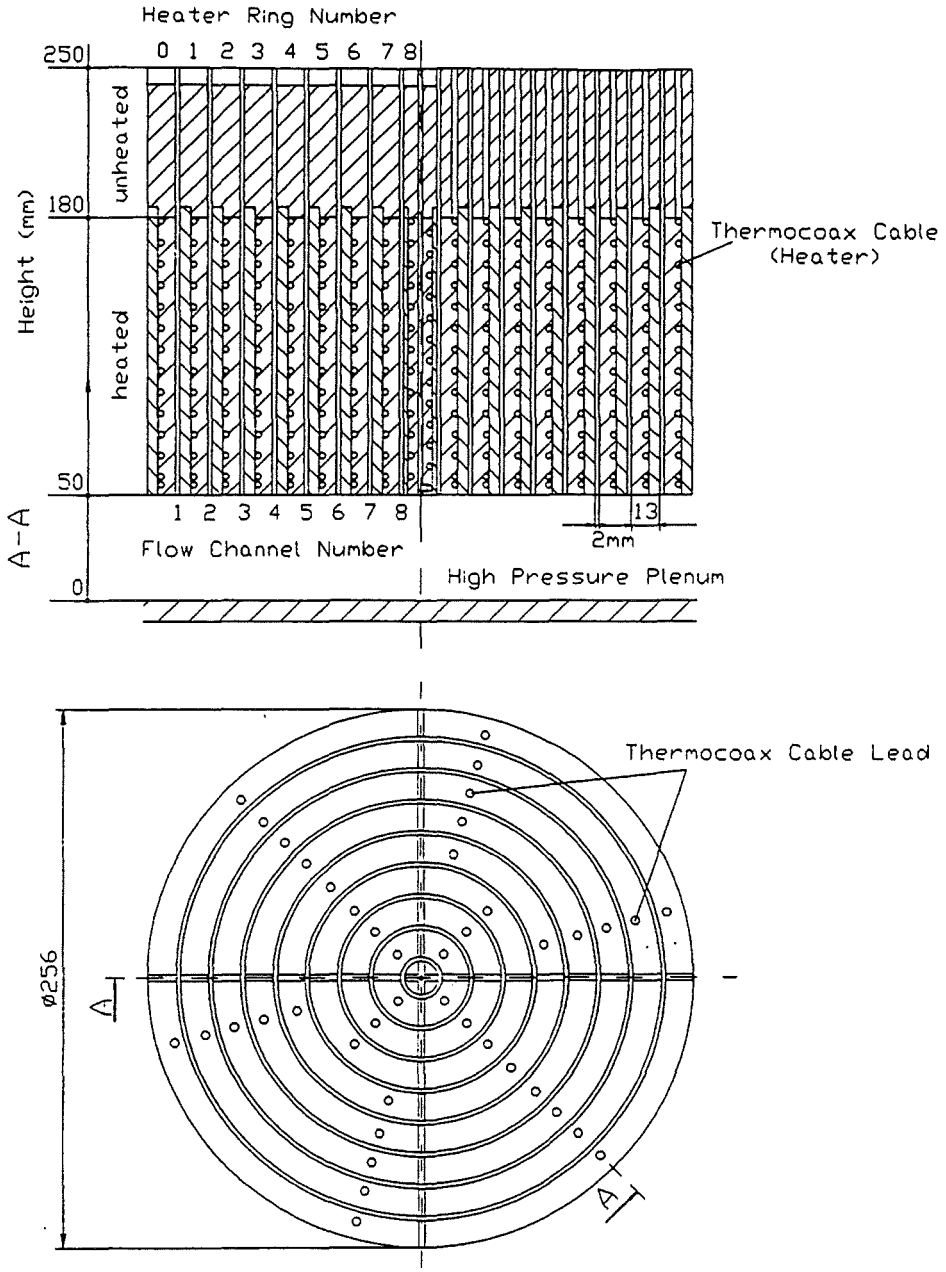

Fig. 6 Vertical and horizontal cross sections of the RAMONA core

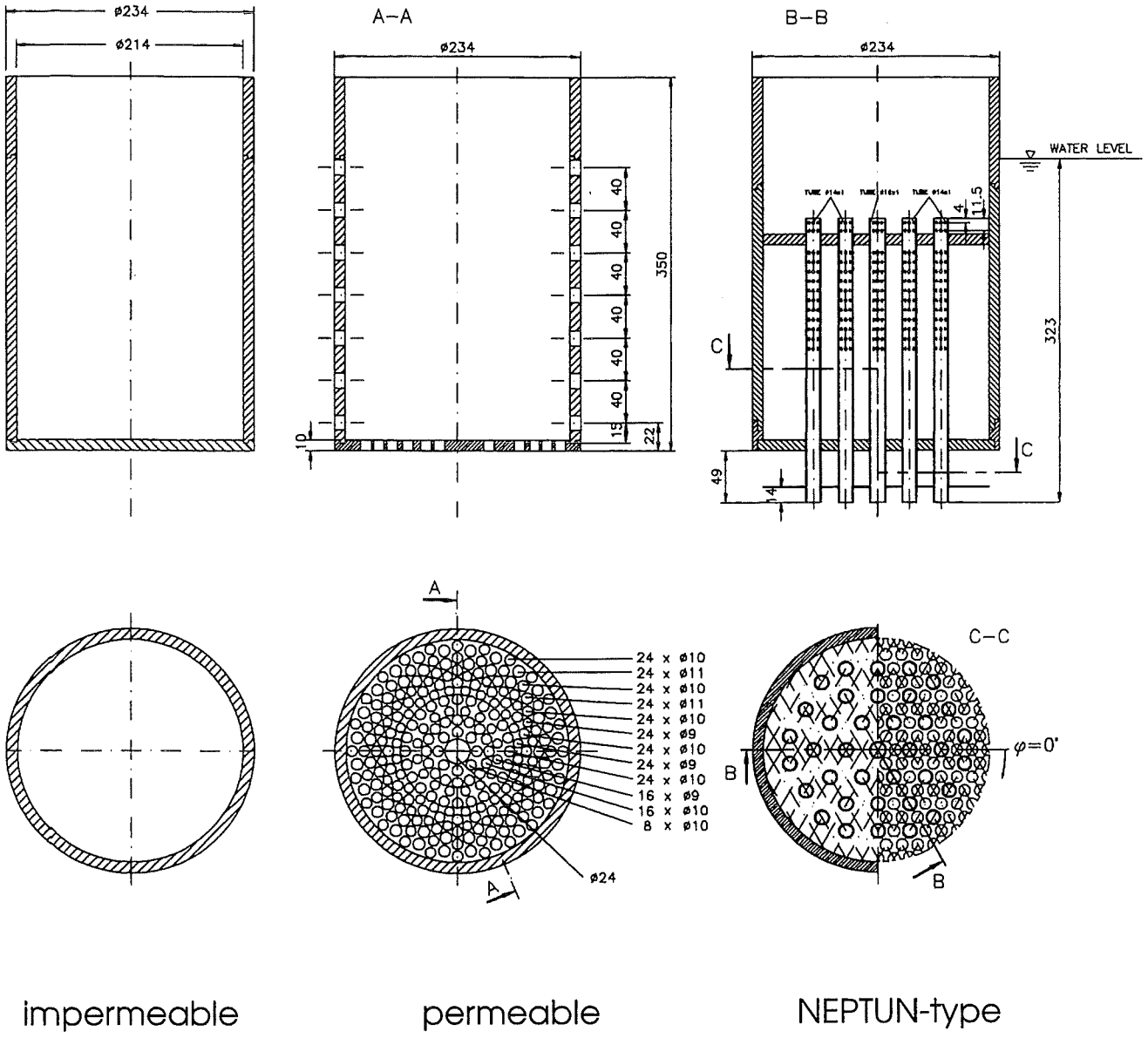

Fig. 7 Different designs of the above-core structure (dimensions in millimeters)

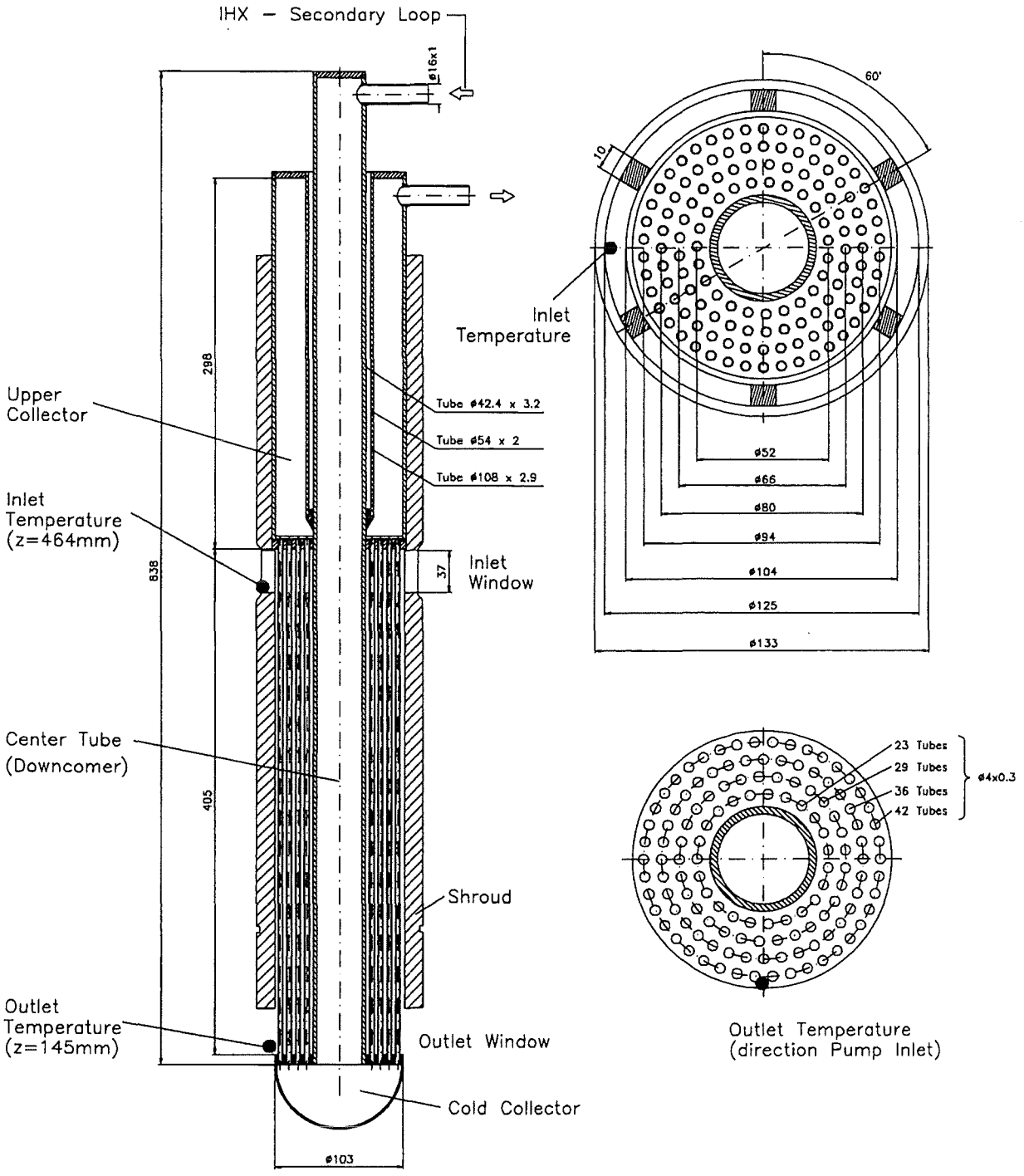

Fig. 8 Cross-sections of the intermediate heat exchanger (dimensions in millimeters)

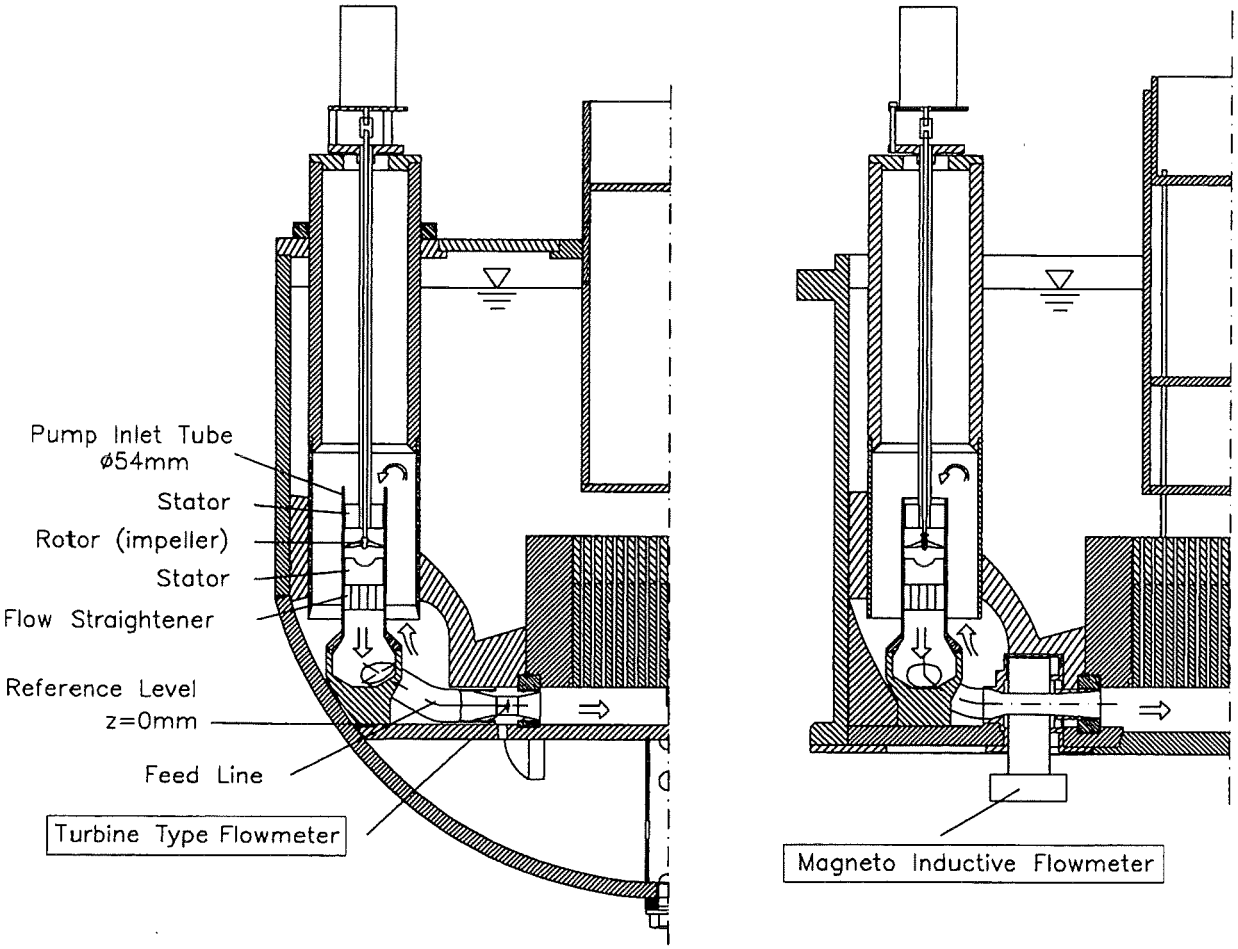

RAMONA I

RAMONA II
RAMONA III

Fig. 9 Installation of the primary pumps (dimensions in millimeters)

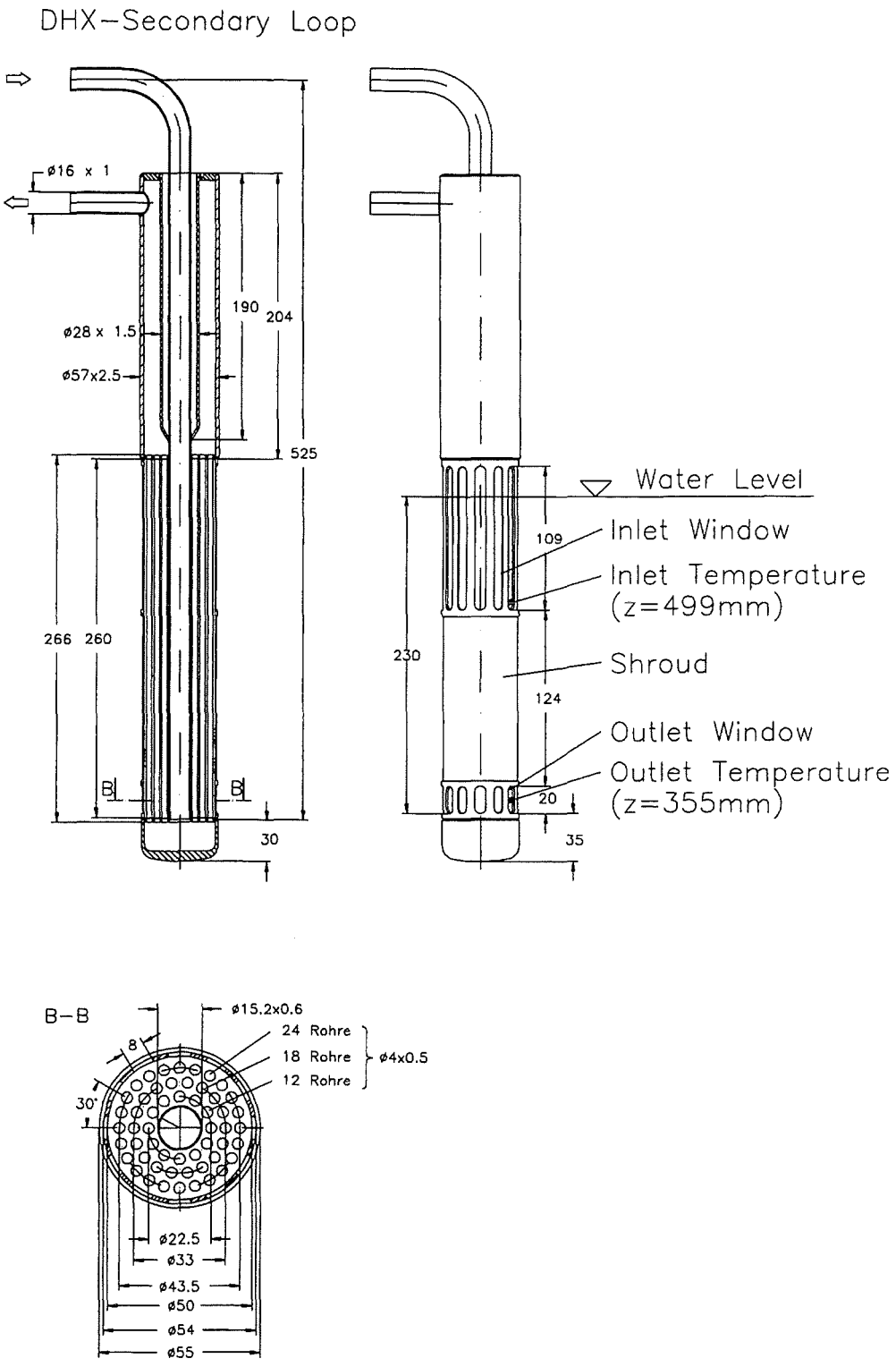

Fig. 10 Cross-sections of the decay heat exchanger (dimensions in millimeters)

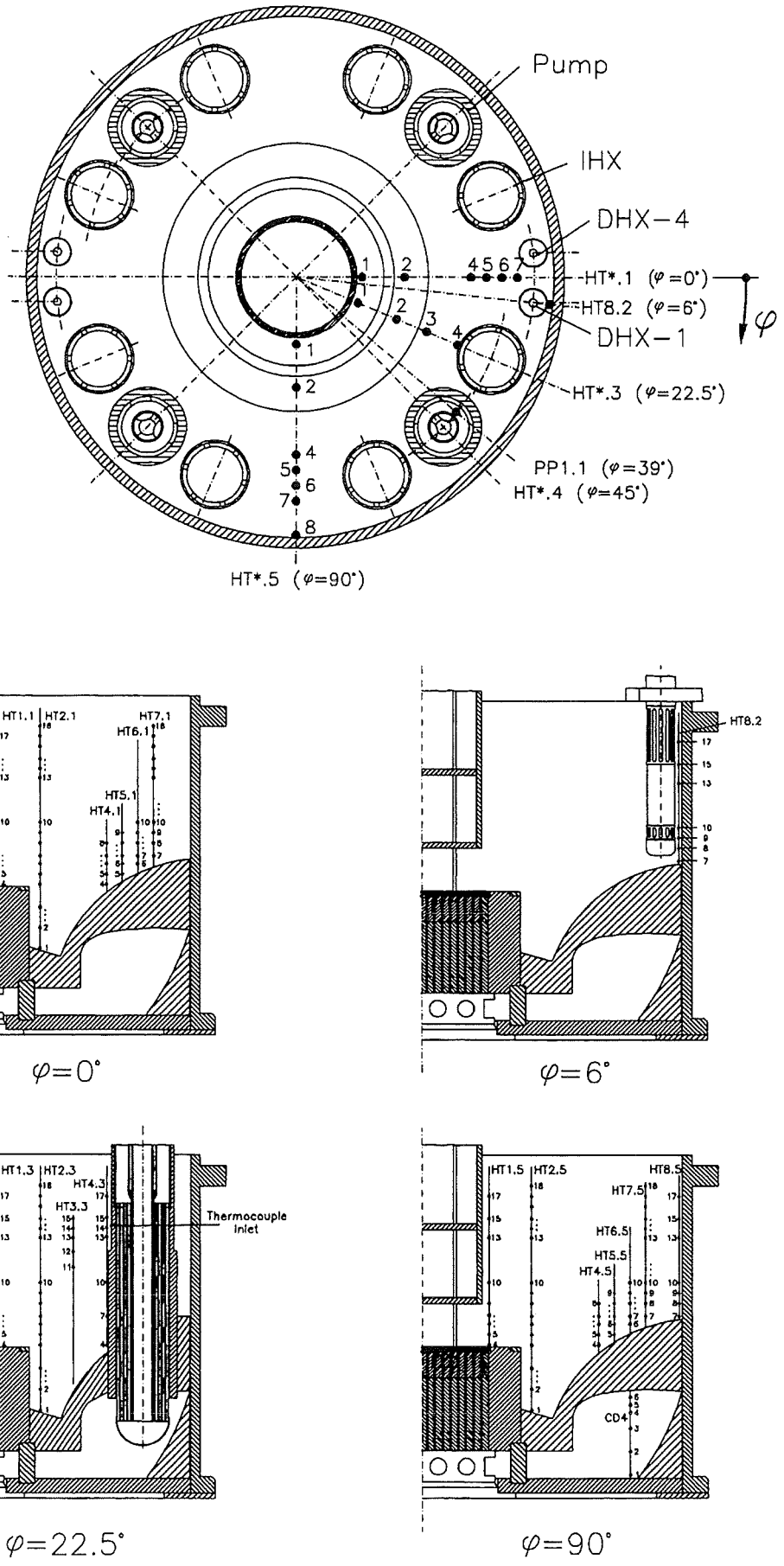

Fig. 11 Instrumentation of the upper plenum

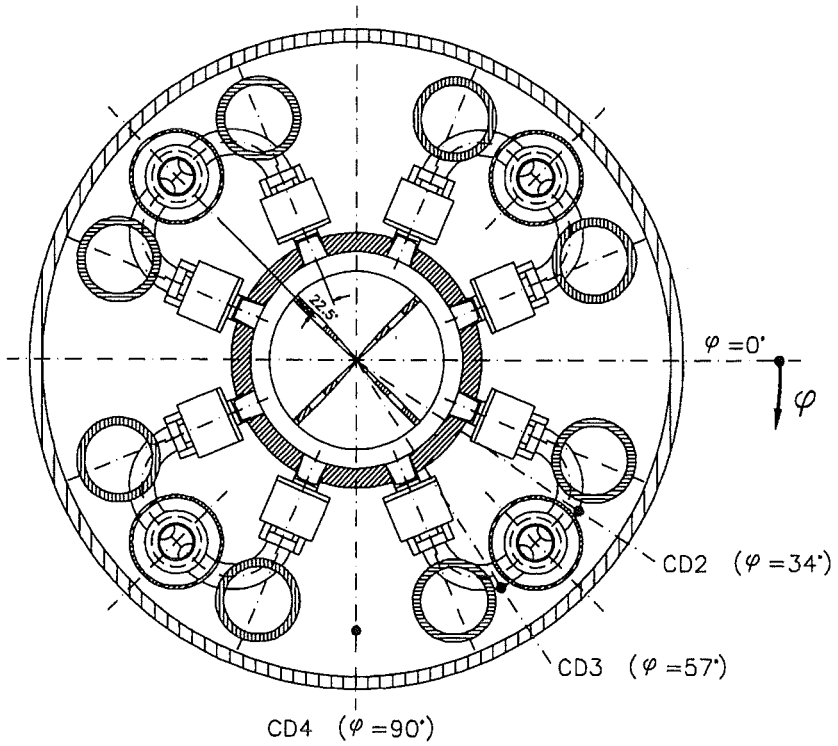

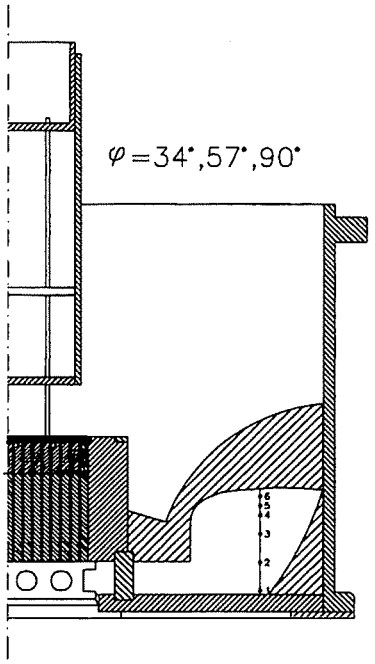

Fig. 12 Instrumentation of the lower plenum

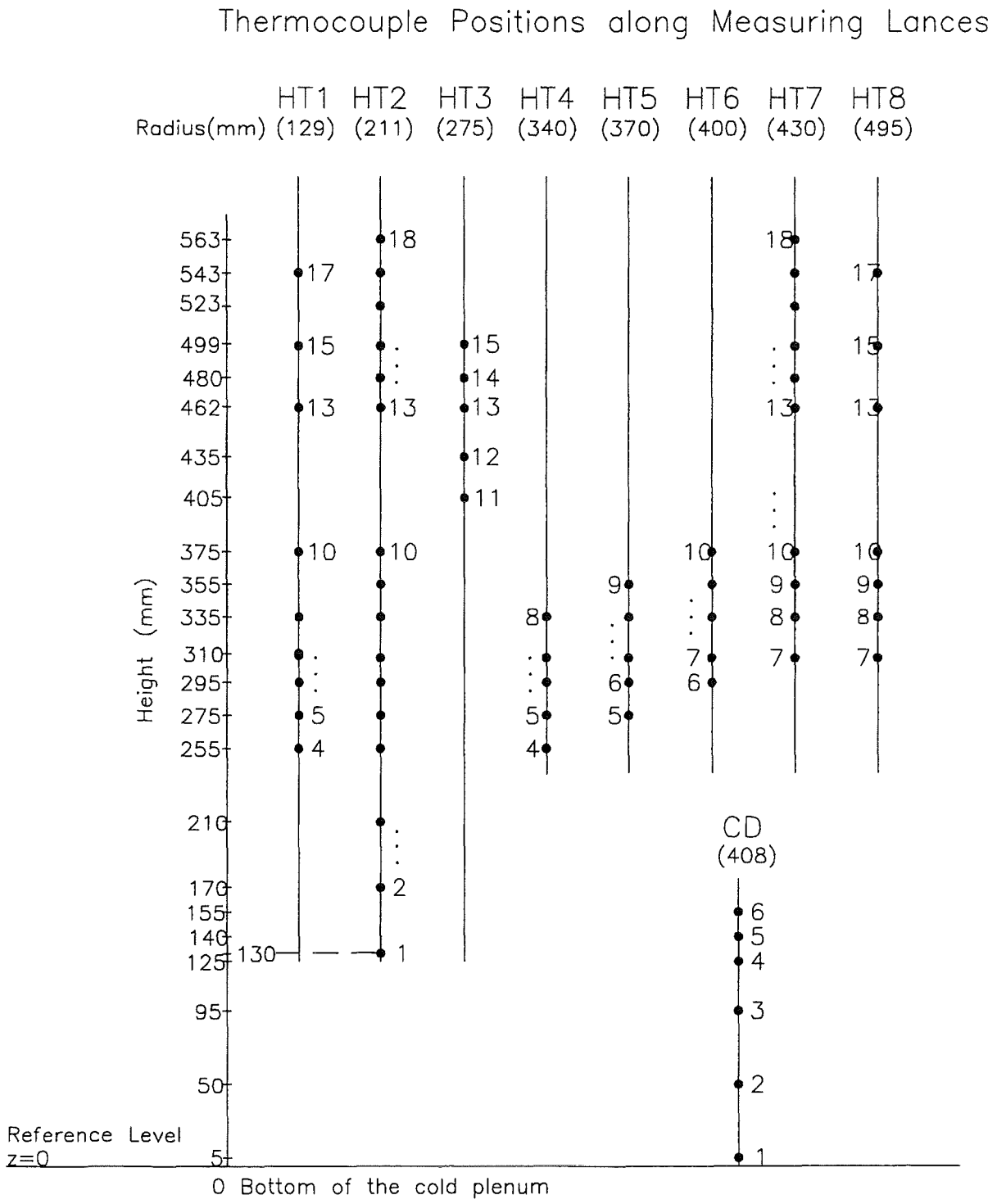

Fig. 13 **Thermocouple positions along the measuring lances**

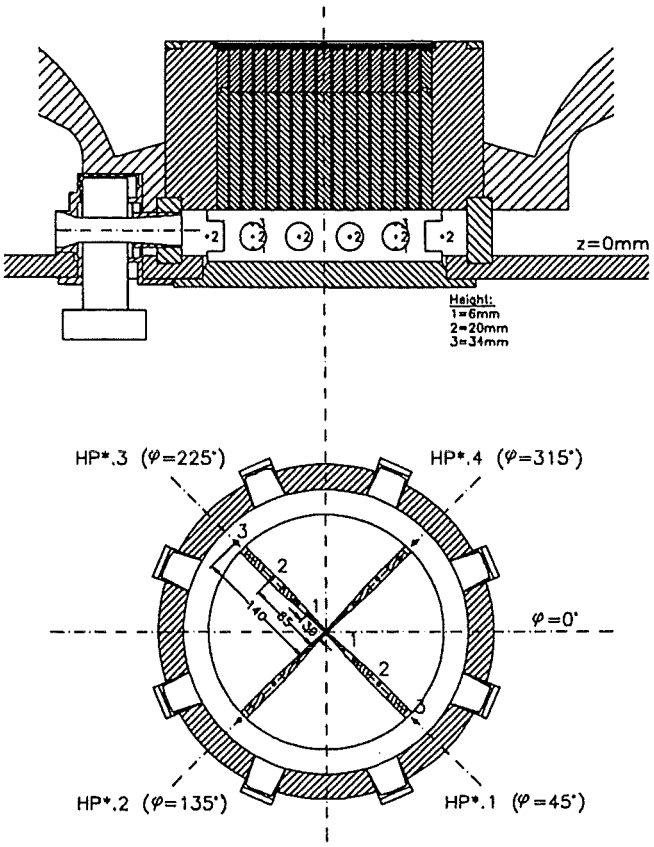

Fig. 14 Instrumentation of the high-pressure plenum

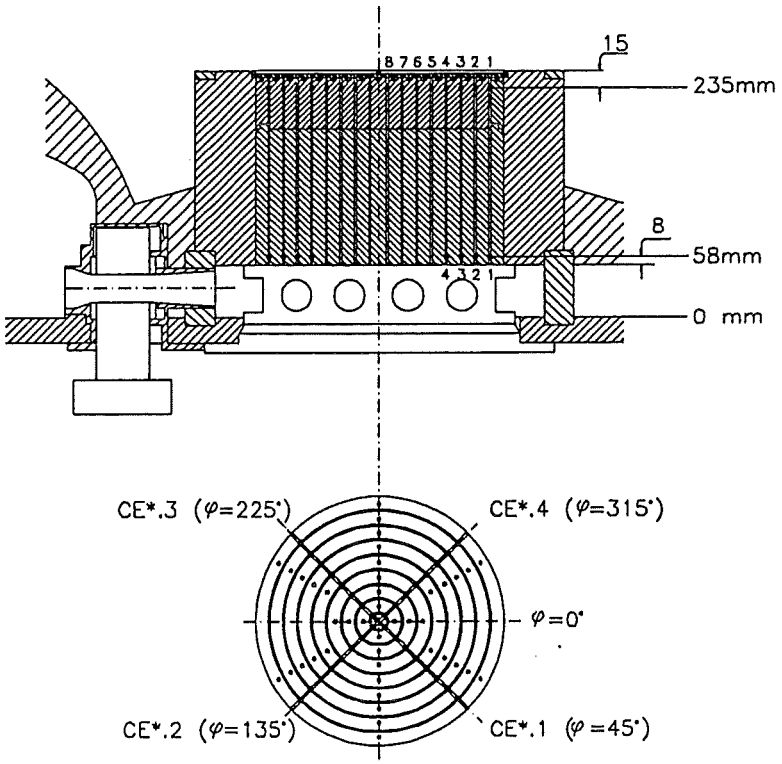

Fig. 15 Instrumentation of the core

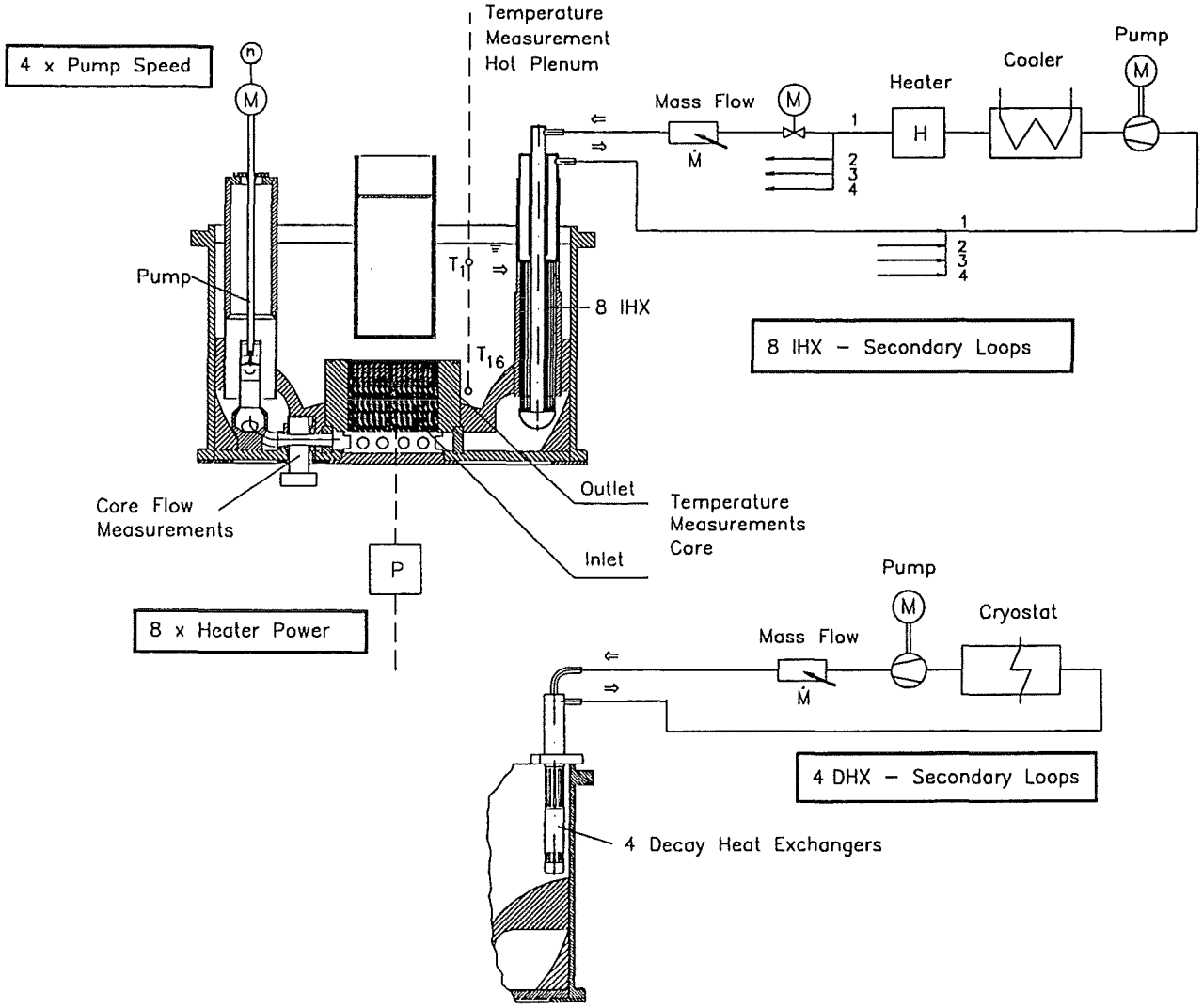

Fig. 16 Secondary heat transport circuits and instrumentation of the test facility

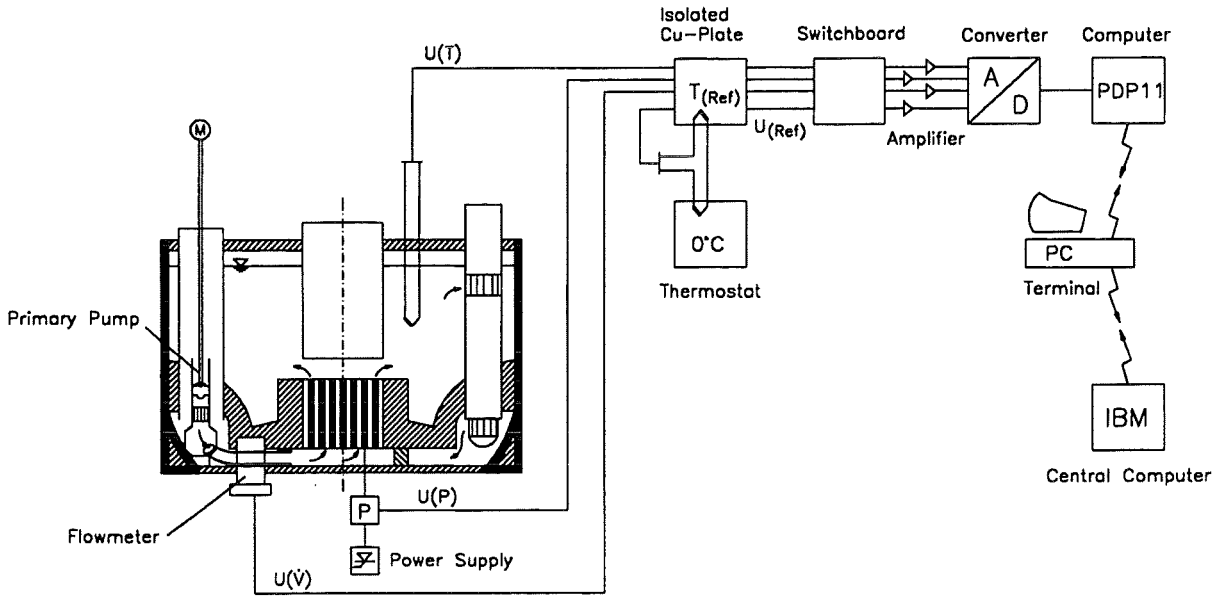

Fig. 17 Data acquisition system

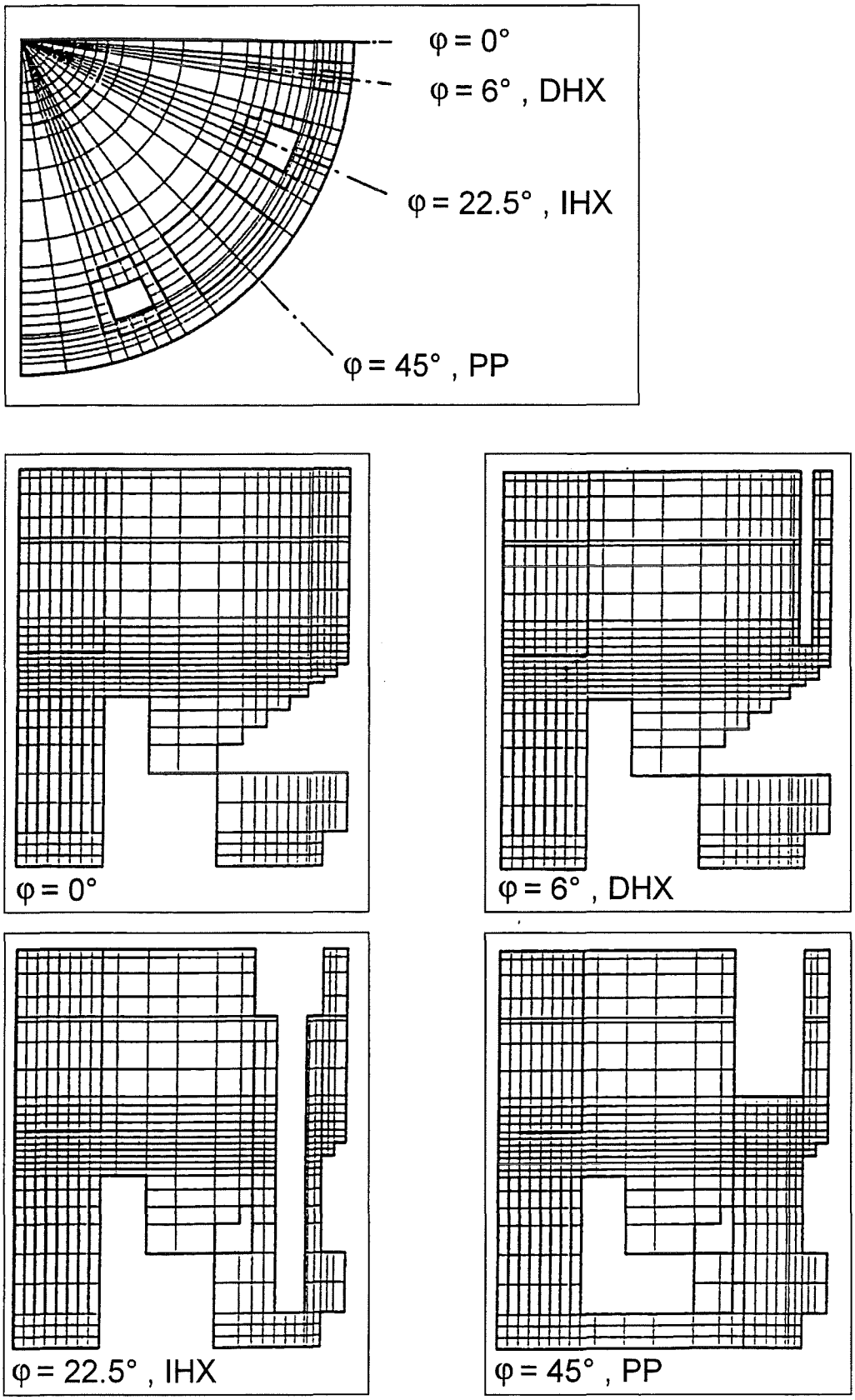

Fig. 18 Nodalization of the RAMONA geometry

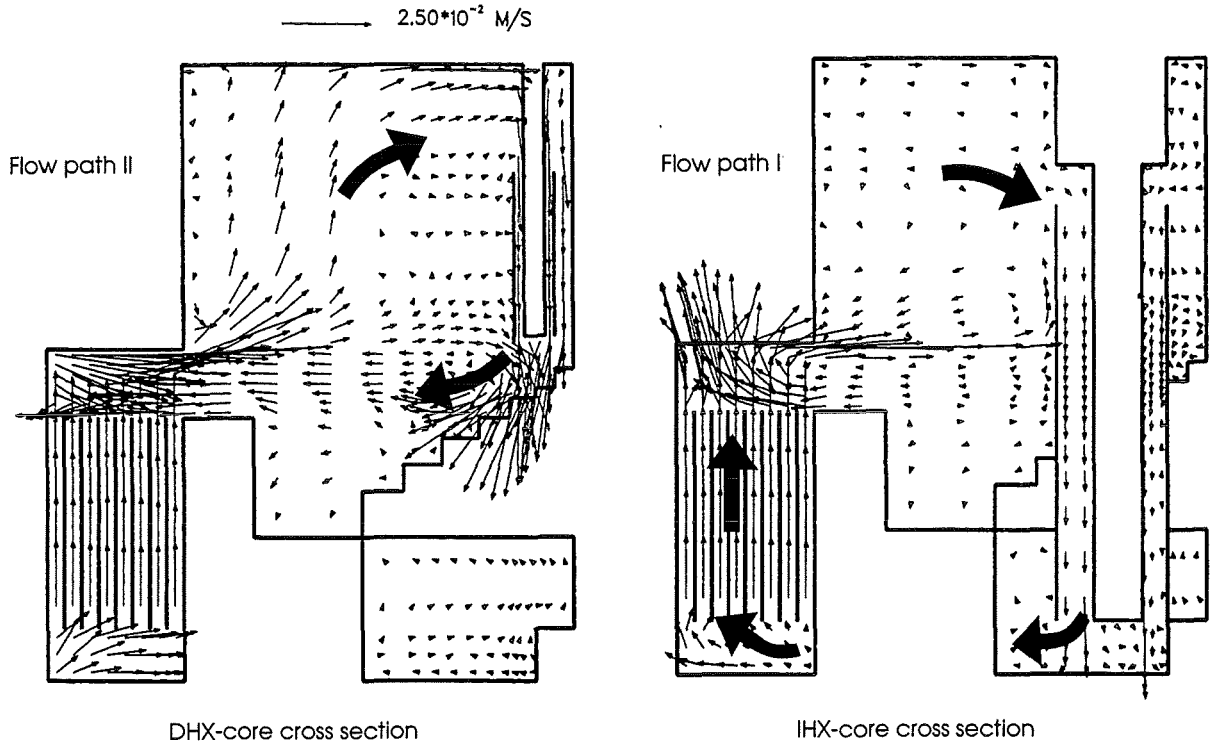

a) velocity fields and flow paths

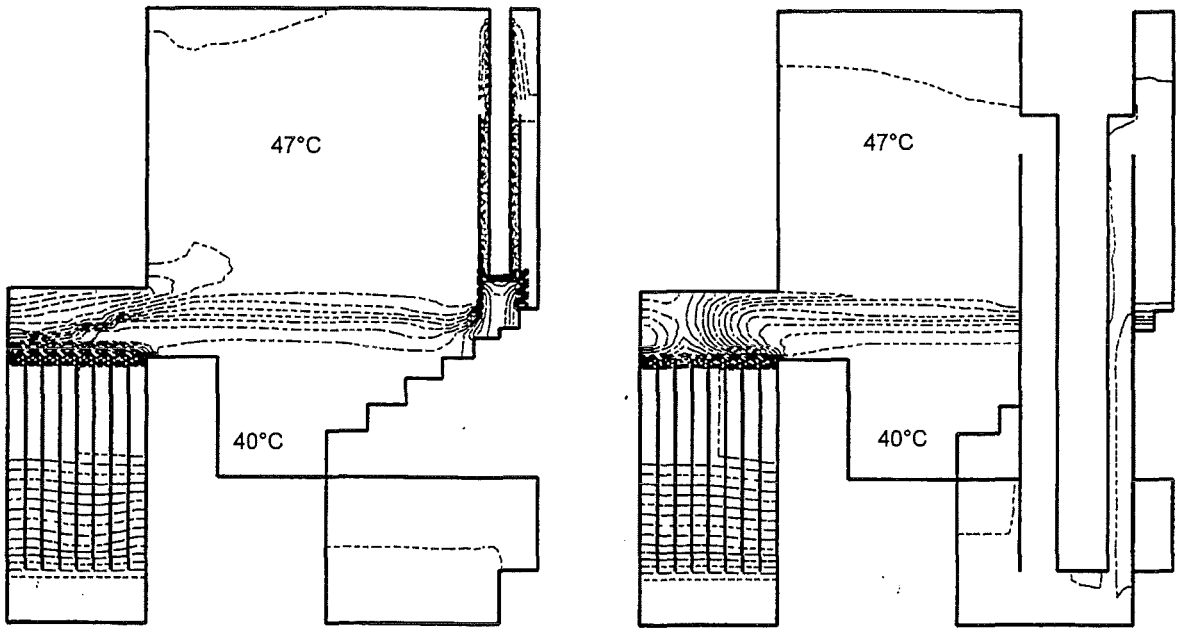

b) temperature fields

Fig. 19 Computed typical velocity and temperature fields of RAMONA

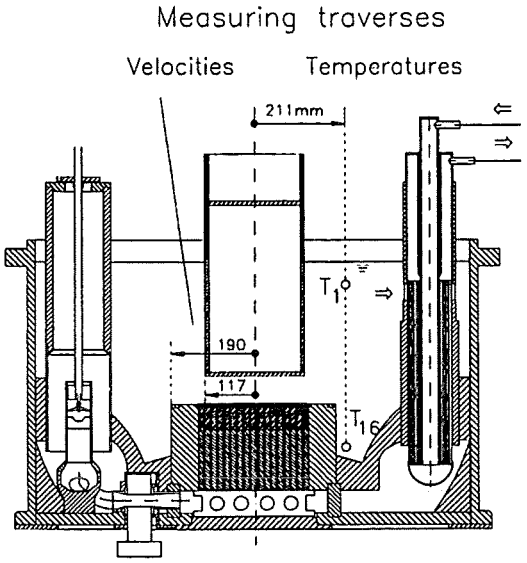

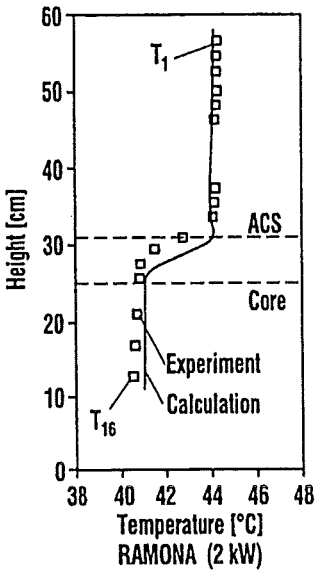

a) Temperatures along vertical traverse r=211mm (2kW)

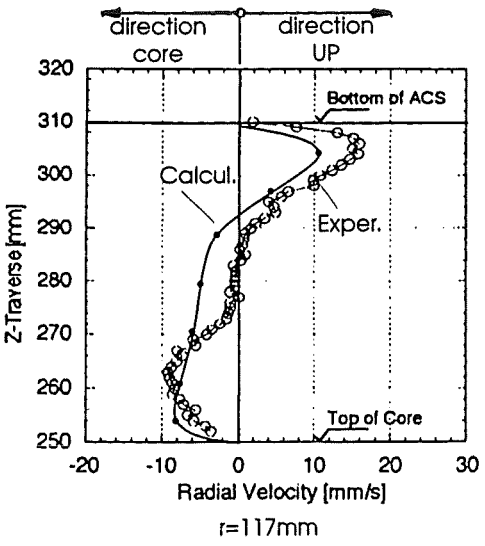

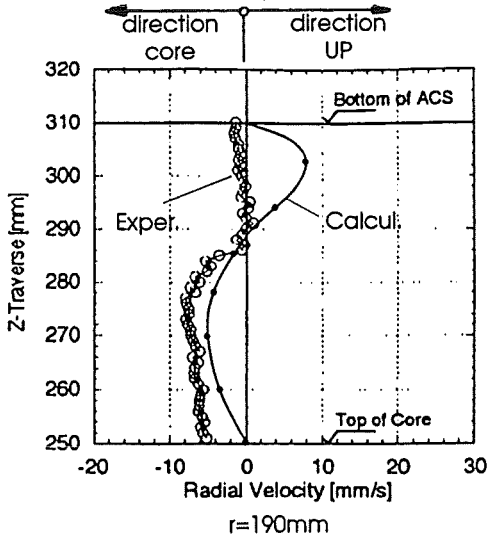

b) Velocities along vertical traverses r=117mm and r= 190mm (1kW)

Fig. 20 Measured and computed velocities and temperatures along vertical traverses in the upper plenum (impermeable ACS)

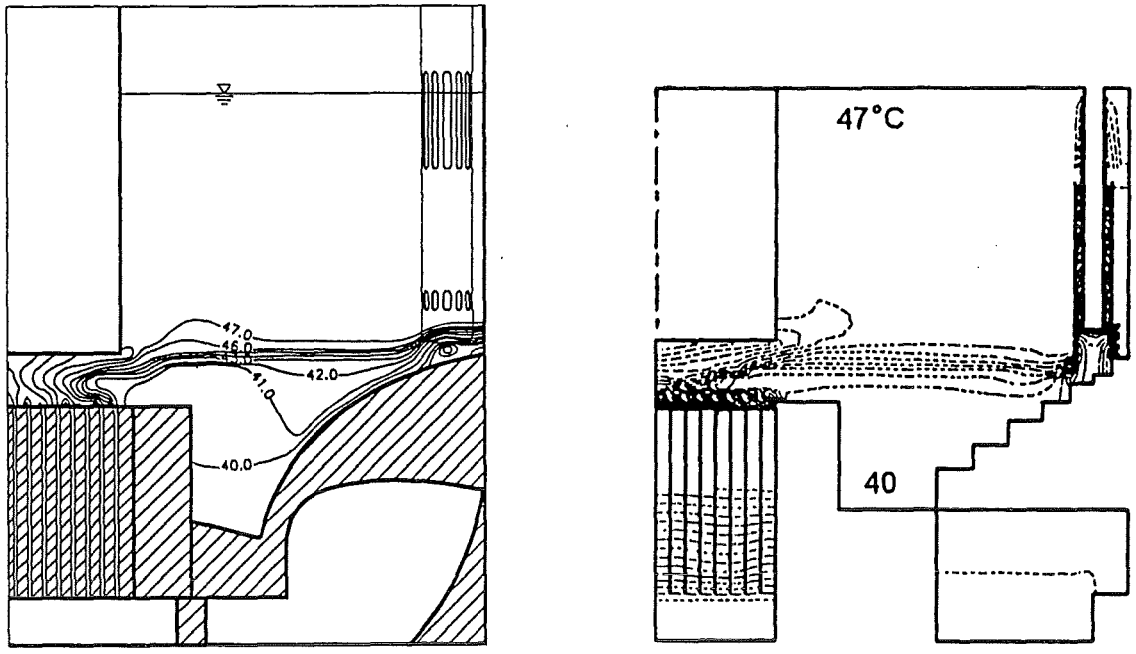

Measurement Calculation

a.) Measured and calculated isotherms ($\phi = 0°$)

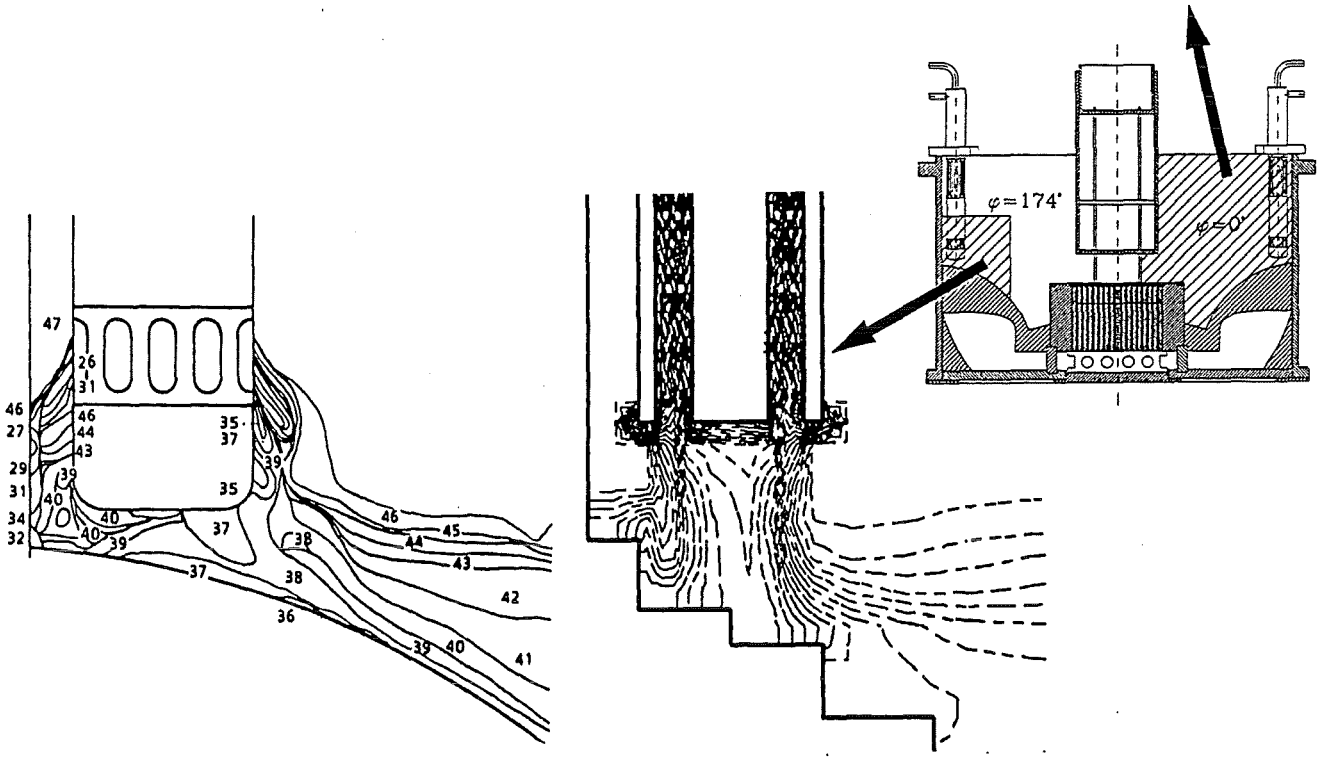

b.) Measured and calculated isotherms - DHX outlet
Cross section ($\phi = 174°$)

Fig. 21 Comparison of measured and computed isotherm fields (isotherm interval of 1 K, $P_t = 8$ kW)

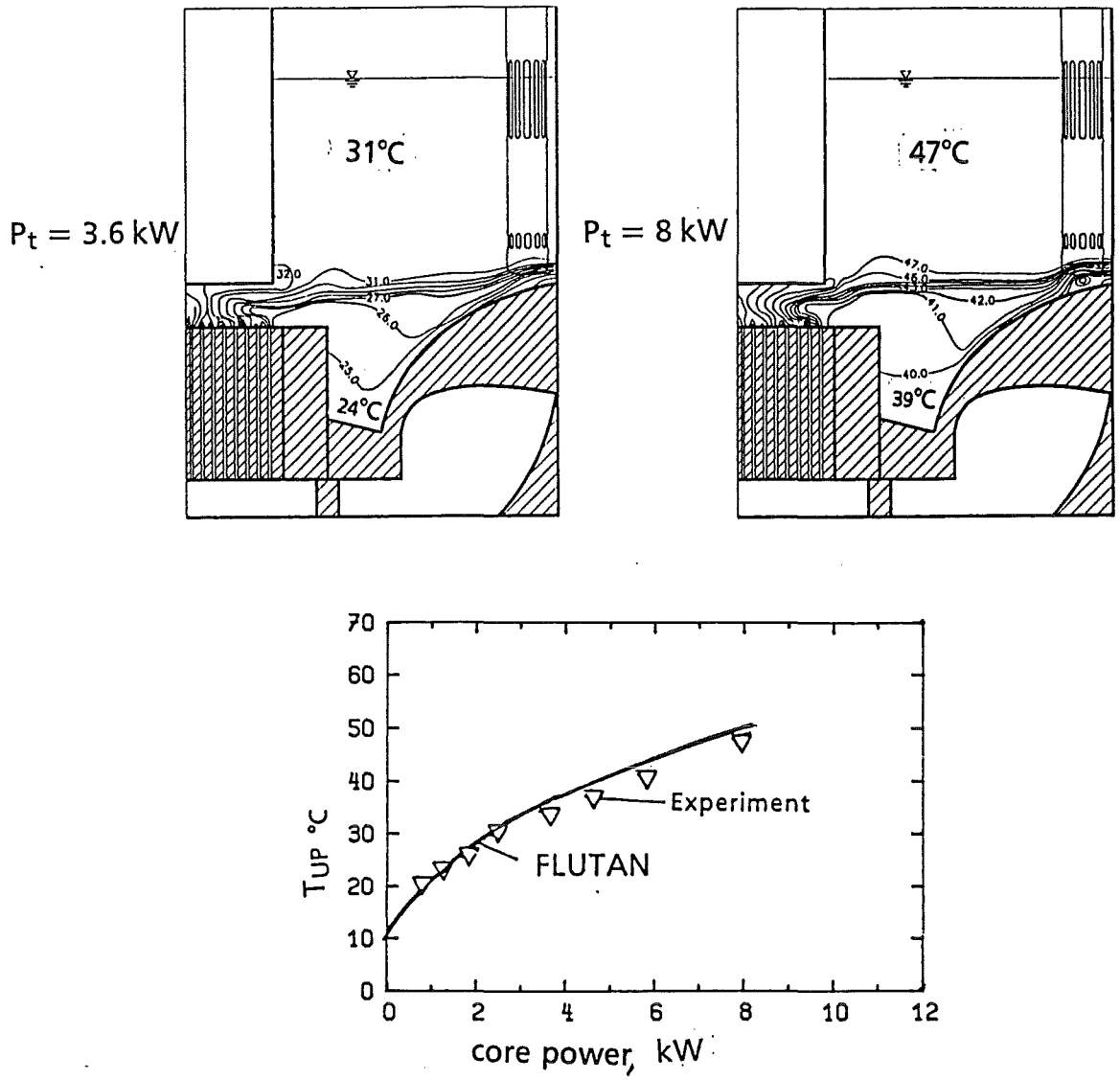

a.) Isotherm fields and upper plenum temperatures versus core power

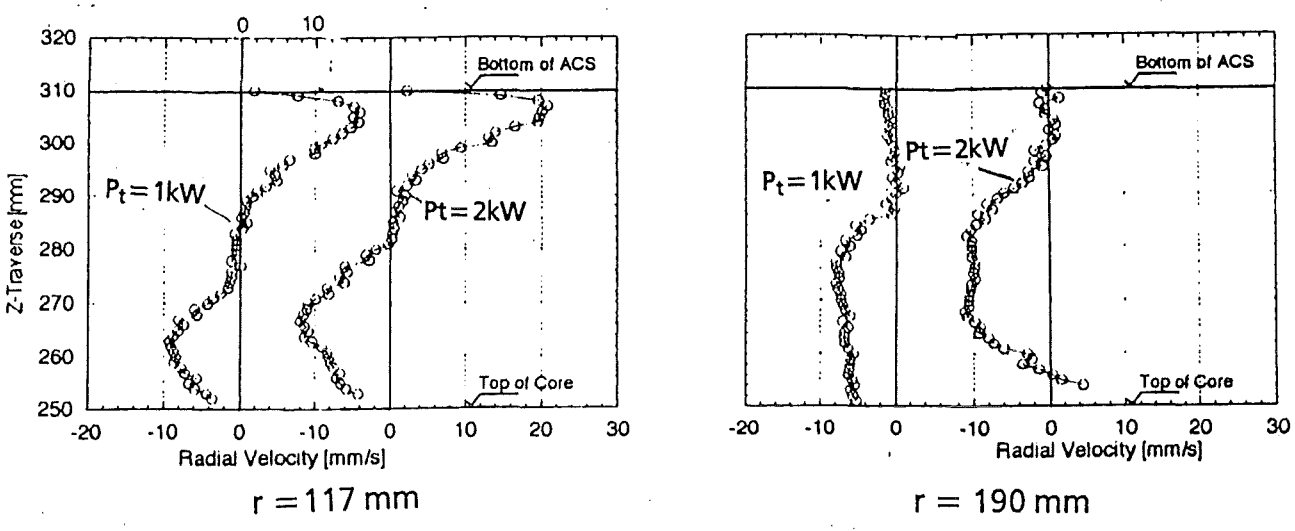

b.) Velocity distributions for two different core powers, measured at r = 117, 190 mm

Fig. 22 Influence of the core power on the comparison of the computed and measured upper plenum temperatures and velocities.

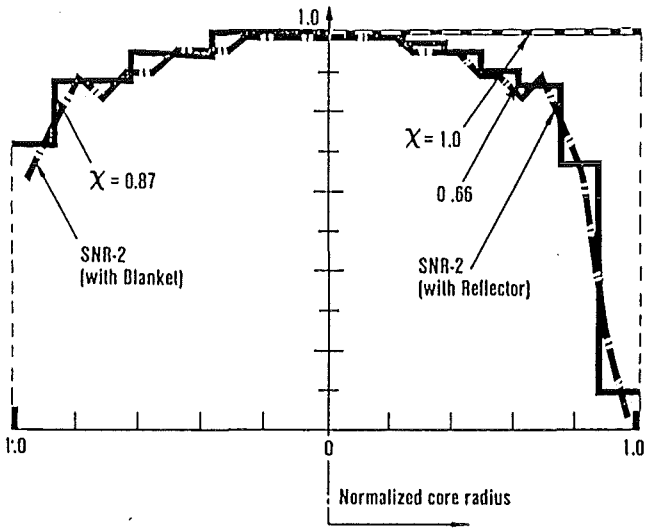

a.) Normalized power distribution $X = X_{avg}/X_{max}$

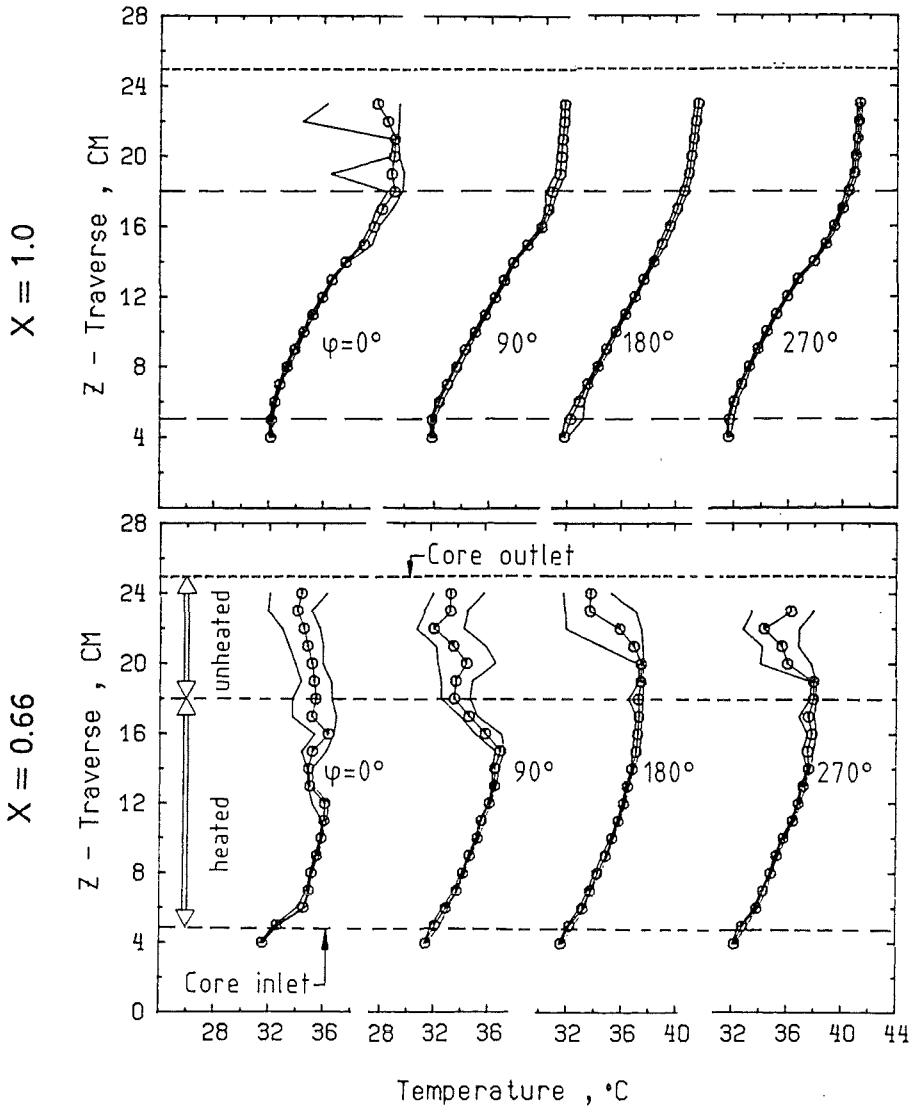

b.) Measured vertical temperatures along flow channel No. 8

Fig. 23 Measured vertical temperatures of the core for different radial core power distributions (P_t = 3.6 kW)

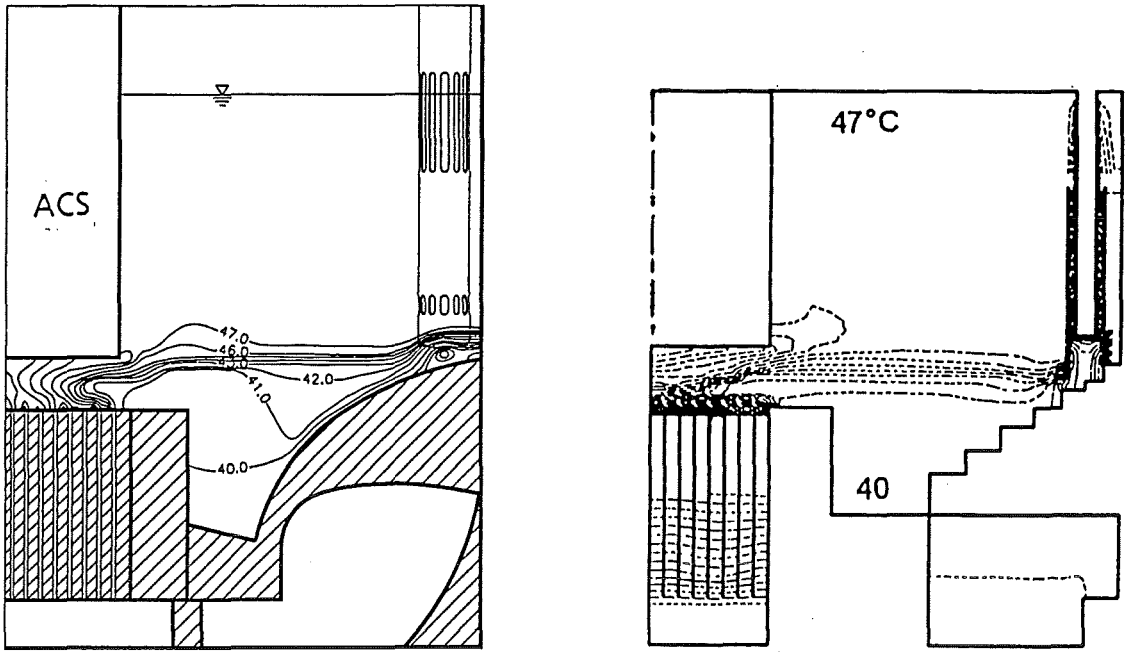

a.) Impermeable ACS

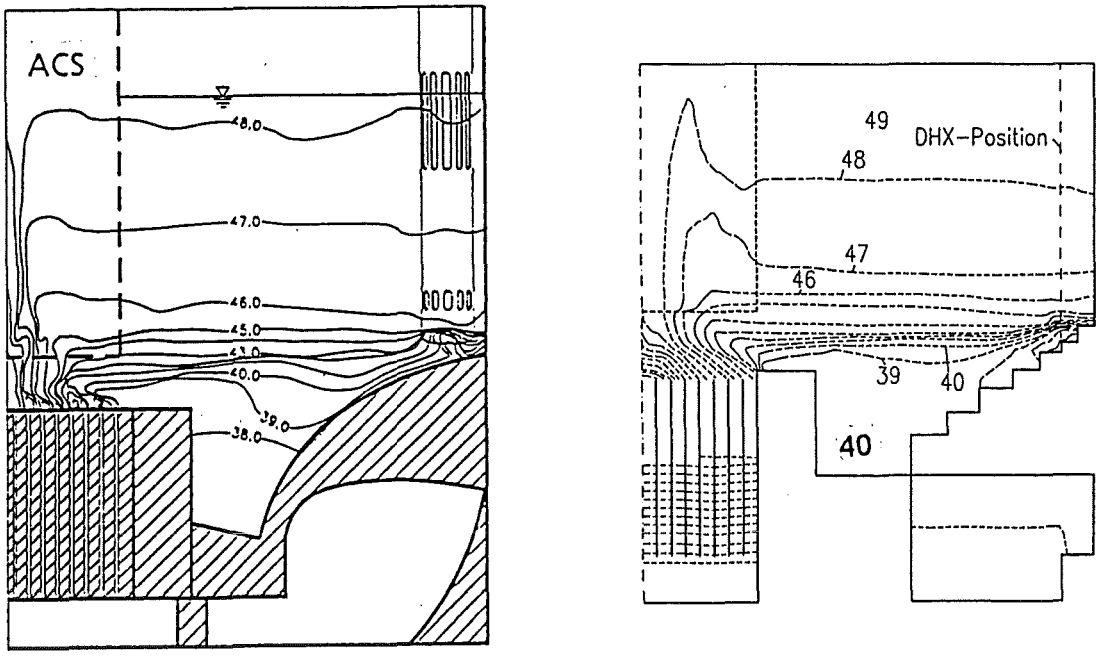

b.) permeable ACS

Measurements Calculations

Fig. 24 Influence of the ACS design on the comparison of computed and measured isotherm fields (isotherm interval of 1 K, $P_t = 8$ kW)

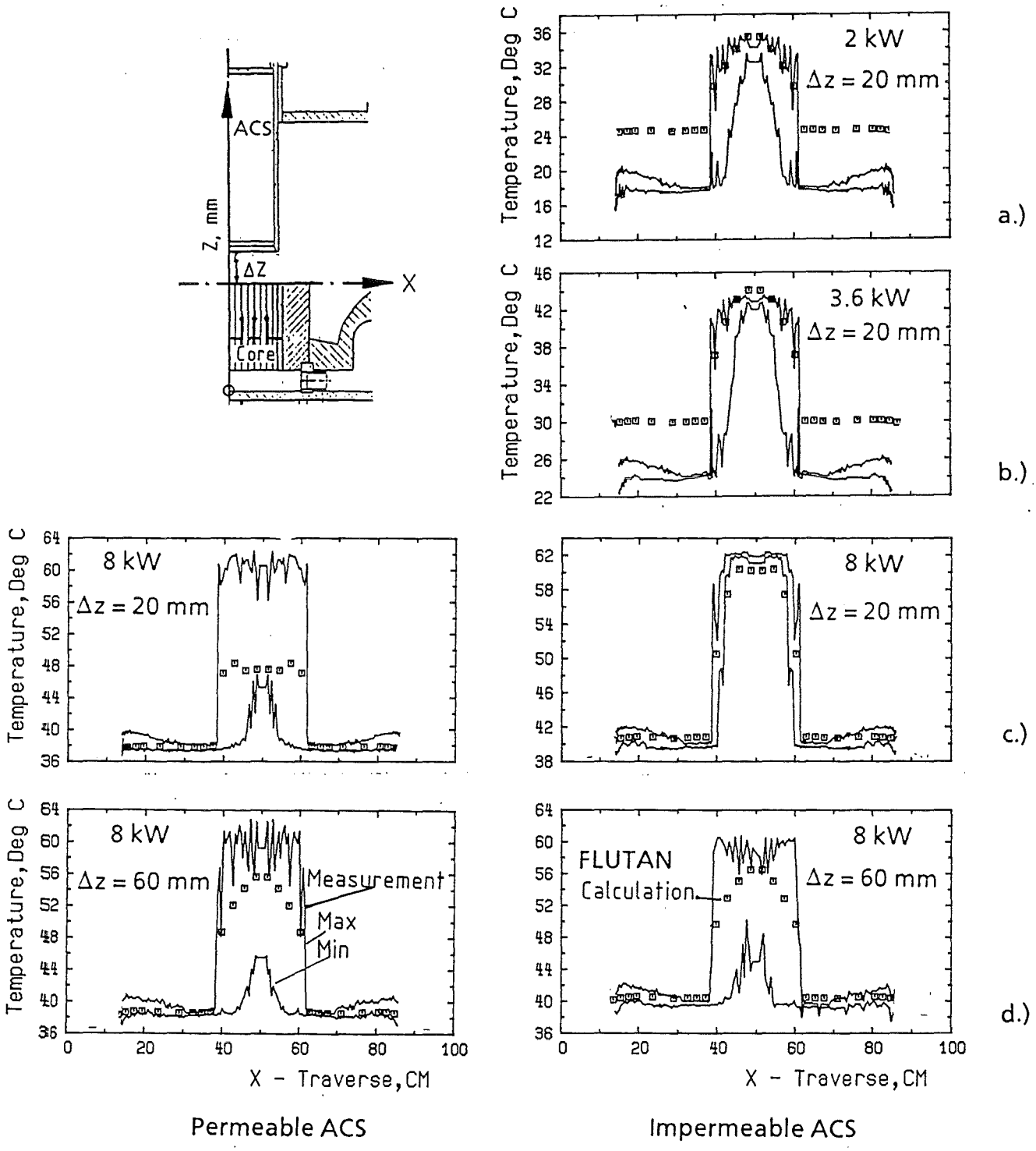

Fig. 25 Influence of the vertical ACS position and core power on the comparison of computed and measured horizontal temperature traverses for permeable and impermeable ACS

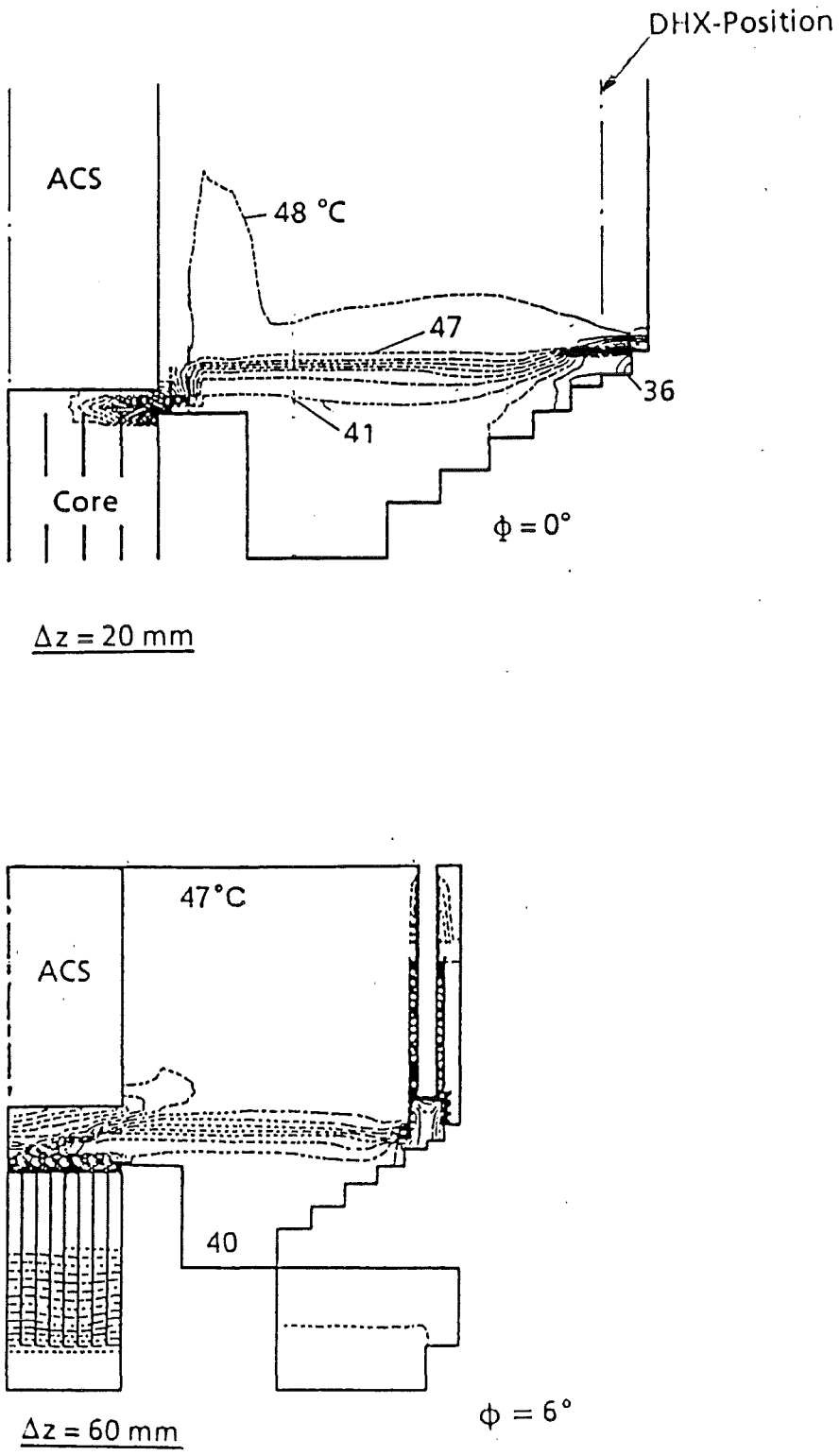

Fig. 26 Influence of the vertical ACS position on the computed isotherm fields (isotherm interval of 1 K, $P_t = 8$ kW)

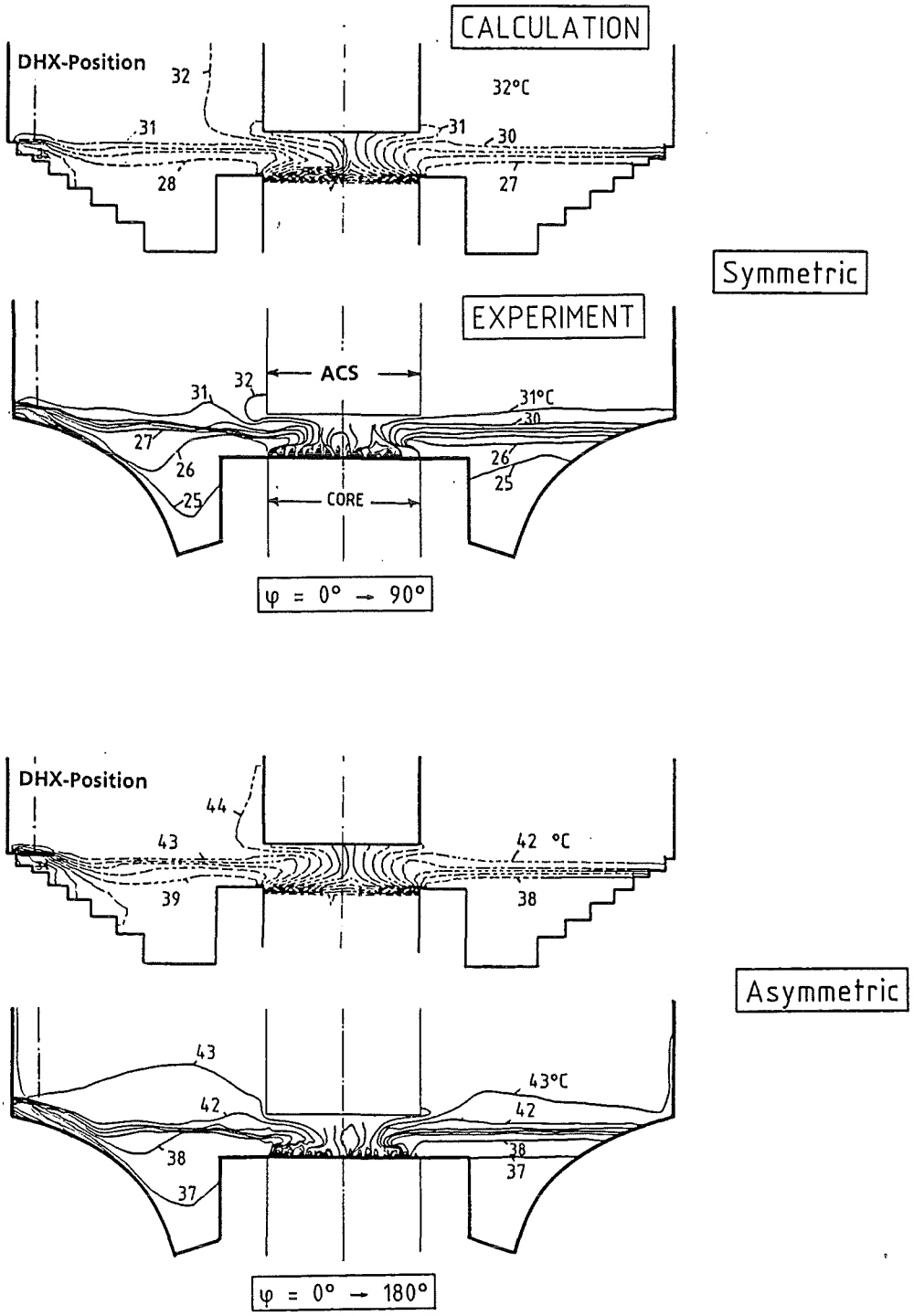

Fig. 27 Influence of the cooling mode on the comparison of computed and measured isotherm fields (isotherm interval of 1 K, $P_t = 3.6$ kW)

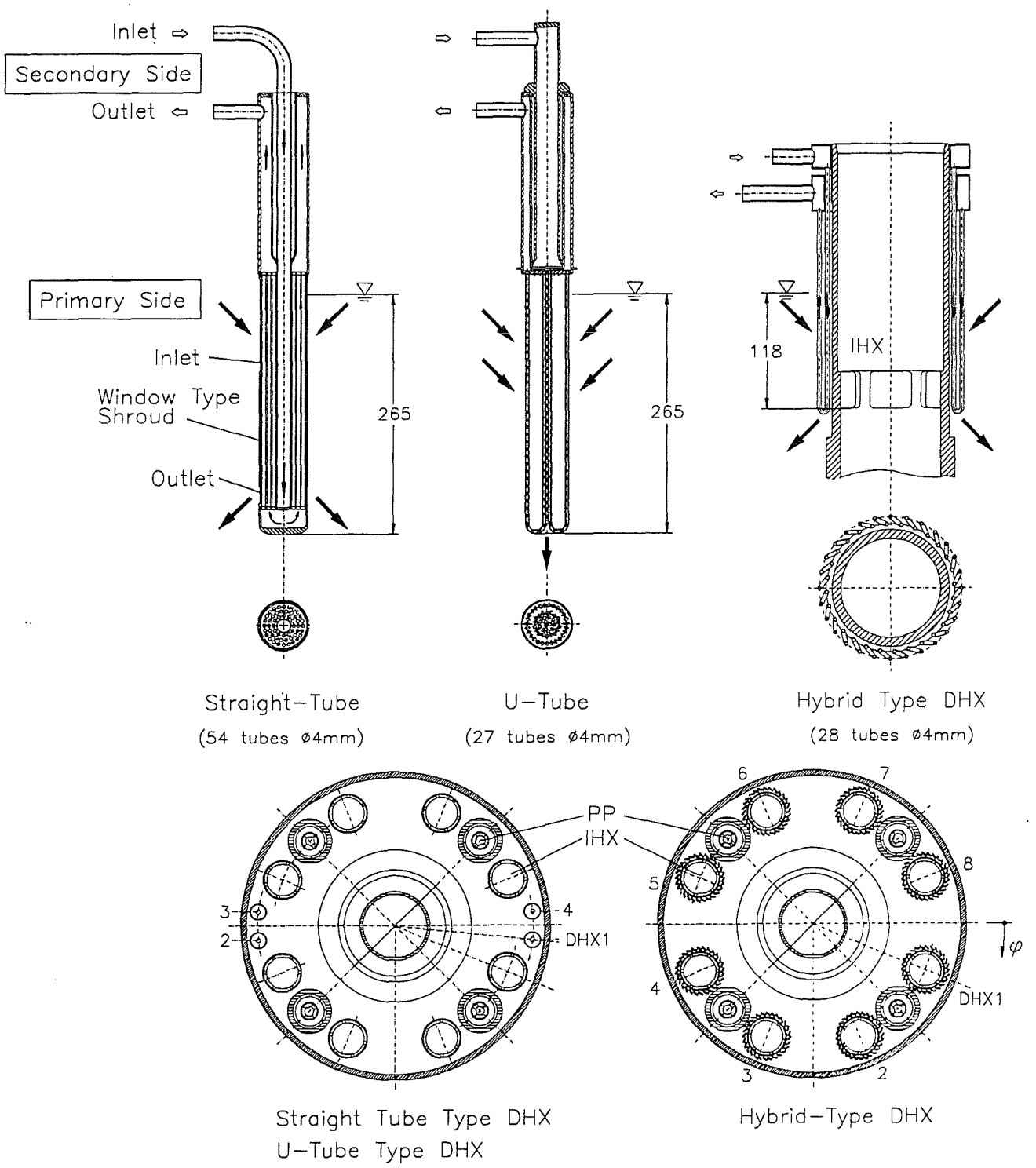

Fig. 28 Different designs of the DHXs

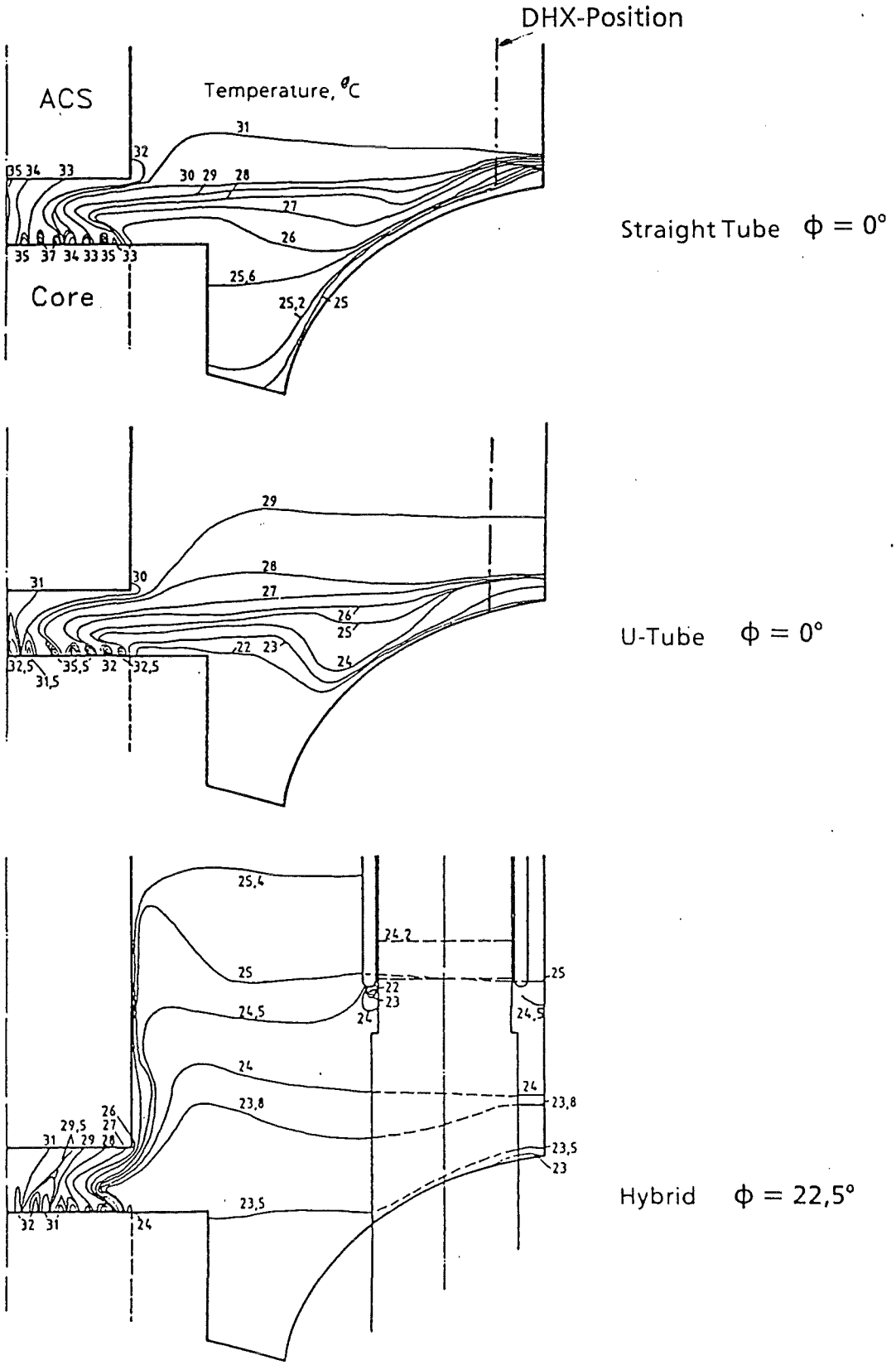

Fig. 29 Influence of the DHX design on the measured isotherm fields (isotherm interval of 1 K, P_t = 3.6 kW)

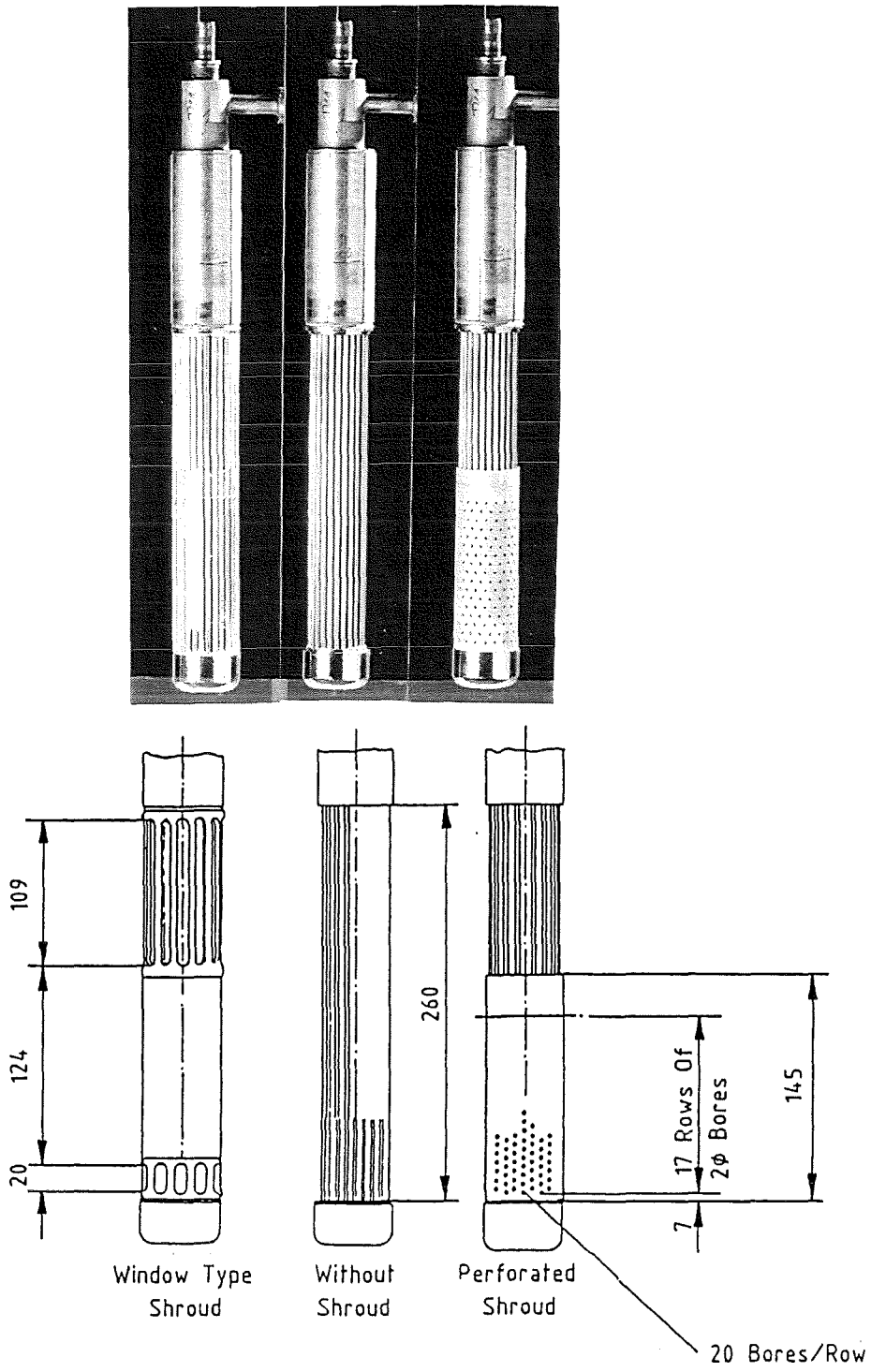

Fig. 30 Straight-tube type DHXs with different shroud geometries

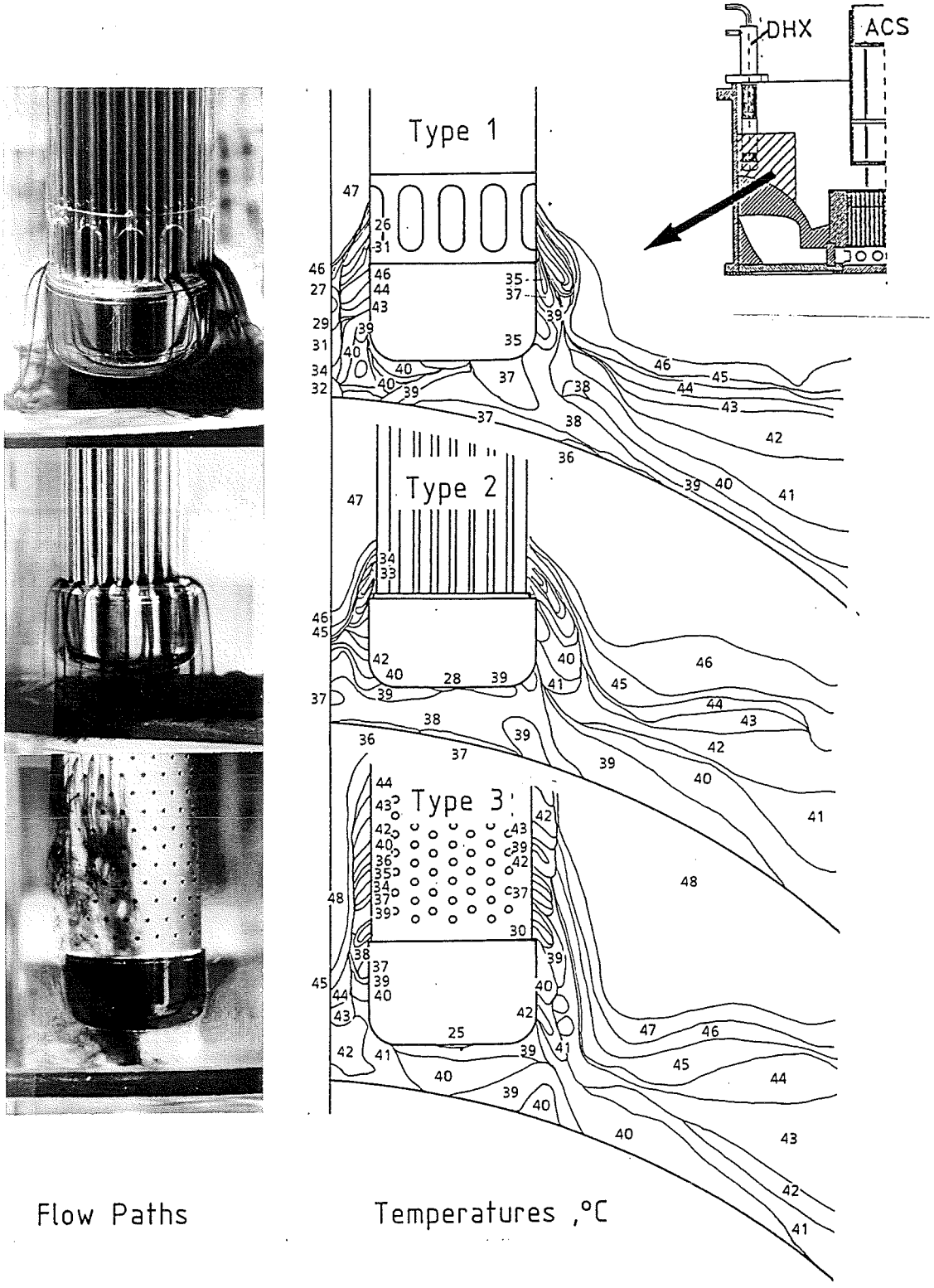

Fig. 31 Influence of the shroud geometries on the measured isotherm fields and flow paths of straight-tube-type DHXs (P_t = 8 kW)

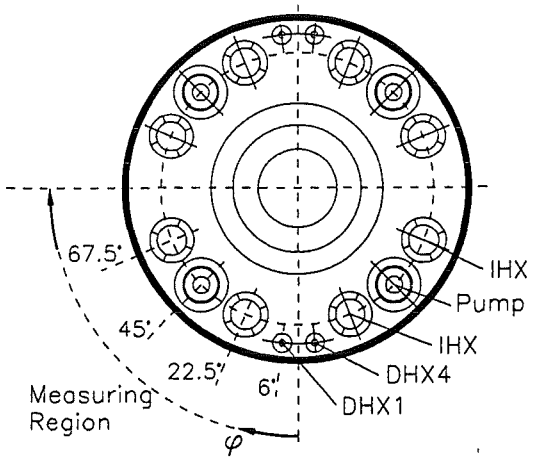

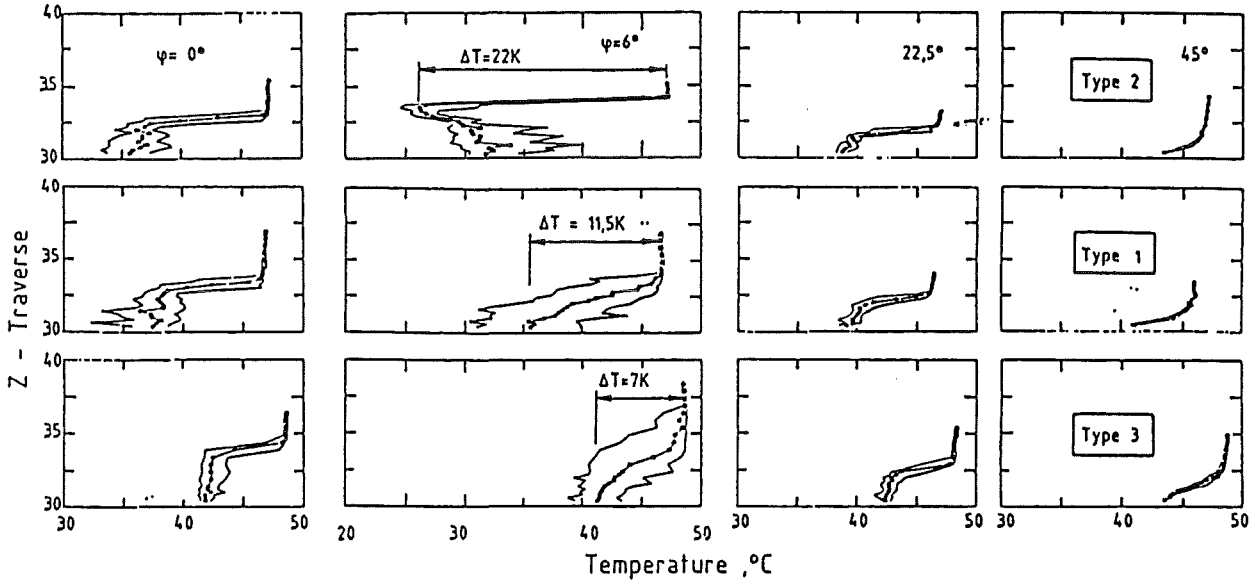

Fig. 32 Influence of the shroud geometries on the measured vertical temperatures at different circumferential positions of the tank wall (P_t = 8 kW)

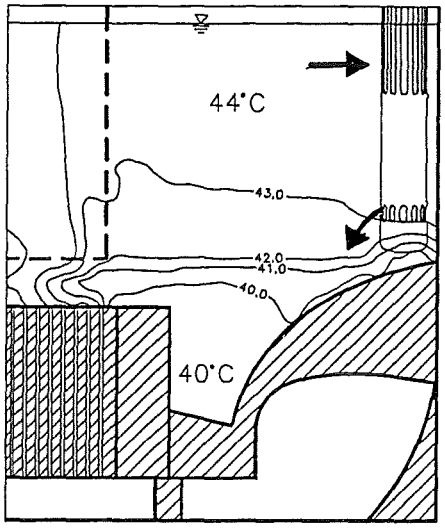

flow paths

a) nominal fluid level

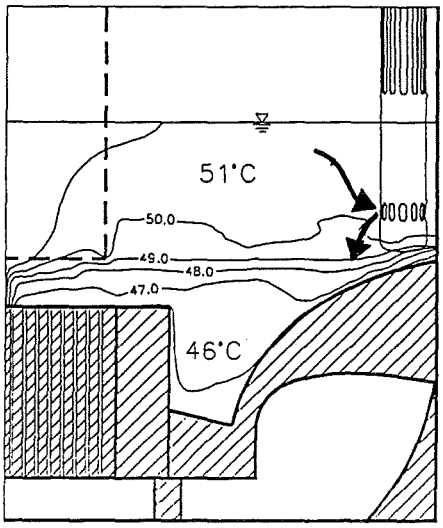

DHXs with shroud

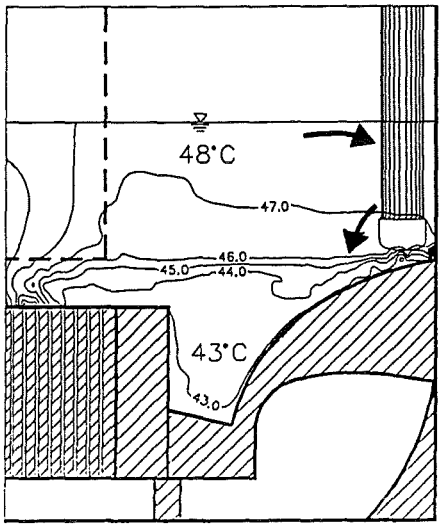

DHXs without shroud

b) lowered fluid level

Fig. 33 Influence of the fluid level on the isotherm fields in the upper plenum (P_t = 2 kW)

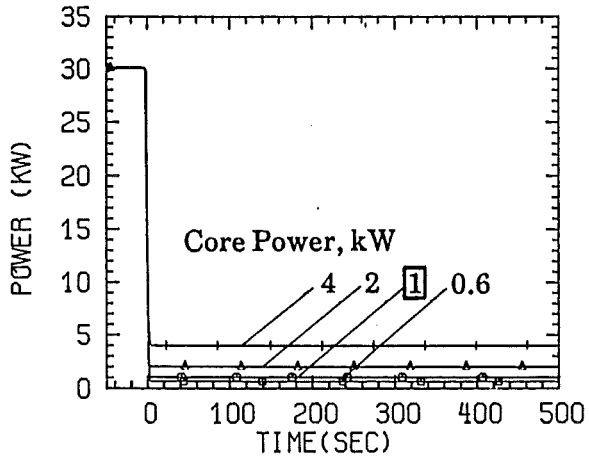

a.) Core Power

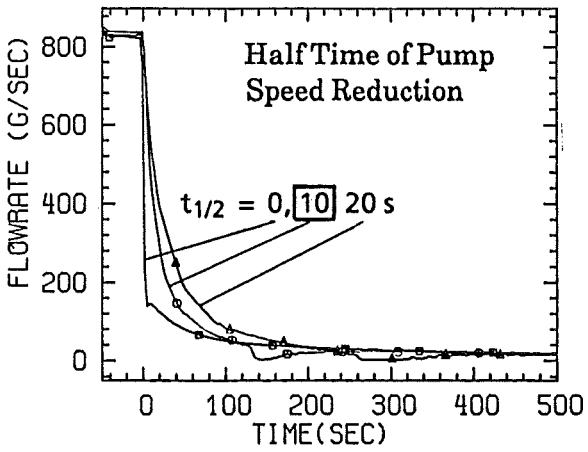

b.) Core Flow Rates

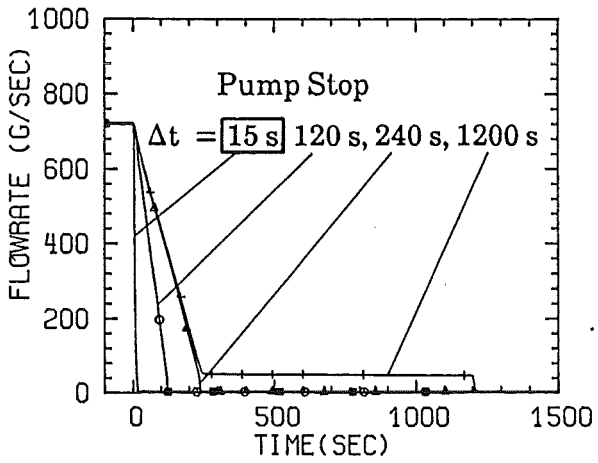

c.) IHX Secondary Side Flow Rates

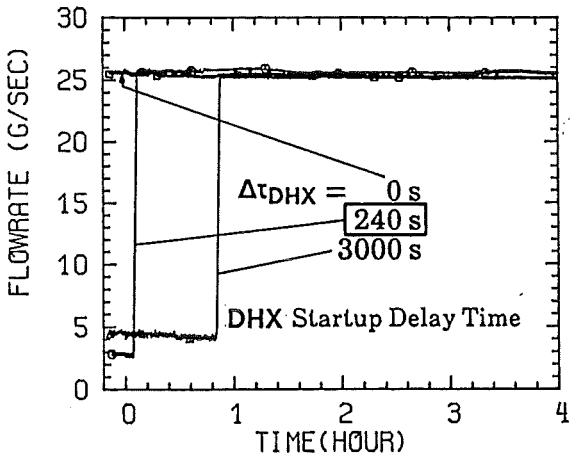

d.) DHX Secondary Side Flow Rates

Reference conditions

Fig. 34 Reference conditions and parameters of the investigations on the transition from forced to natural convection

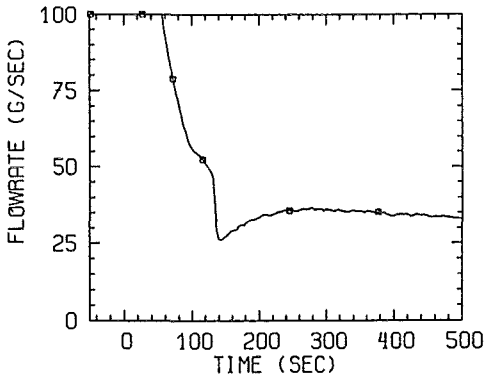

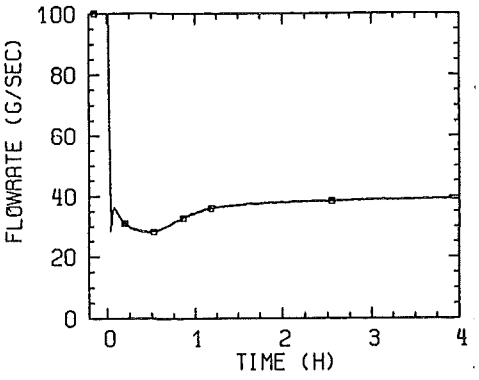

a) core mass flow rate

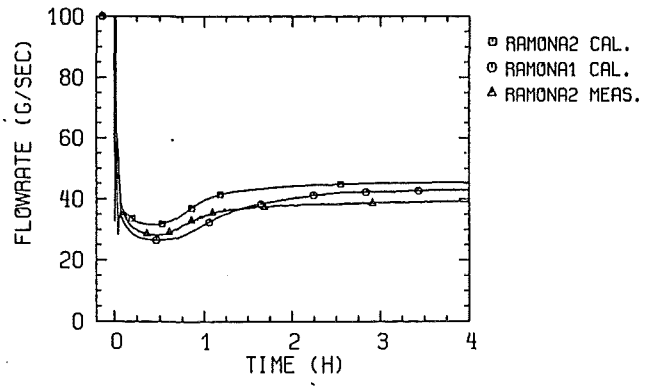

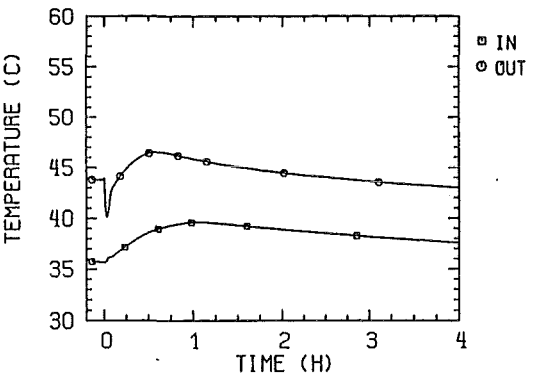

aa.) core mass flow rate

b) core inlet and outlet temperatures

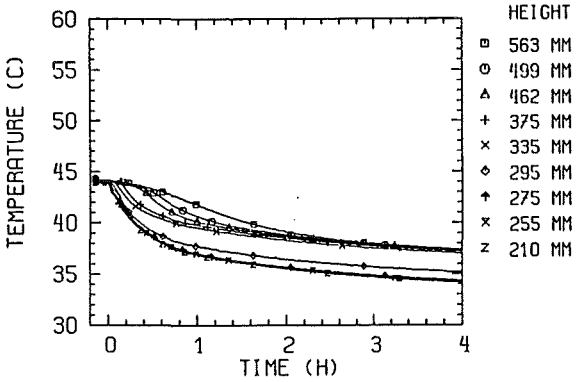

c) upper plenum temperatures

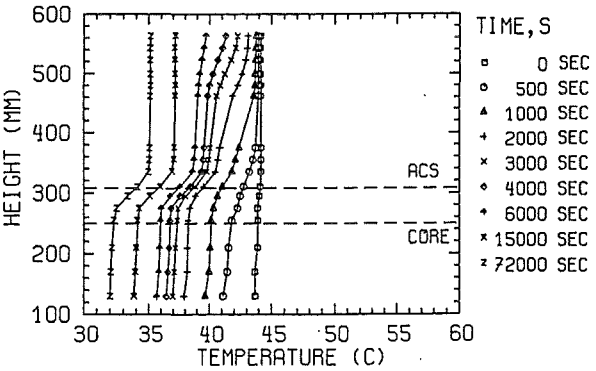

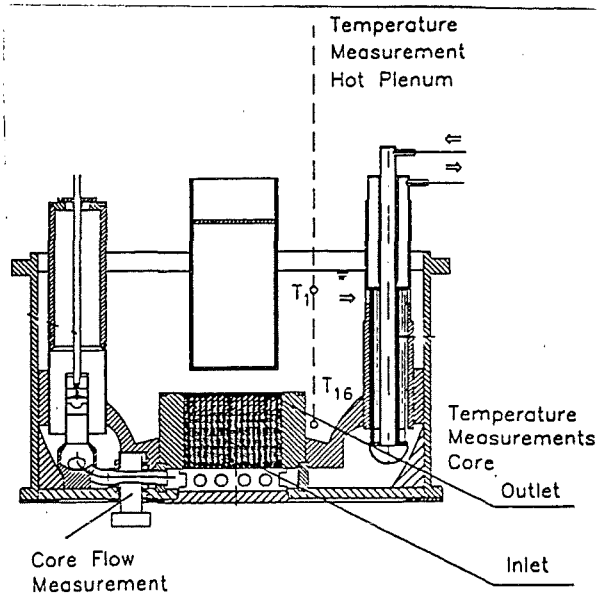

d) vertical temperature distributions in the upper plenum

Fig. 35 The development of core mass flow, core and UP temperatures during the transition from forced to natural convection - reference conditions.

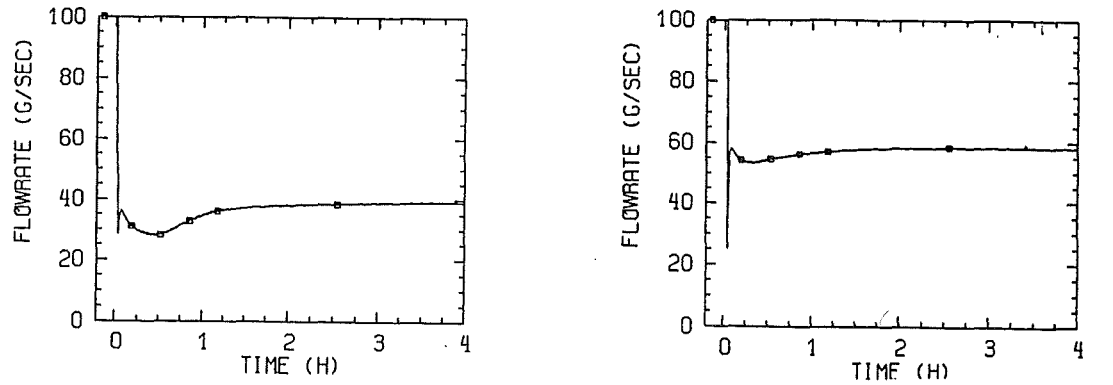

a) core mass flow rate

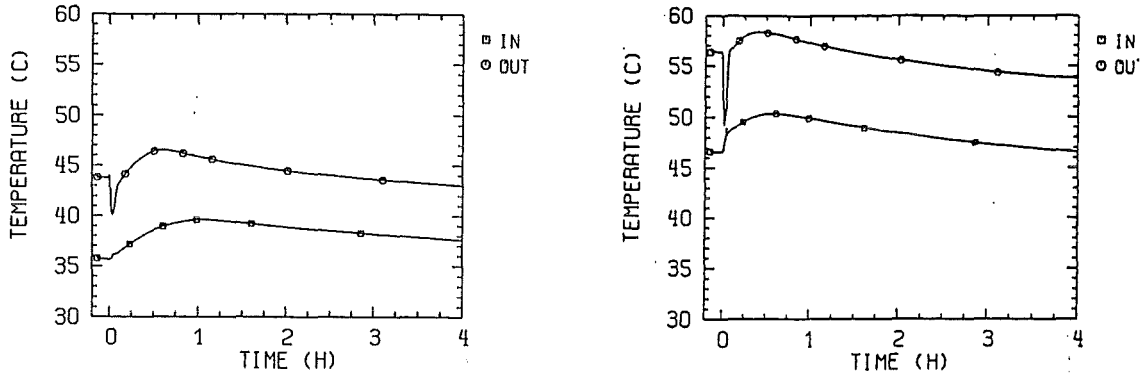

b) core inlet and outlet temperatures

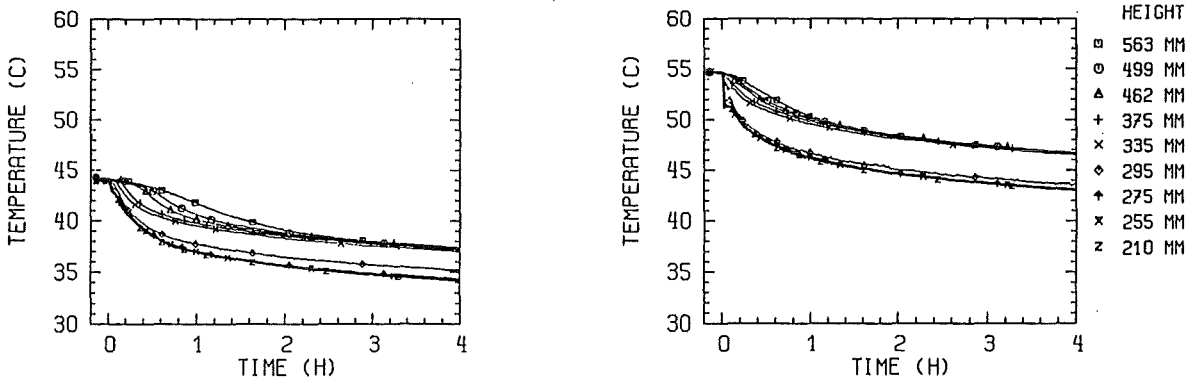

c) upper plenum temperatures

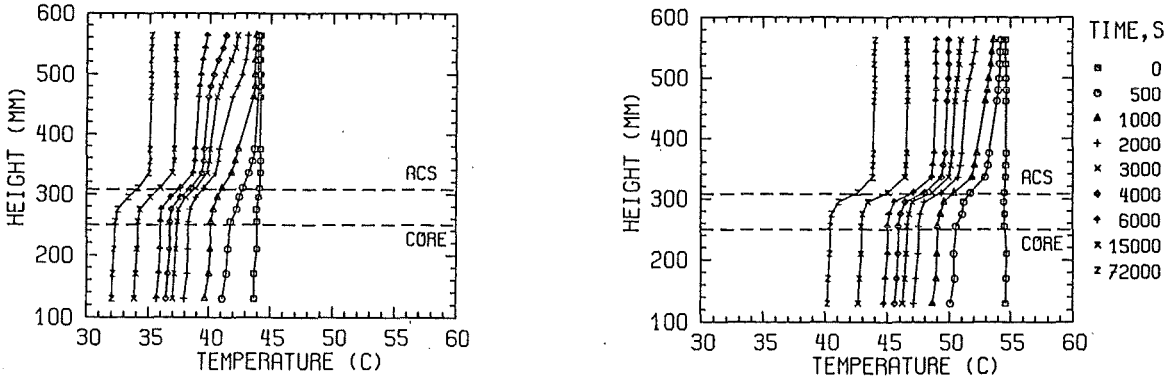

d) vertical temperature distributions in the upper plenum

30 kW → 1 kW

75 kW → 2 kW

Fig. 36 Influence of the core power before scram on the transition from forced to natural circulation (τ_{IHX} = 15 s; ACS impermeable)

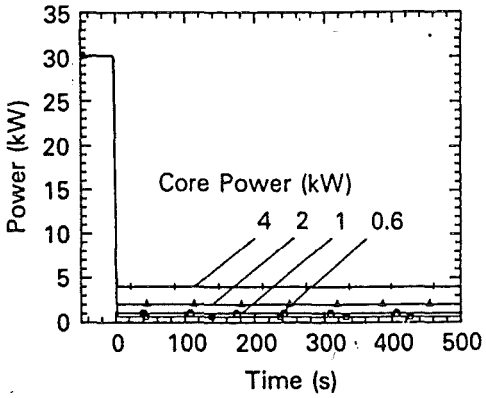

a) core power

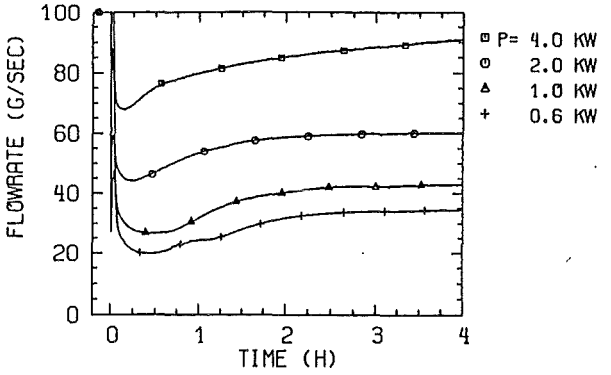

b) core flow rate

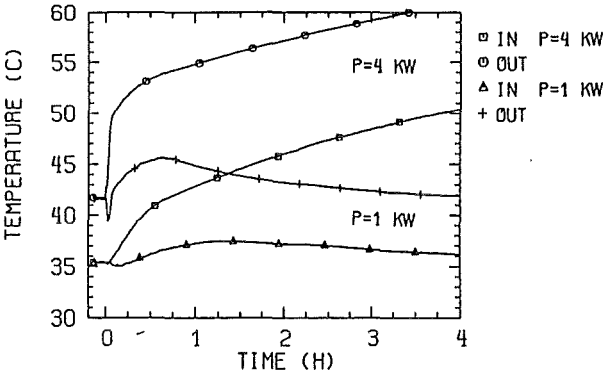

c) core inlet and outlet temperatures

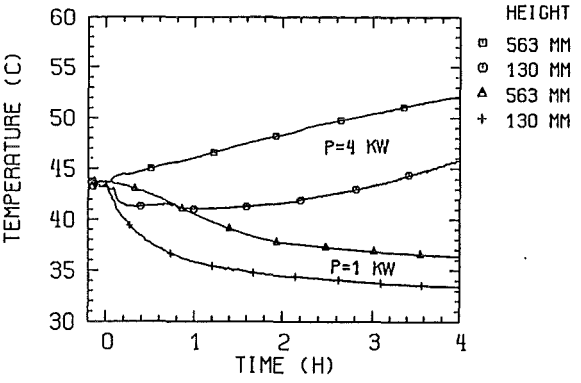

d) upper plenum temperatures

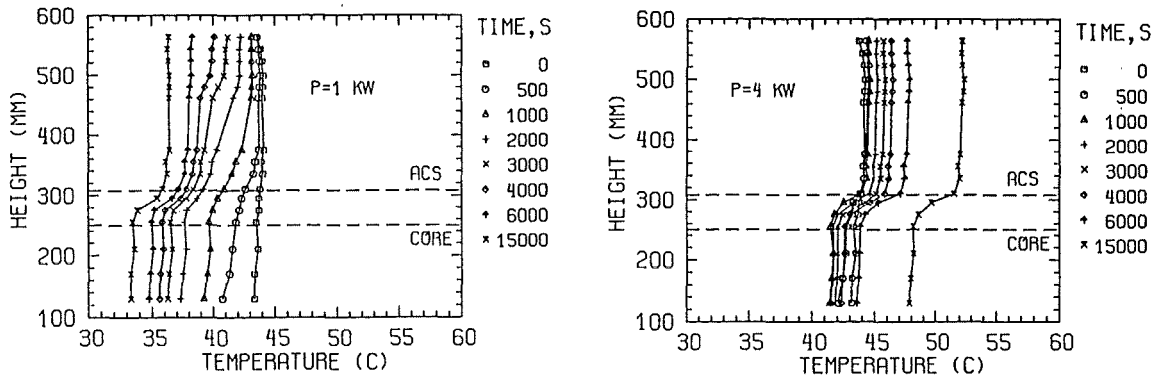

e) vertical temperature distributions in the upper plenum

Fig. 37 Influence of the core power after scram on the transition from forced to natural convection (τ_{IHX} = 15 s; ACS impermeable)

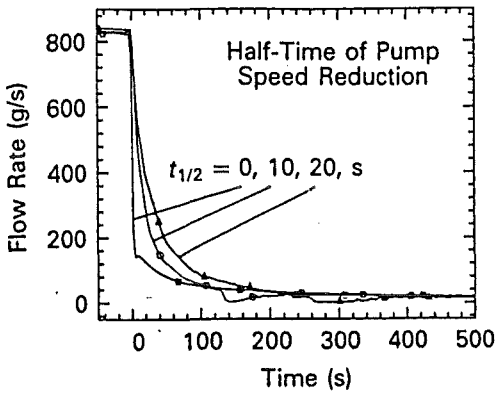

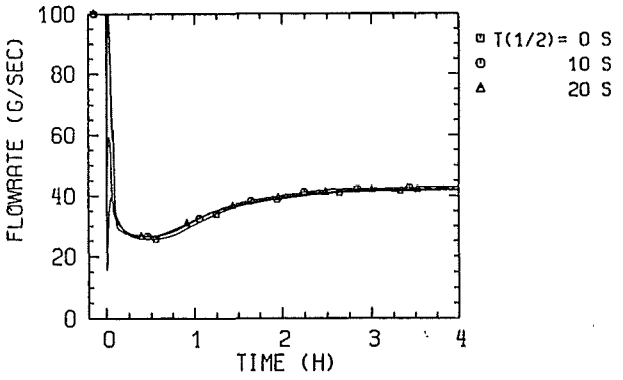

a) core mass flow rate

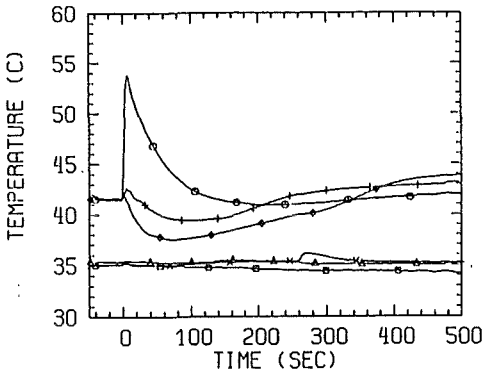

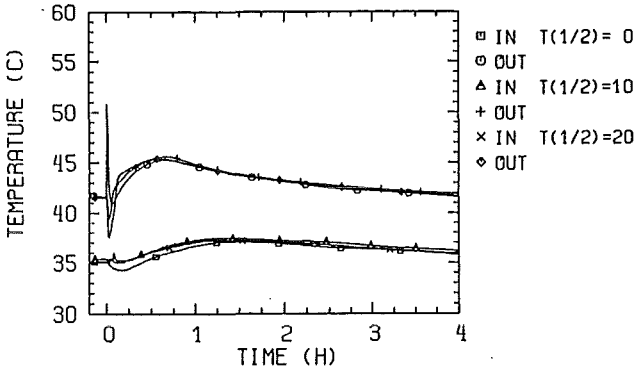

b) core inlet and outlet temperatures

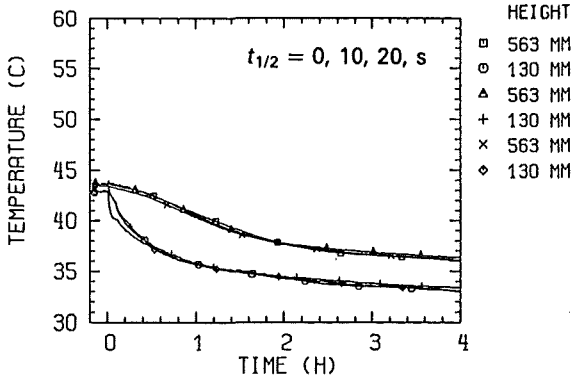

c) upper plenum temperatures

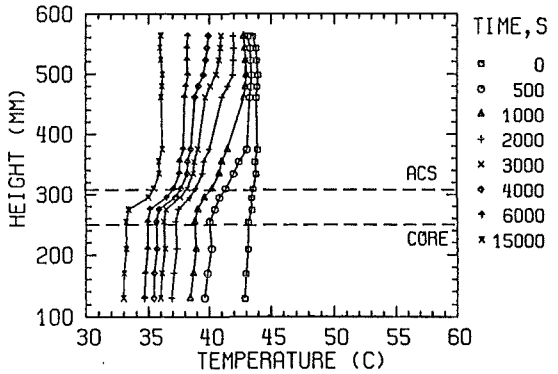

d) vertical temperature distributions in the upper plenum

Fig. 38 Influence of the half-time of the primary pump coastdown on the transition from forced to natural convection (τ_{IHX} = 15 s; ACS impermeable)

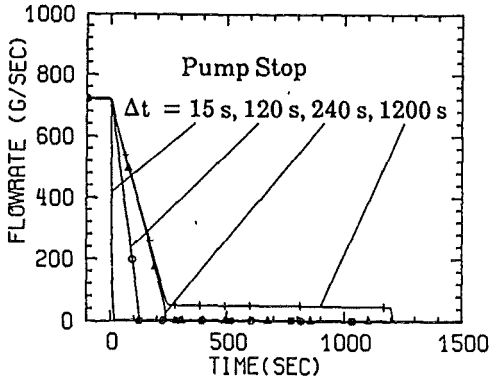

a) IHX secondary-side flow rate

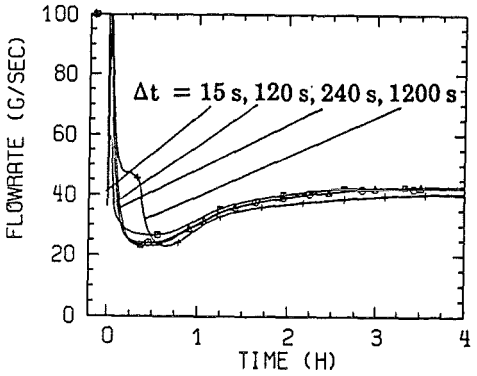

b) core flow rate

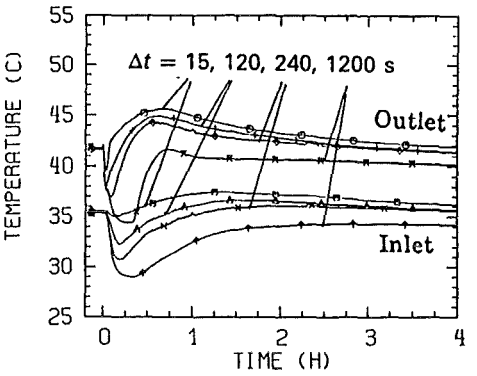

c) core inlet and outlet temperatures

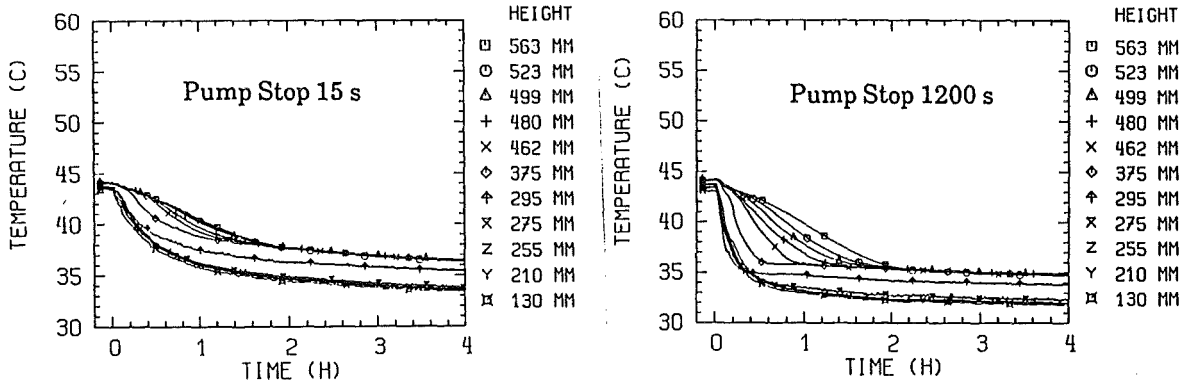

d) upper plenum temperatures

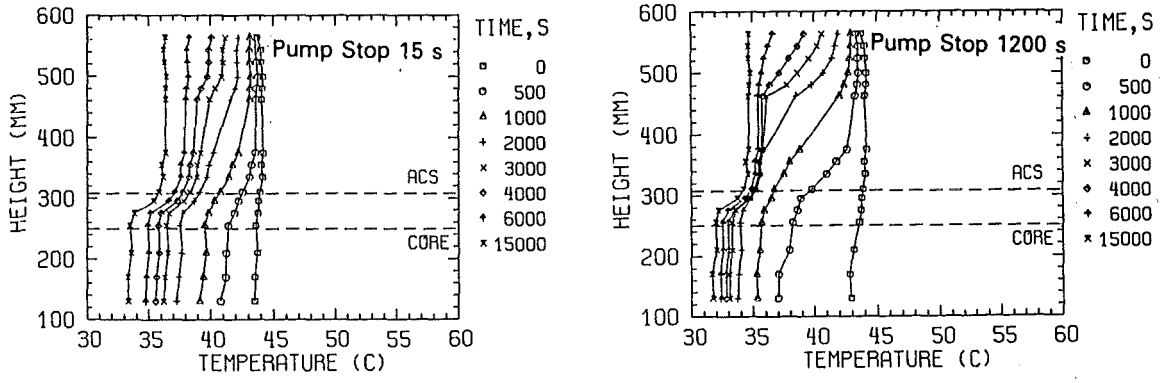

e) vertical temperature distributions in the upper plenum

Fig. 39a Influence of the IHXs secondary-side pump run-down on the transition from forced to natural convection (τ_{IHX} = 15 s; ACS impermeable)

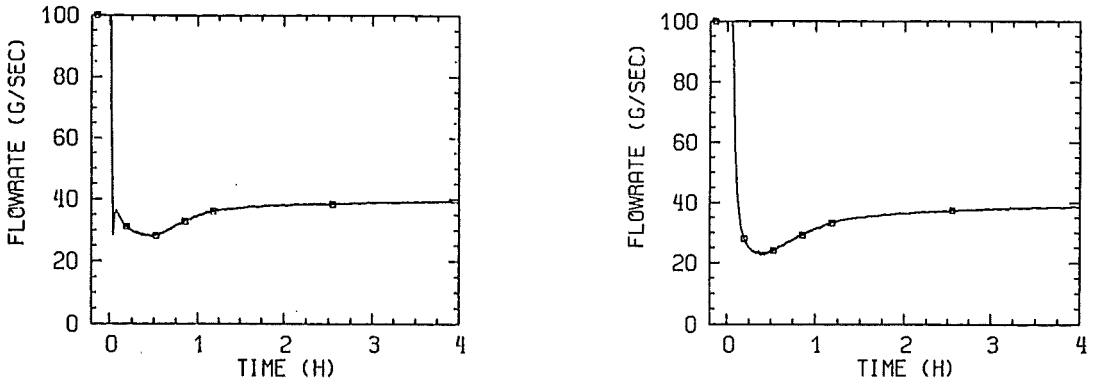

a) core mass flow rate

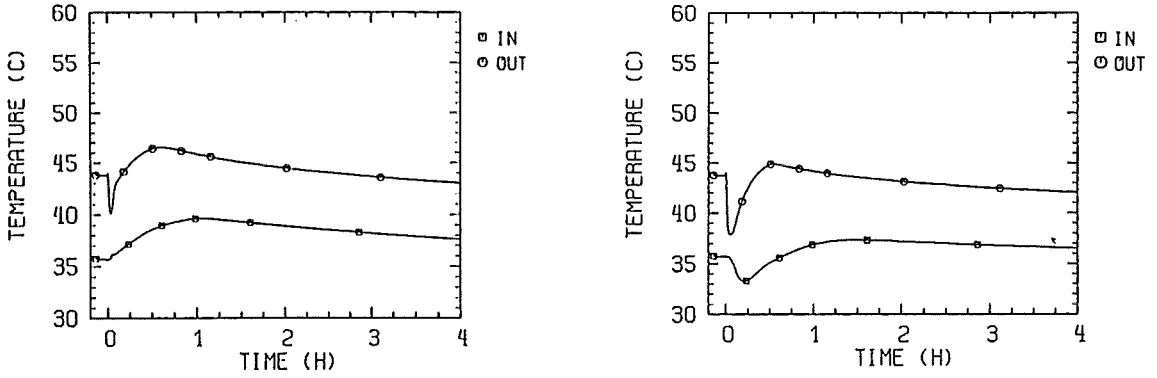

b) core inlet and outlet temperatures

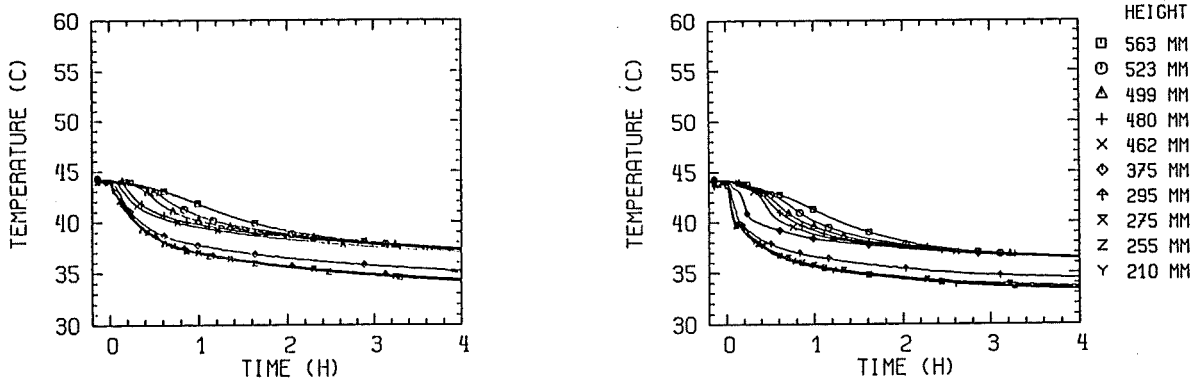

c) upper plenum temperatures

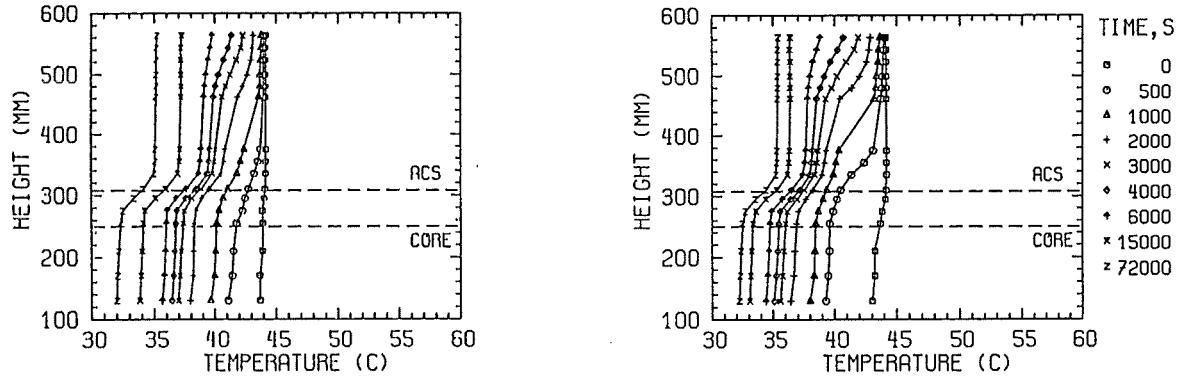

d) vertical temperature distributions in the upper plenum

Fig. 39b Comparison of the transient thermal hydraulic behavior of the primary system for $\tau_{IHX} = 15$ s and $\tau_{IHX} = 240$ s (ACS impermeable)

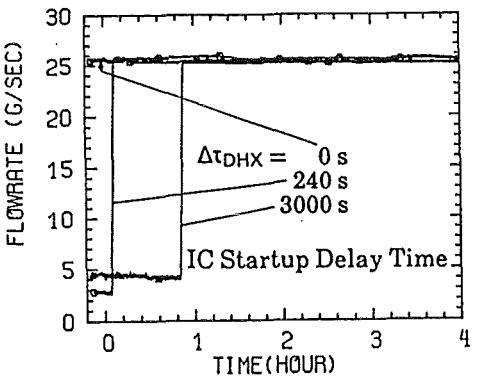

a) DHX secondary-side flow rate

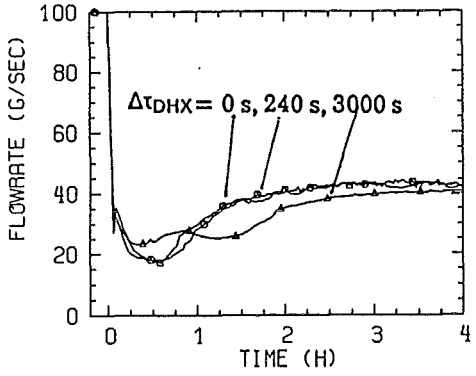

b) core flow rate

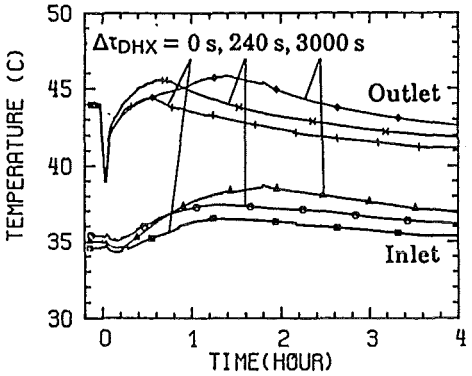

c) core inlet and outlet temperatures

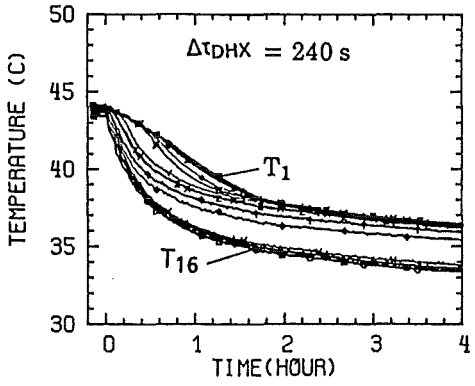

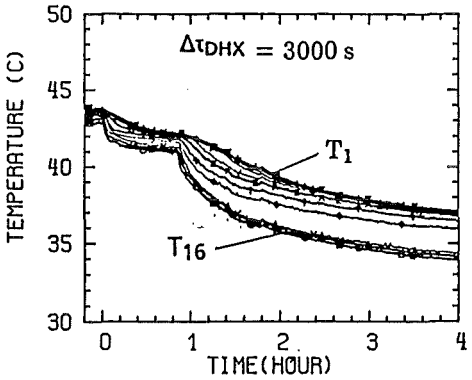

d) upper plenum temperatures

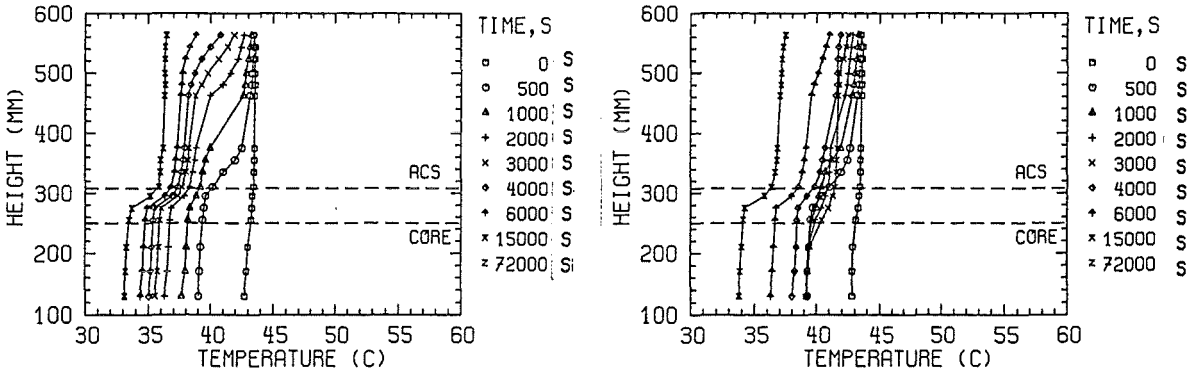

e) vertical temperature distributions in the upper plenum

Fig. 40 Influence of the DHX startup delay time on the transition from forced to natural convection (τ_{IHX} = 15 s; ACS impermeable)

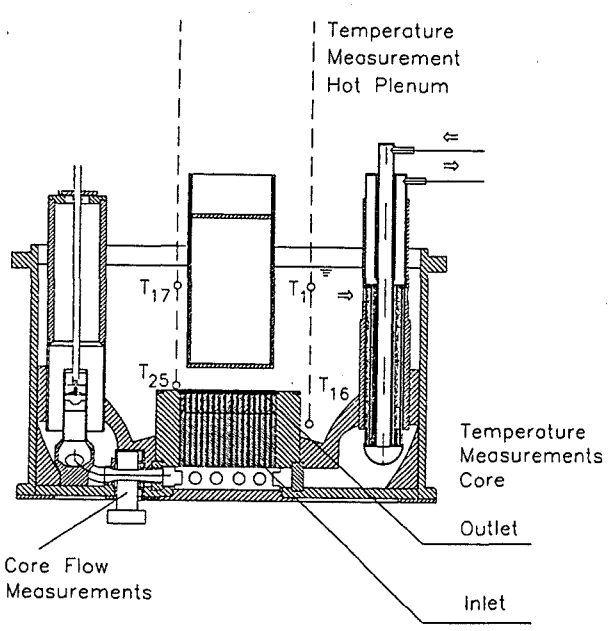

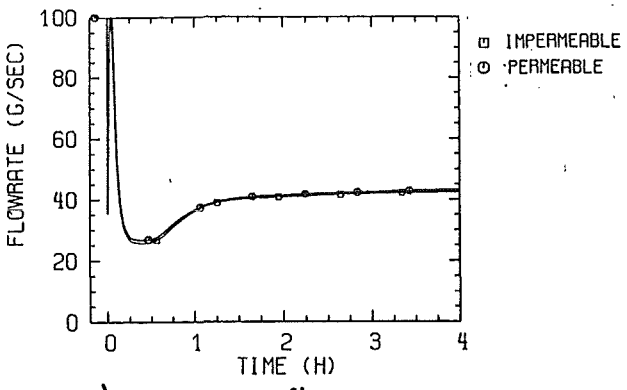

a) core mass flow rate

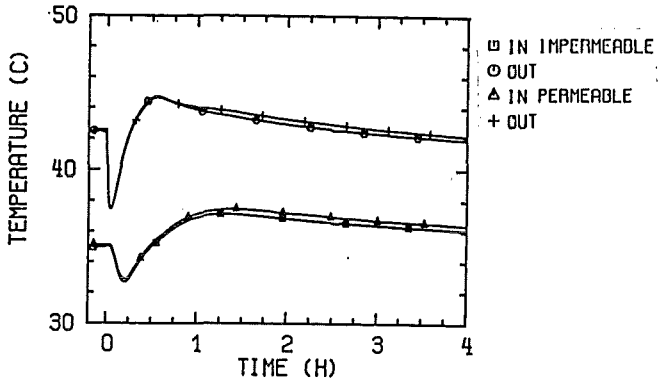

b) core inlet and outlet temperatures

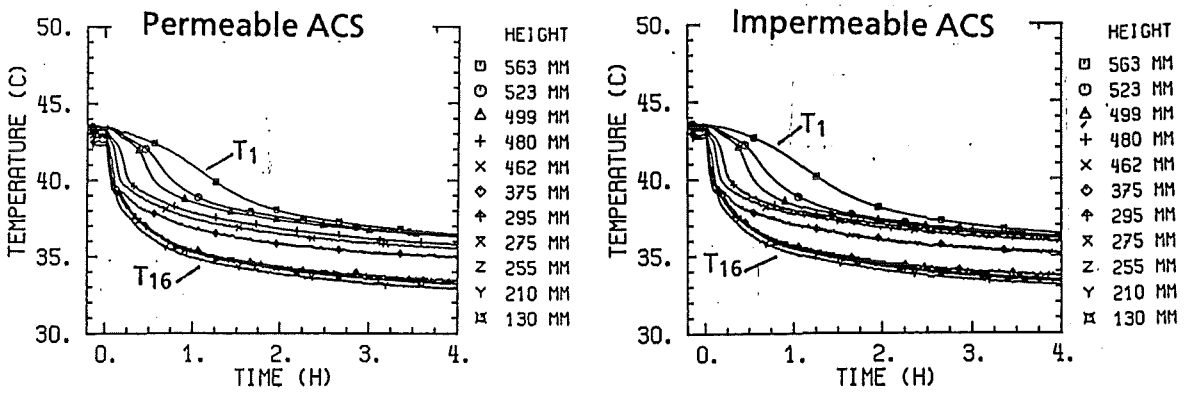

c) upper plenum temperatures

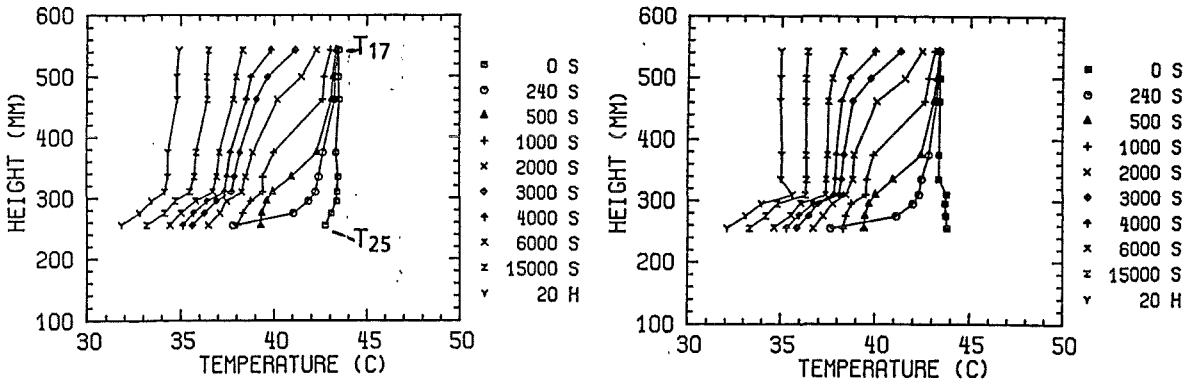

d) vertical temperature distributions in the upper plenum

Fig. 41 Influence of the ACS design on the transition from forced to natural convection (τ_{IHX} = 240 s)

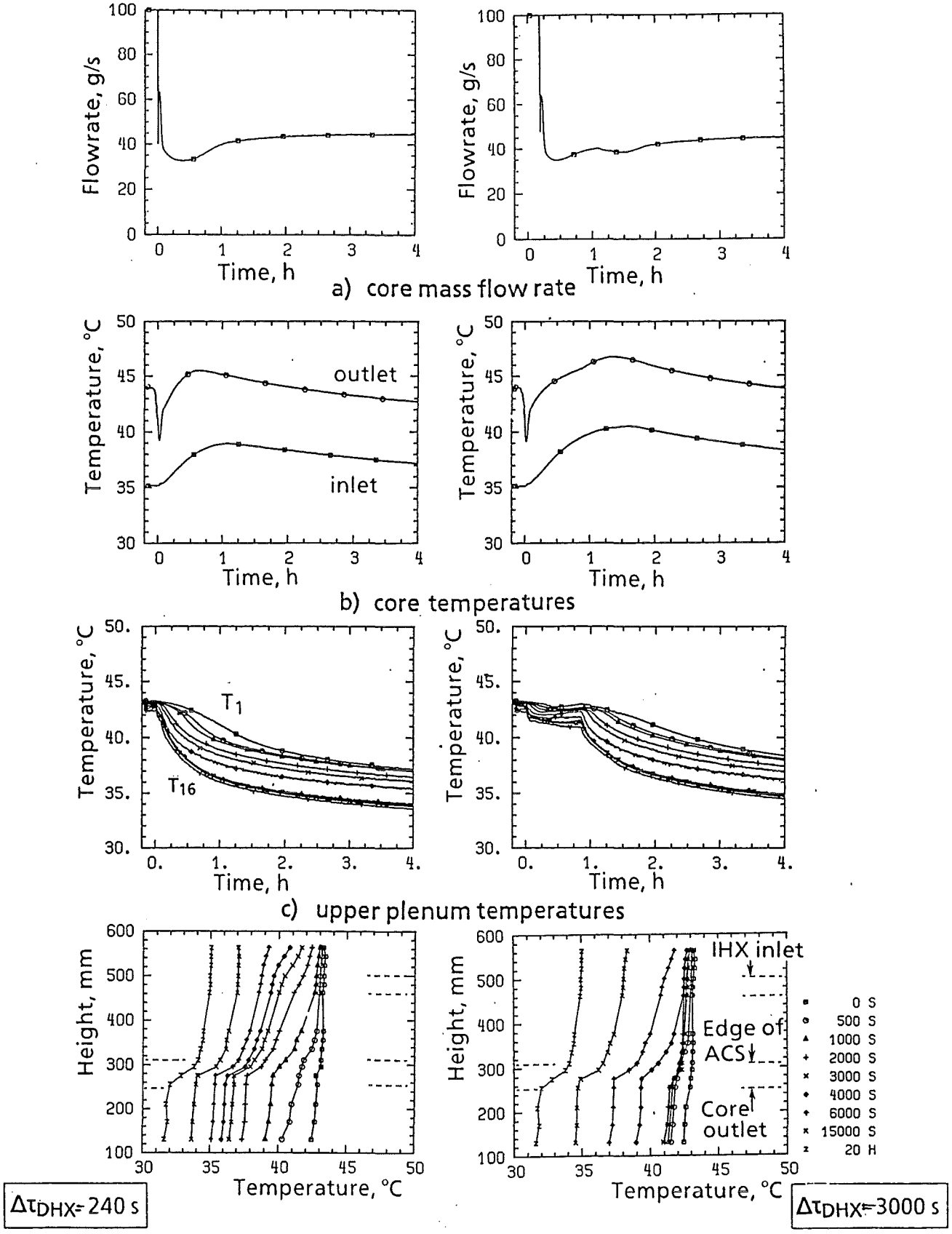

Fig. 42 Influence of the DHX startup delay time on the transition from forced to natural convection for straight-tube-type DHXs (τ_{IHX} = 15 s; ACS permeable)

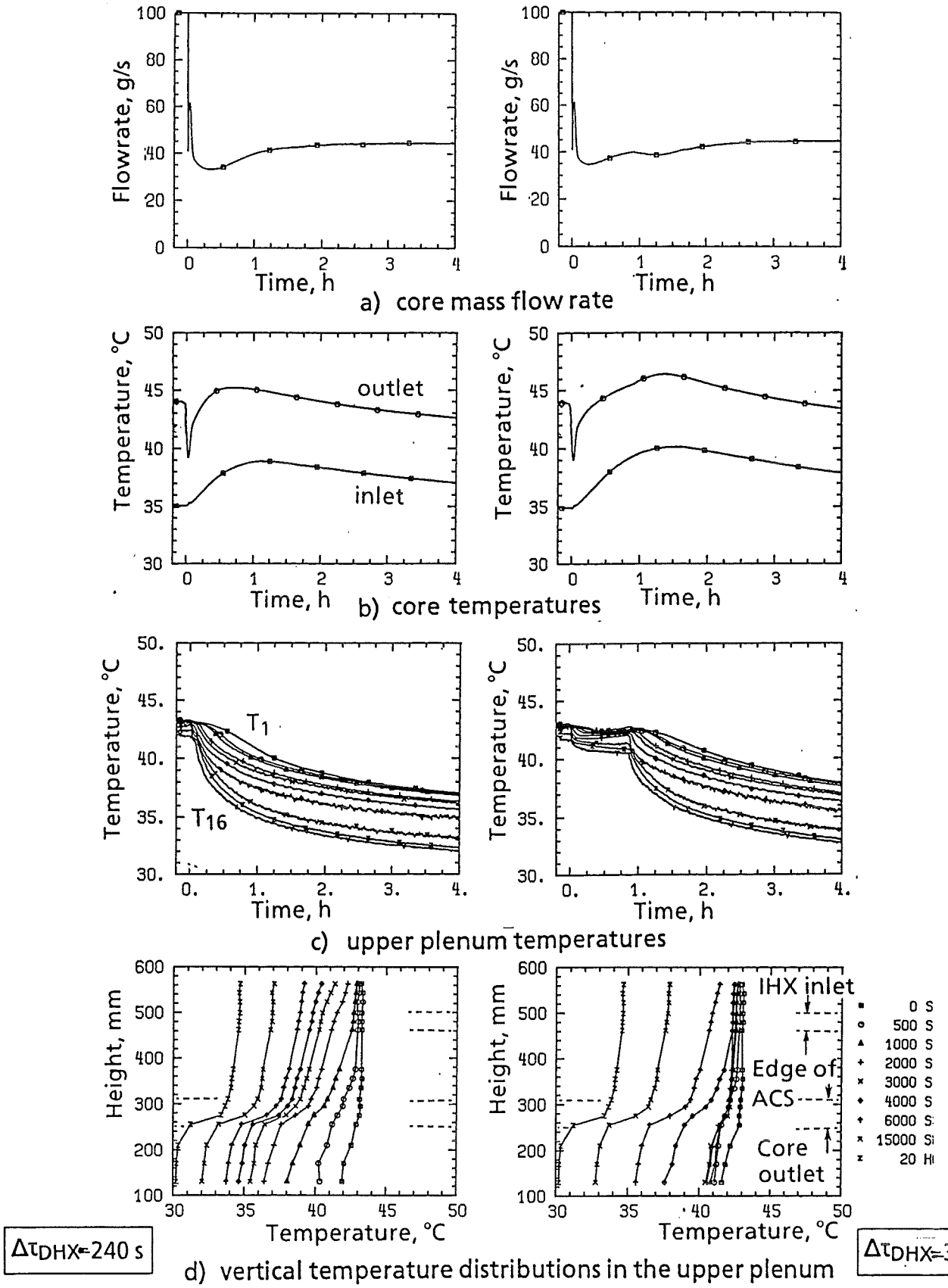

Fig. 43 Influence of the DHX startup delay time on the transition from forced to natural convection for U-tube-type DHXs (τ_{IHX} = 15 s, ACS permeable)

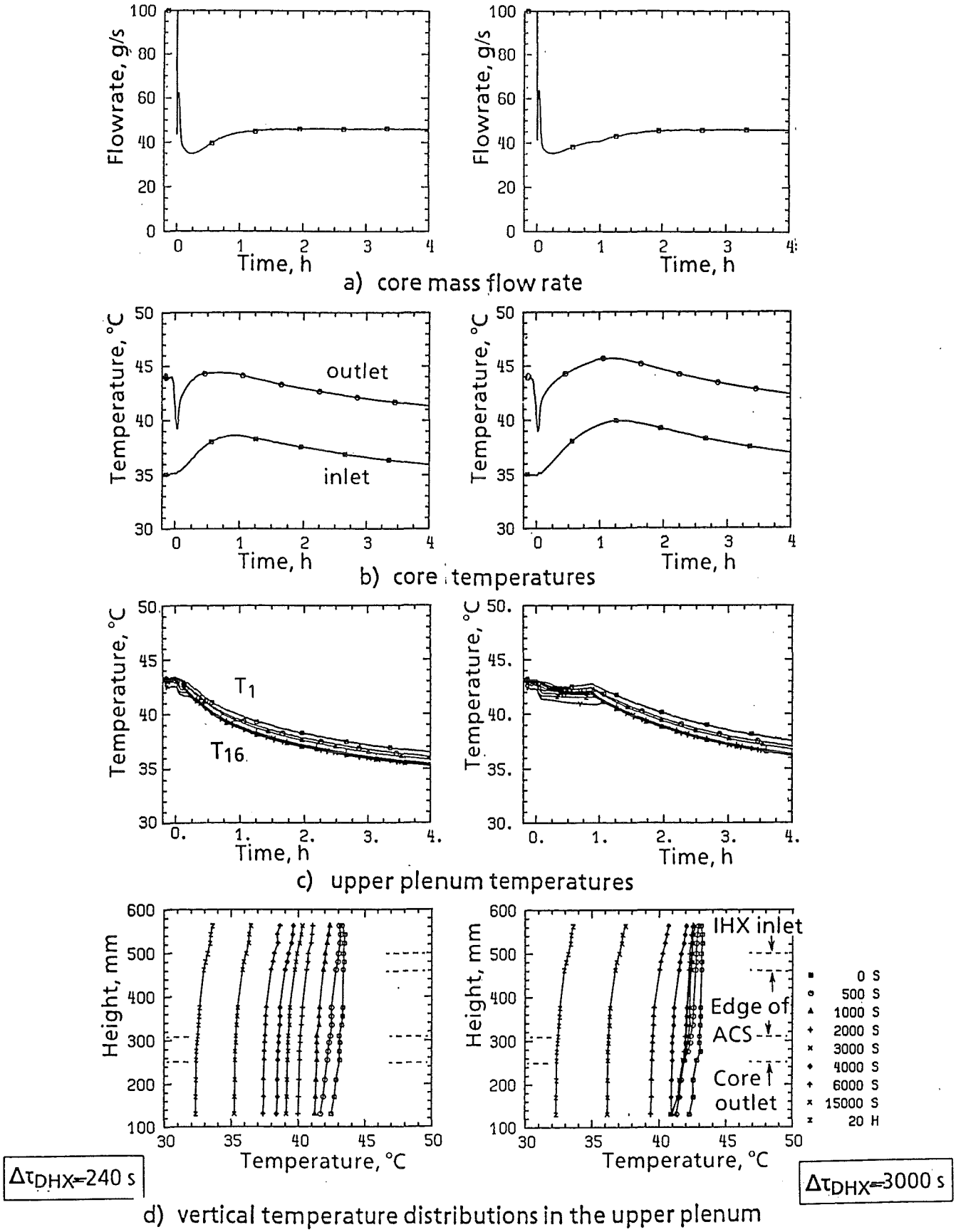

Fig. 44 Influence of the DHX startup delay time on the transition from forced to natural convection for hybrid-type DHXs (τ_{IHX} = 15 s, ACS permeable)

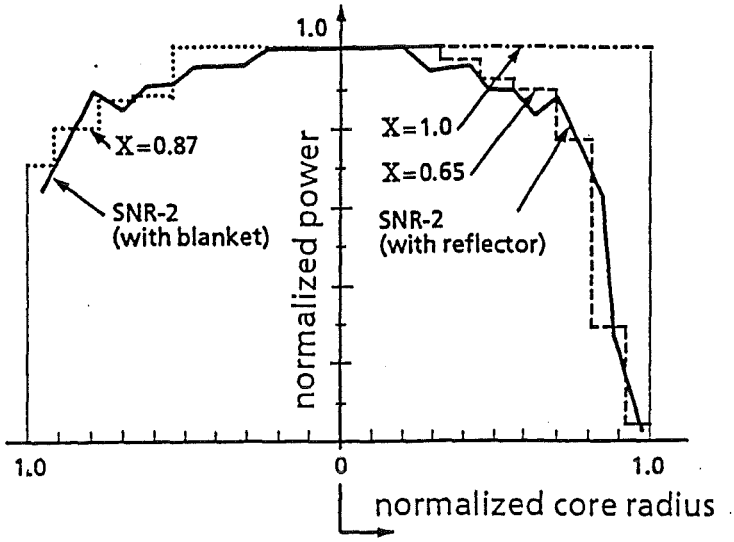

a) normalized radial power distribution

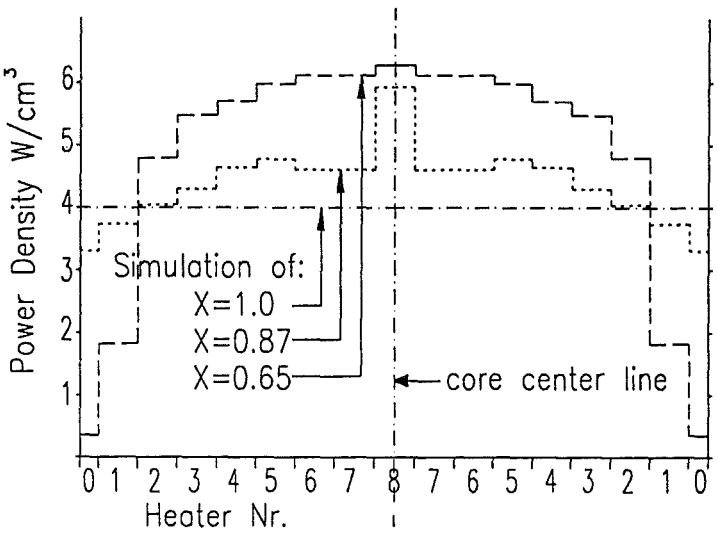

b) typical radial power distributions

Fig. 45 Typical radial power distributions across the core

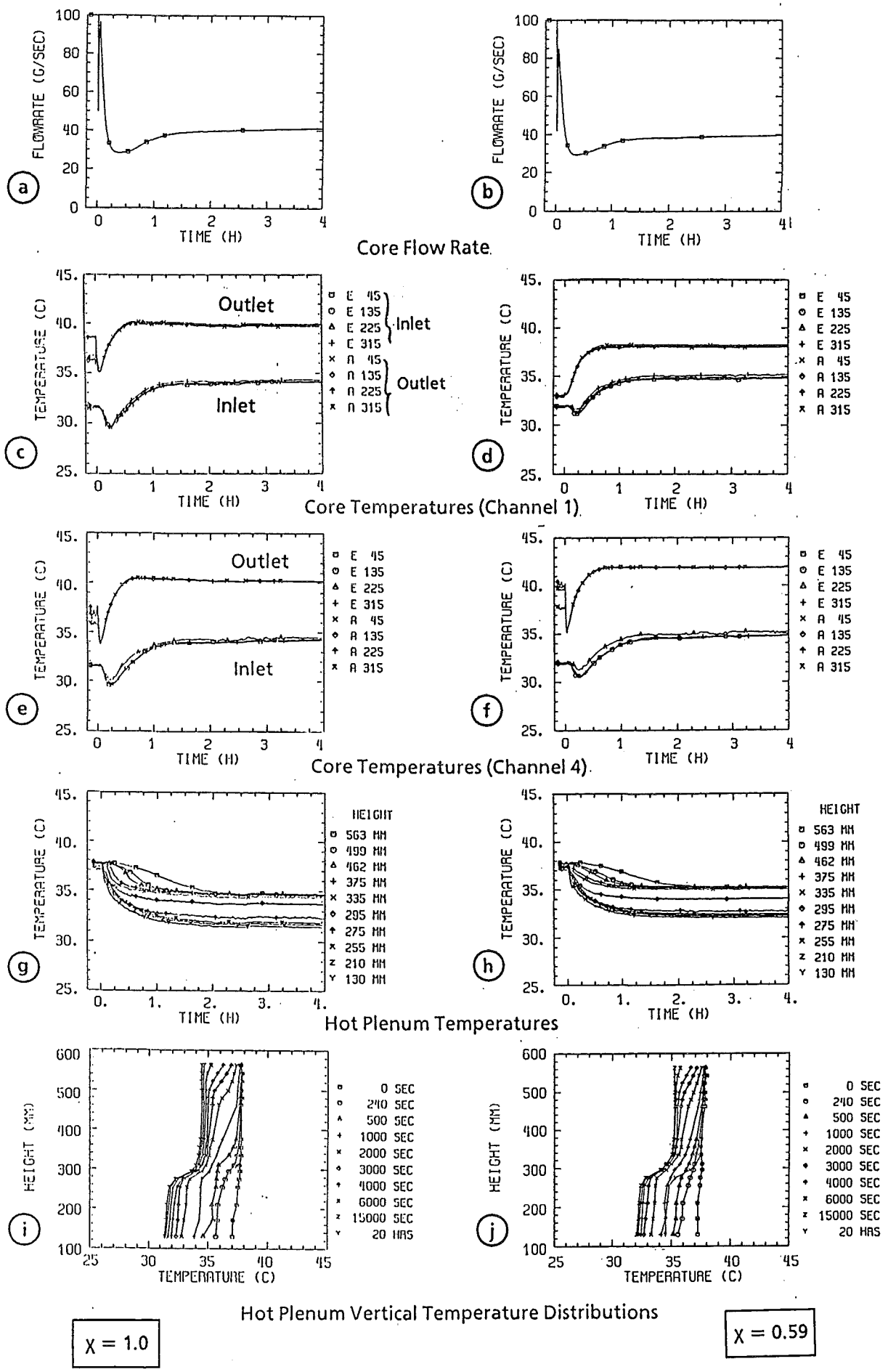

Fig. 46 Influence of the radial power distribution on the transition from forced to natural circulation (P_t = 21 kW; τ_{IHX} = 240 s; ACS impermeable)

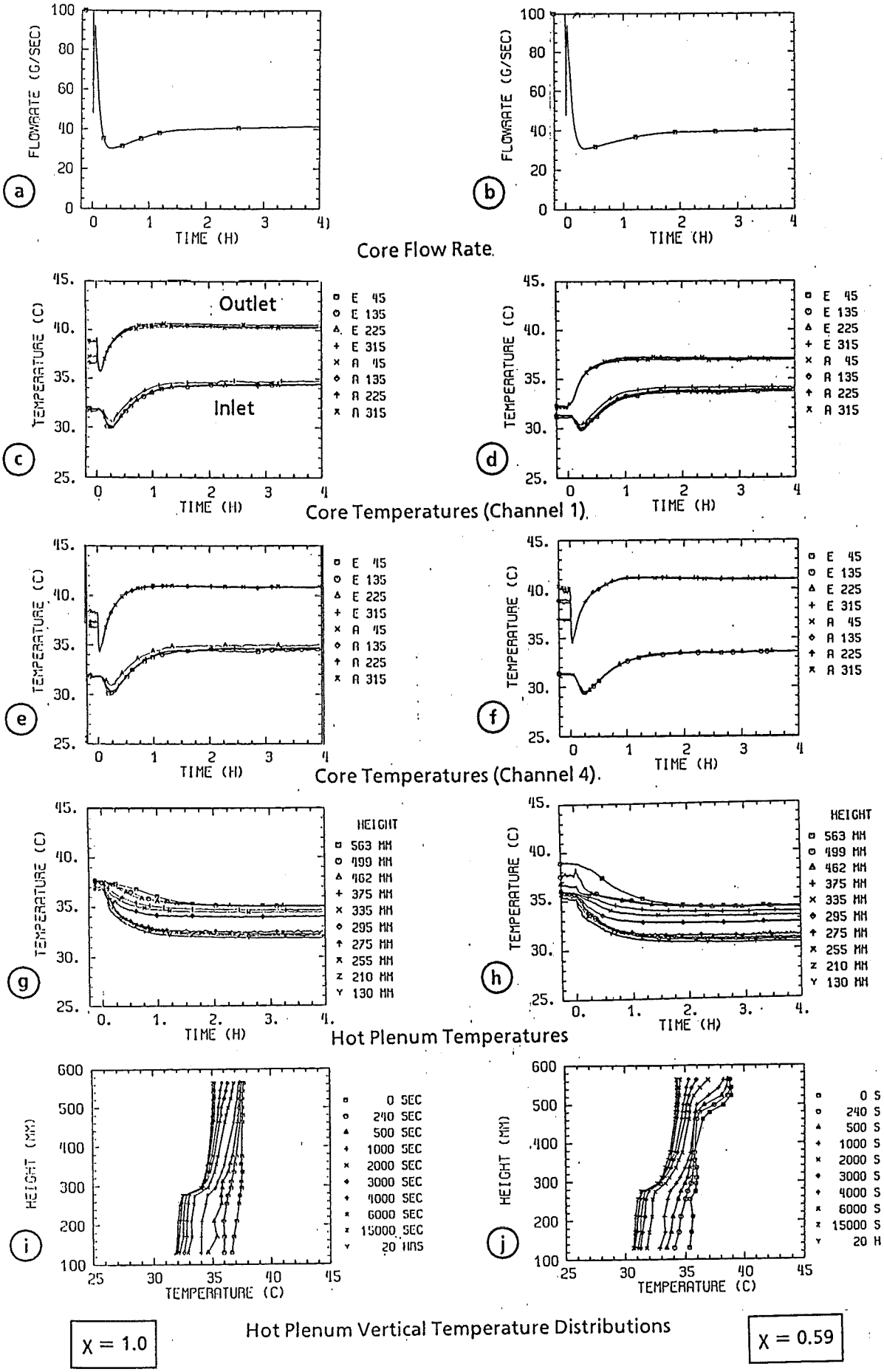

Fig. 47 Influence of the radial power distribution on the transition from forced to natural circulation (P_t = 21 kW; τ_{IHX} = 240 s; ACS permeable)

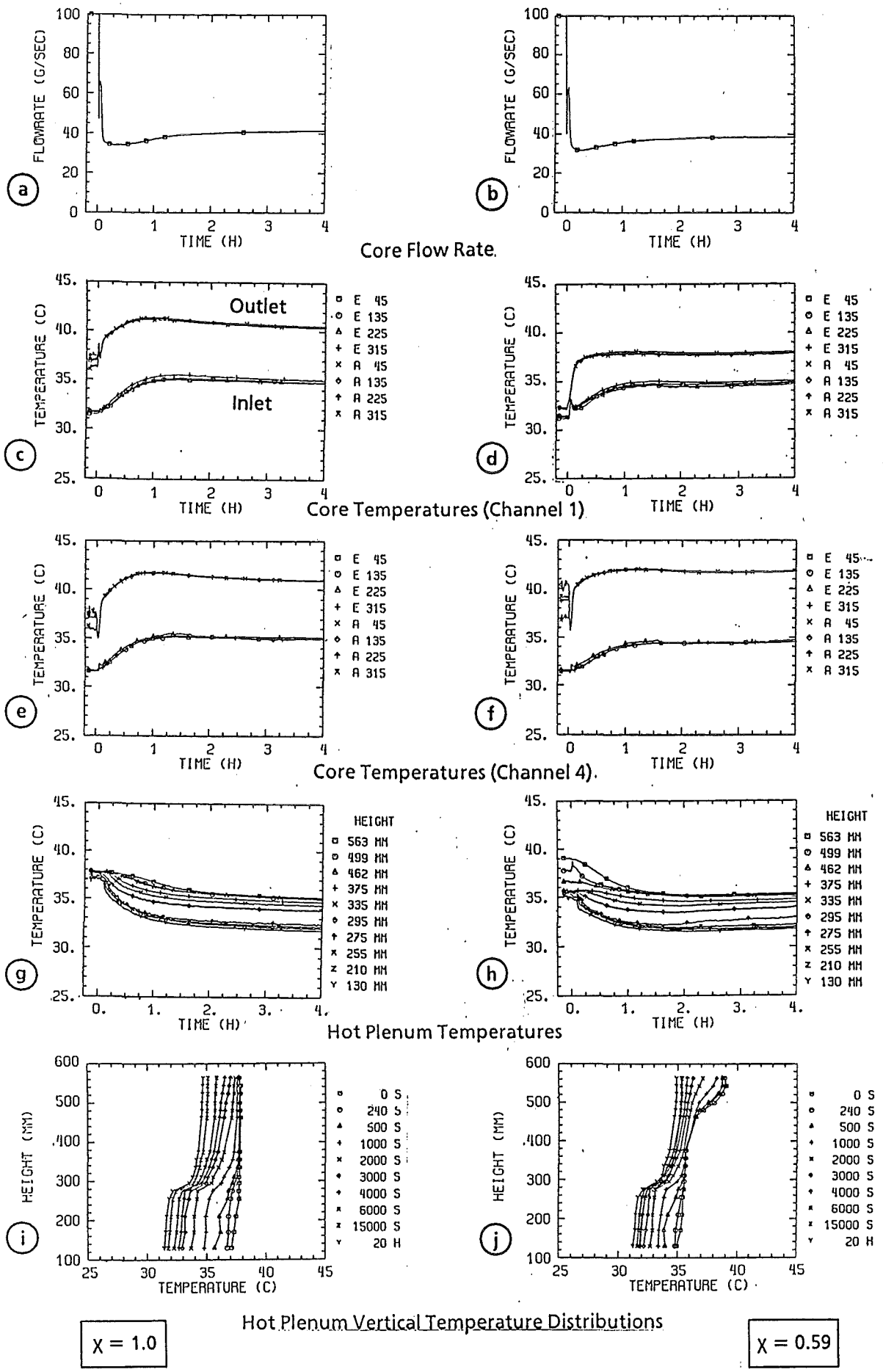

Fig. 48 Influence of the radial power distribution on the transition from forced to natural circulation (P_t = 21 kW; τ_{IHX} = 15 s; ACS permeable)

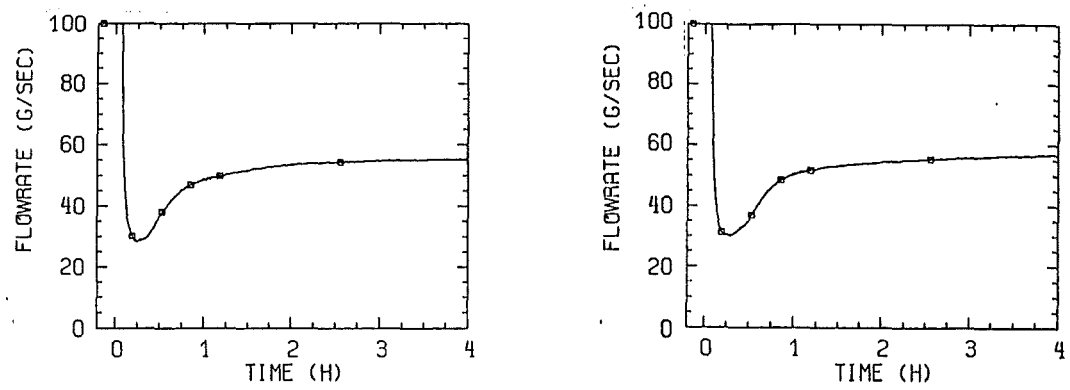

a) core mass flow rate

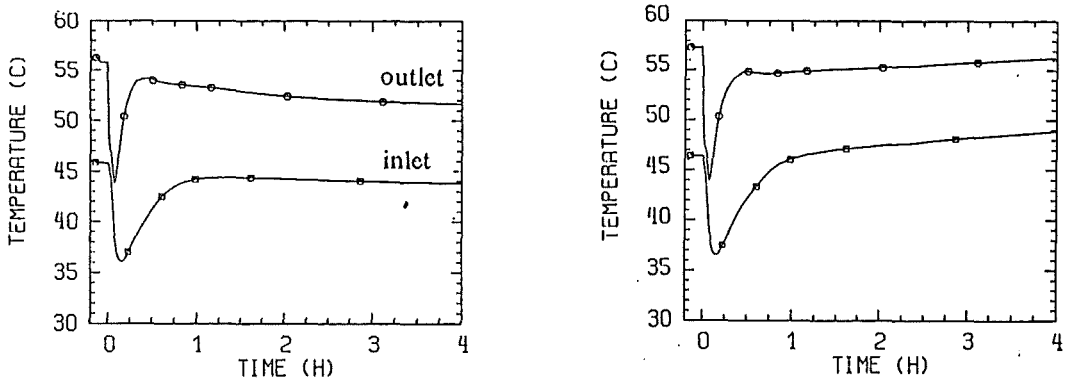

b) core inlet and outlet temperatures

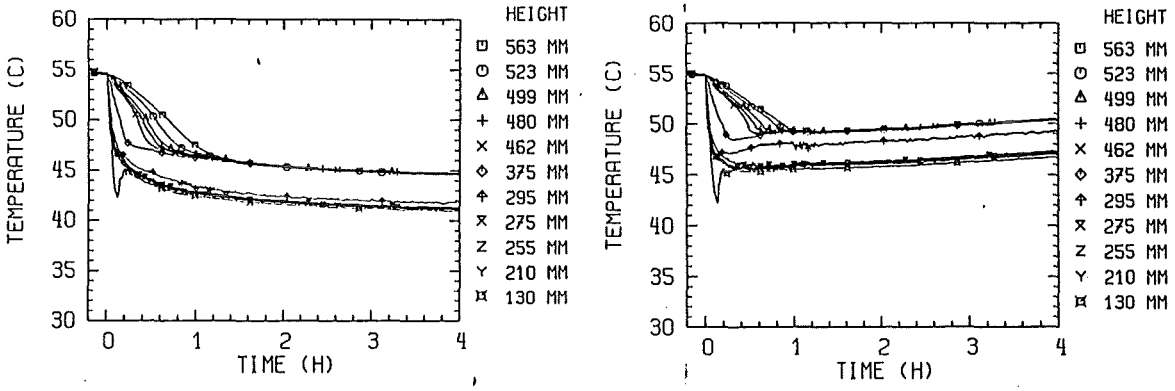

c) upper plenum temperatures

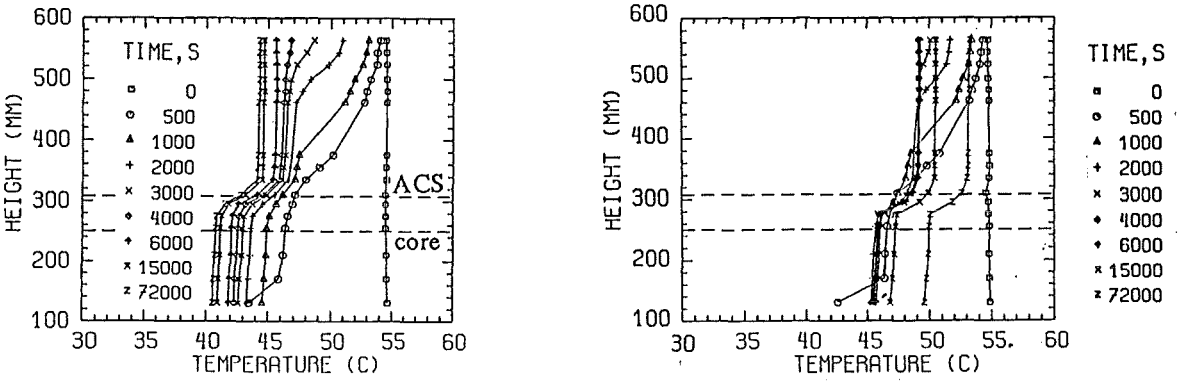

d) vertical temperature distributions in the upper plenum

4 DHXs in operation

2 DHXs in operation

Fig. 49 Influence of the cooling mode on the transition from forced to natural convection for straight-tube-type DHXs (P_t = 75 kW; τ_{IHX} = 240 s; ACS impermeable)

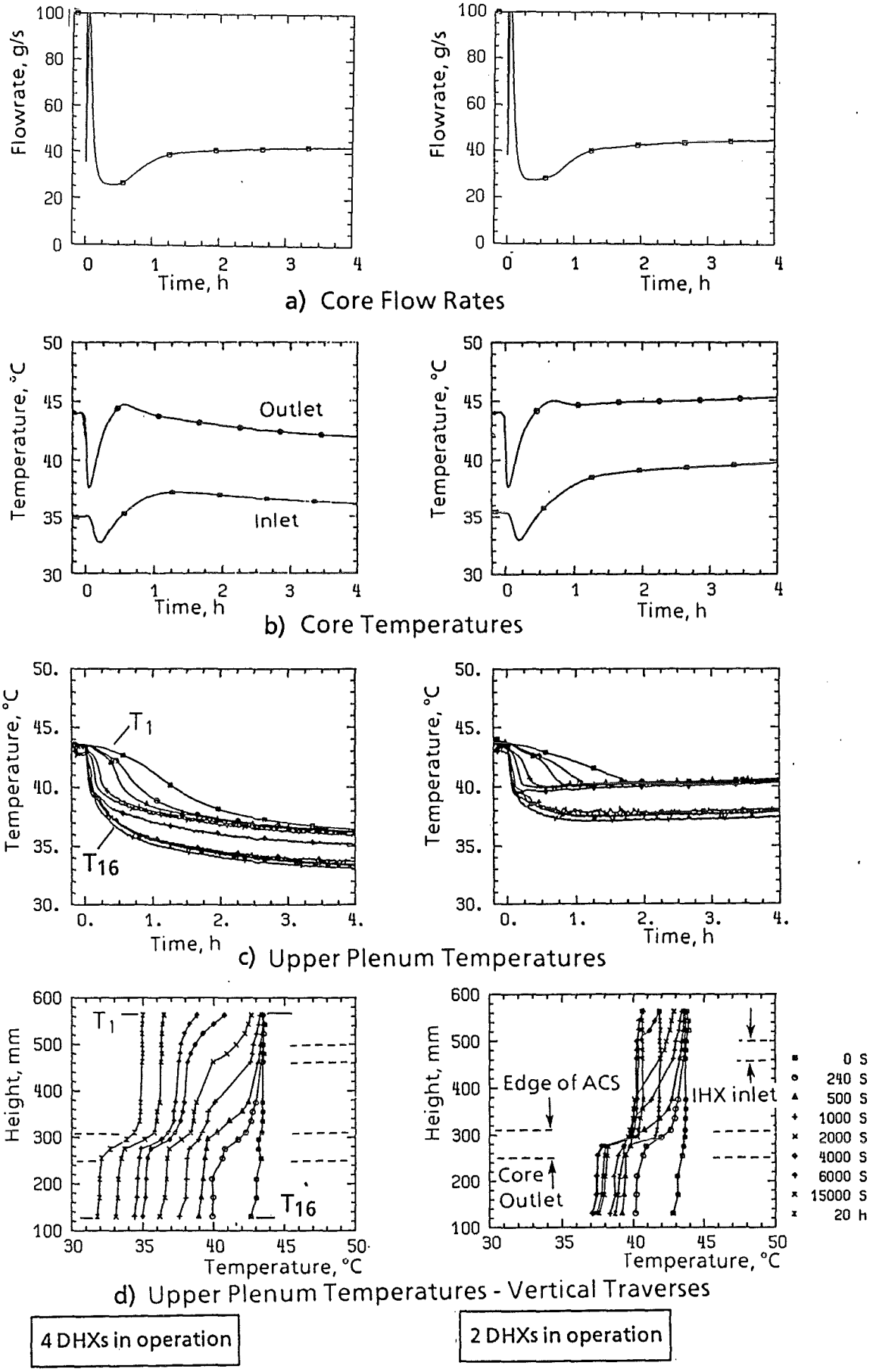

Fig. 50 Influence of the cooling mode on the transition from forced to natural convection for straight-tube-type DHXs (P_t = 30 kW; τ_{IHX} = 240 s; ACS impermeable)

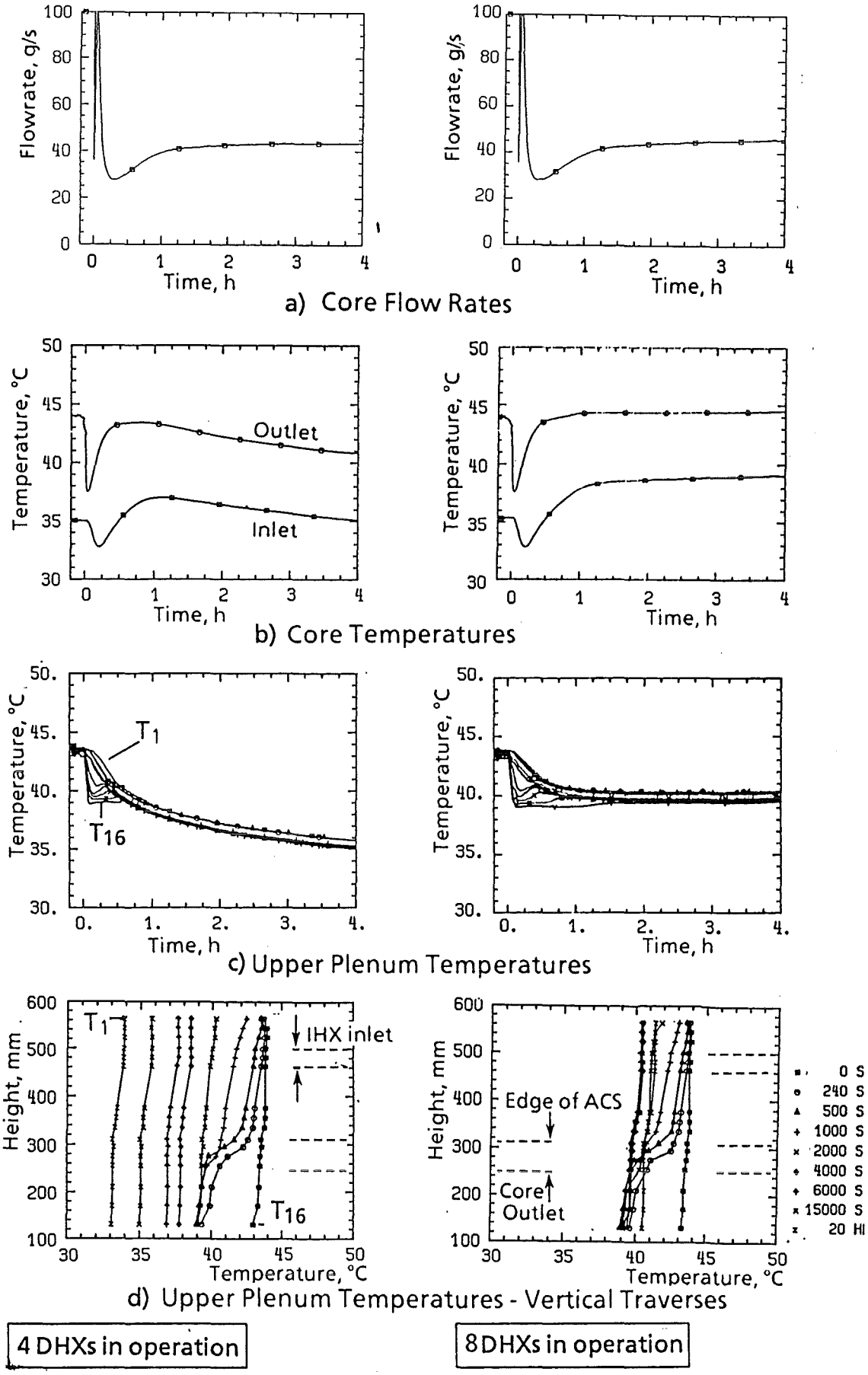

Fig. 51 Influence of the cooling mode on the transition from forced to natural convection for hybrid-type DHXs (P_t = 30 kW; τ_{IHX} = 240 s; ACS impermeable)

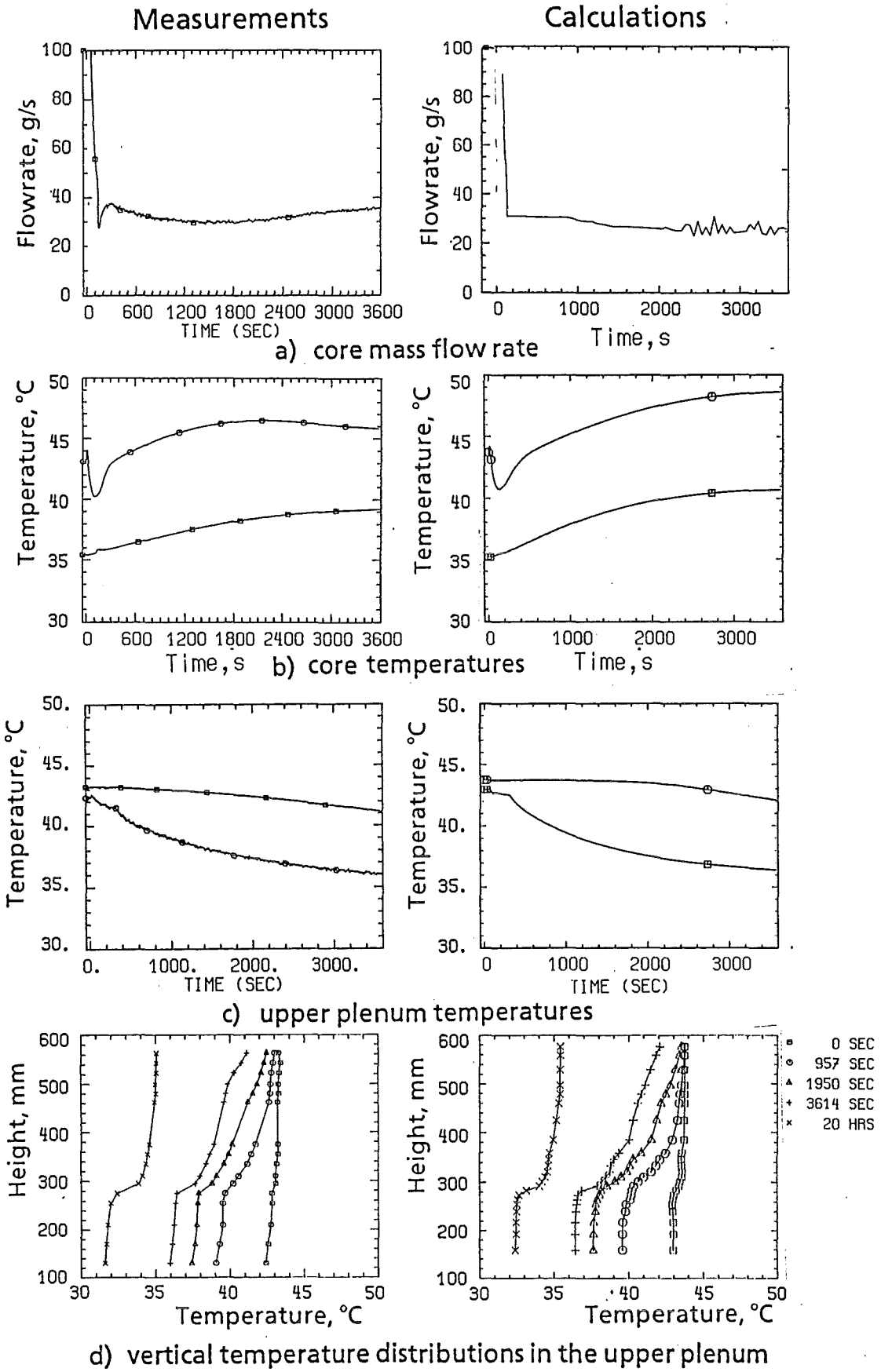

Fig. 52 Comparison of experimental and computed results of investigations on the transition from forced to natural convection (P_t = 30 kW; τ_{IHX} = 15 s; ACS permeable)

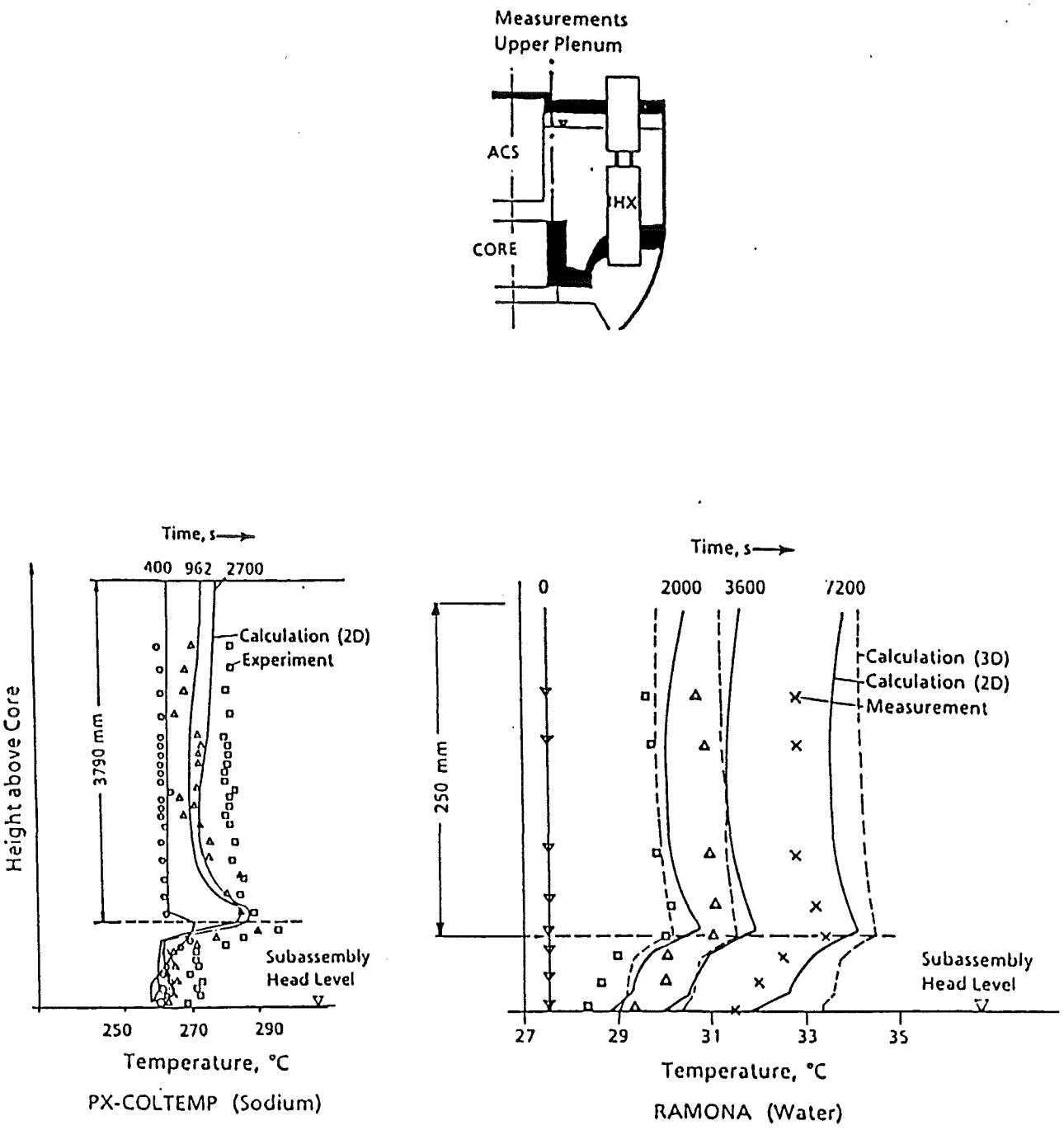

Fig. 53 Comparison of measured and calculated vertical temperature distributions in the upper plena of PHENIX-COLTEMP 4 and RAMONA after a sudden primary pump stop

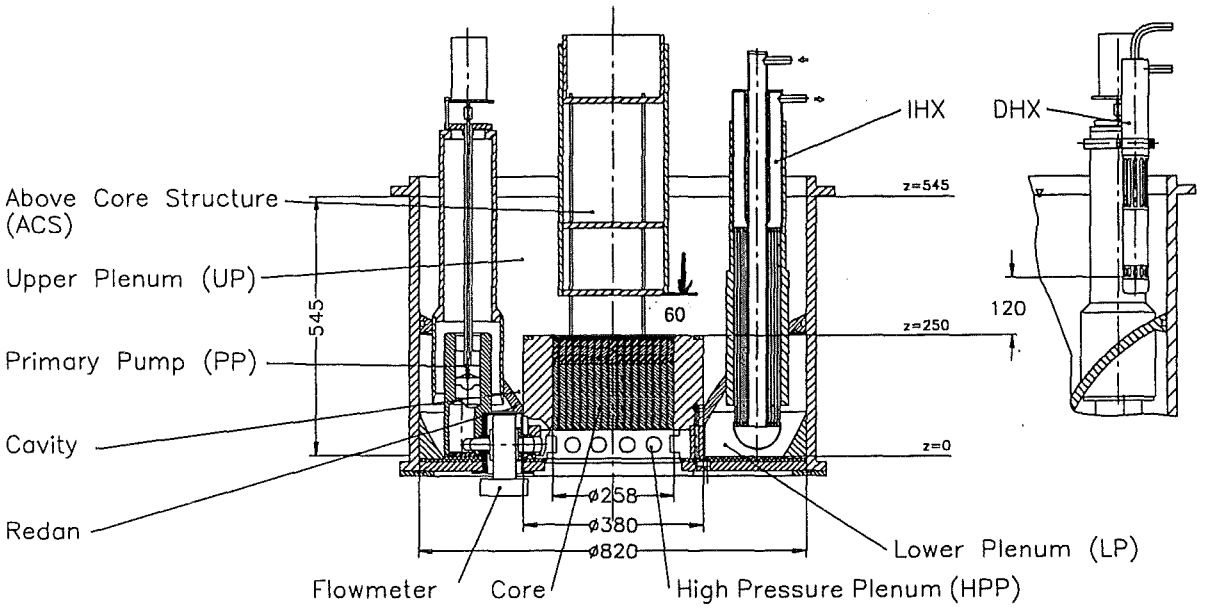

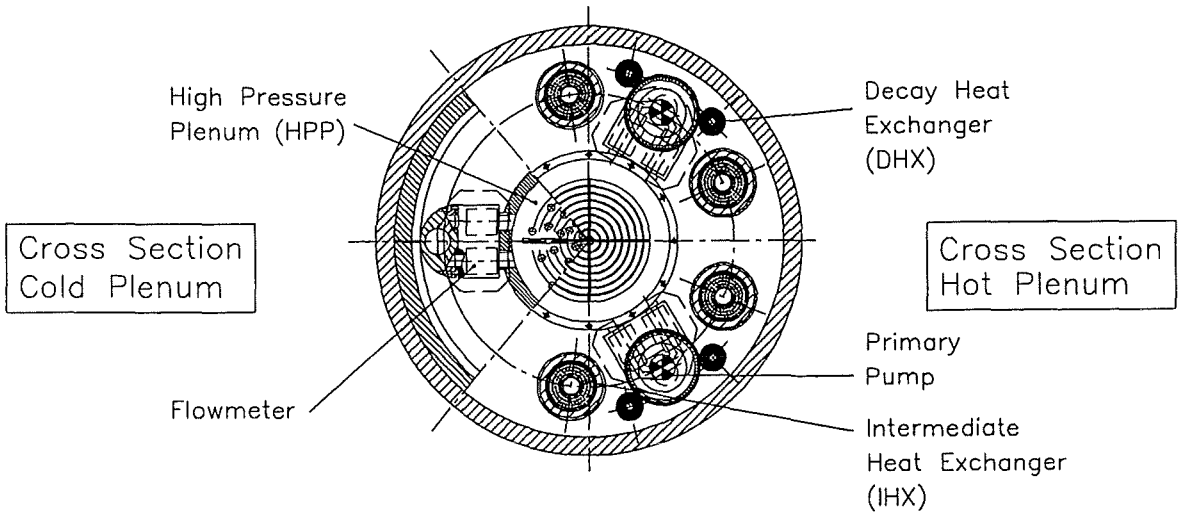

Fig. 54 Vertical and horizontal cross-sections of the RAMONA-III test facility

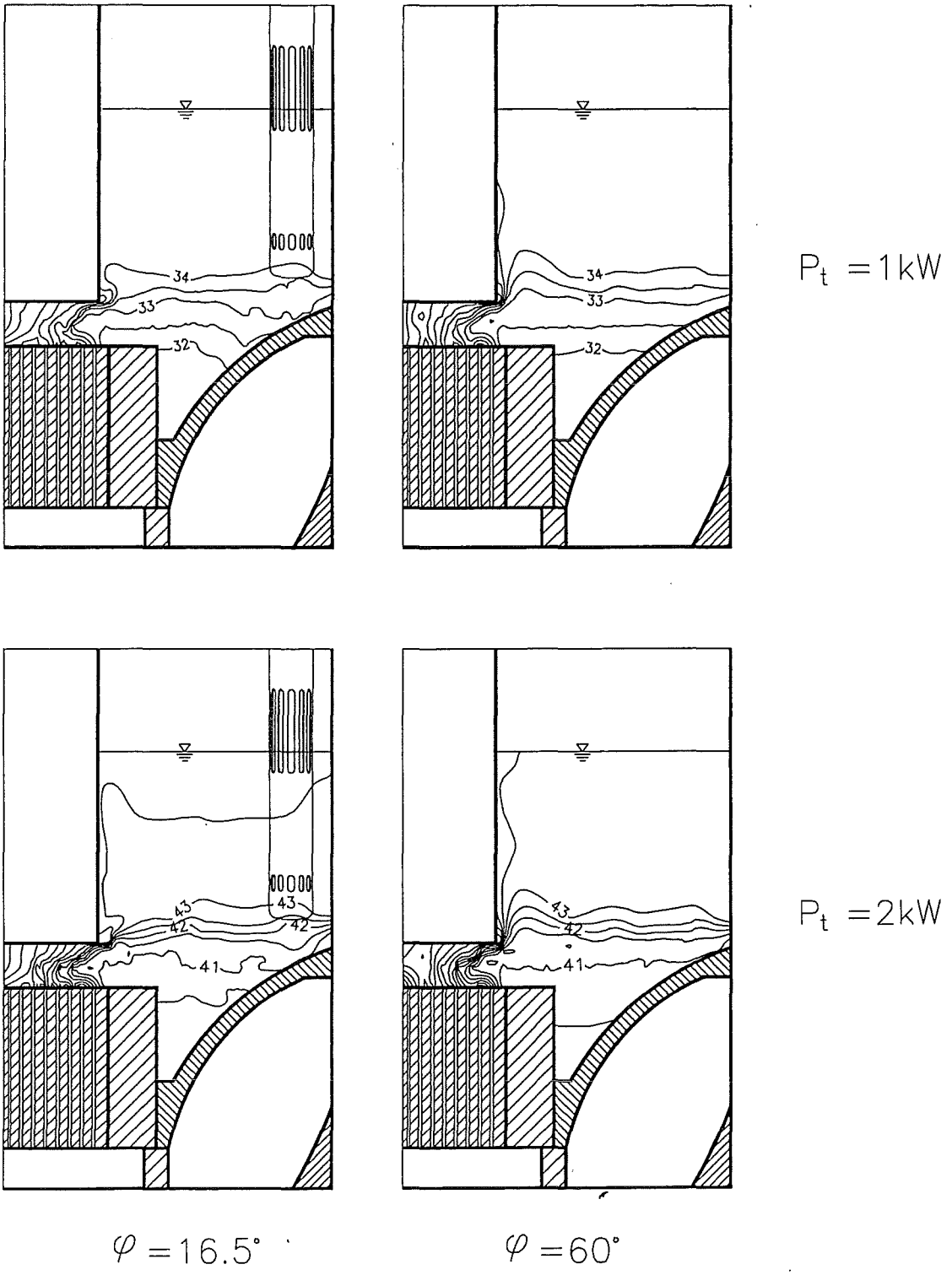

Fig. 55 Influence of the core power on the isotherm fields in RAMONA-III (isotherm interval 0.5 K; ACS: NEPTUN impermeable; t_{DHX} = 24°C).

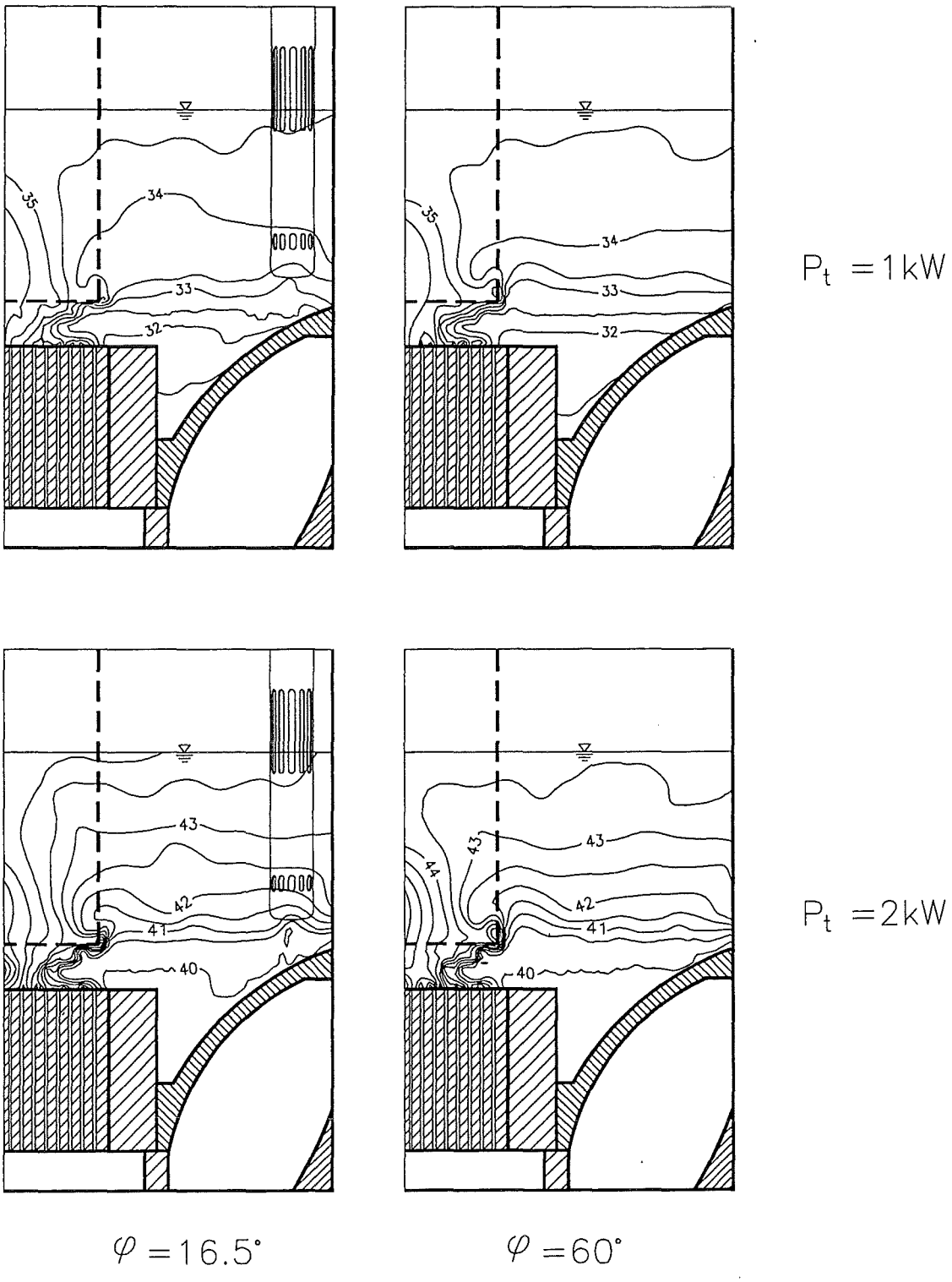

Fig. 56 Influence of the core power on the isotherm fields in RAMONA-III (isotherm interval 0.5 K; ACS: NEPTUN permeable; t_{DHX} = 24°C).

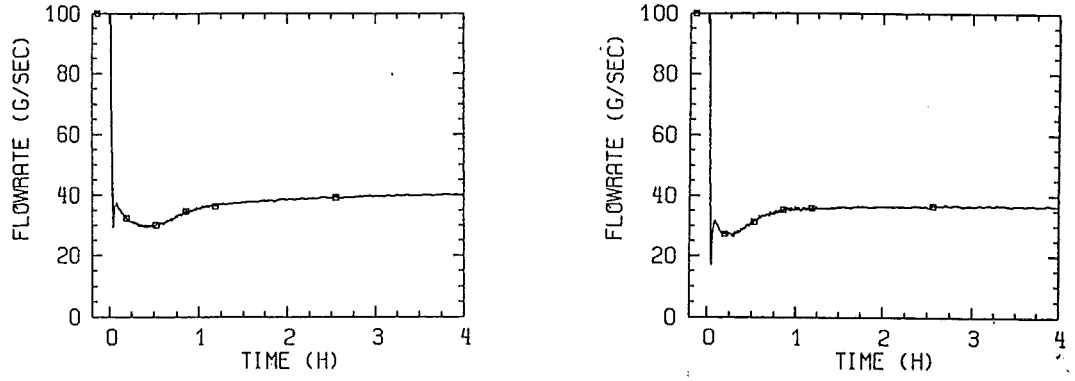

a) core mass flow rate

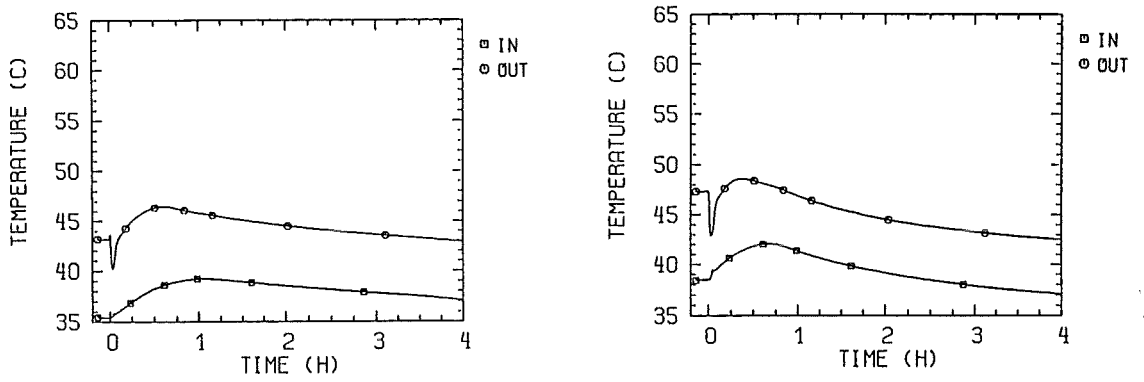

b) core inlet and outlet temperatures

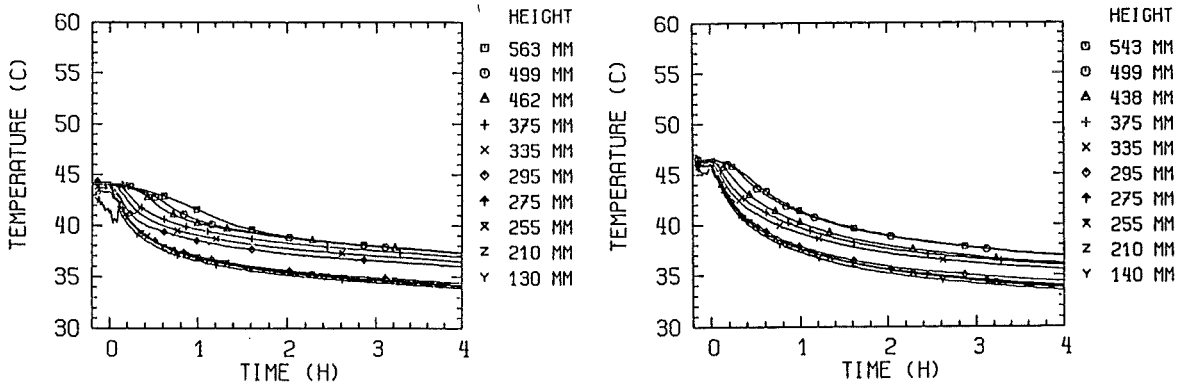

c) upper plenum temperatures

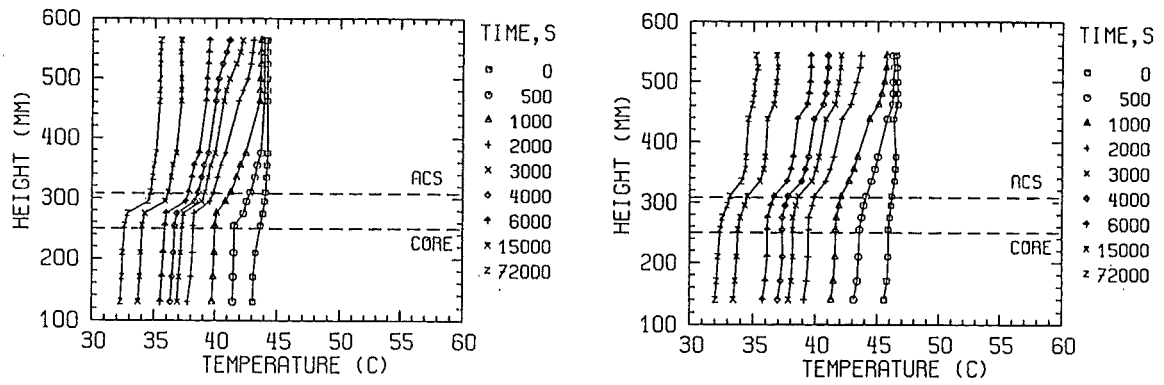

d) vertical temperature distributions in the upper plenum

RAMONA-II

RAMONA-III

Fig. 57 Influence of the number of heat transport loops (RAMONA-II ↔ RAMONA-III) on the transition from forced to natural convection (P_t = 30 kW; τ_{IHX} = 15 s; ACS permeable)

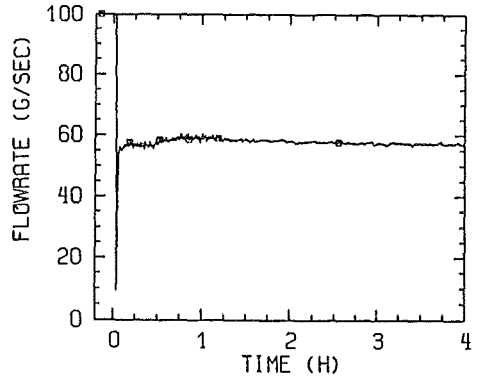

a) core mass flow rate

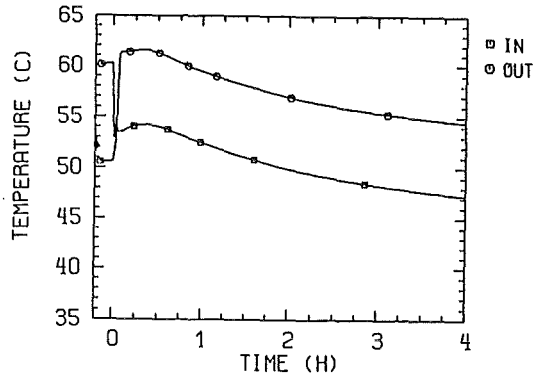

b) core inlet and outlet temperatures

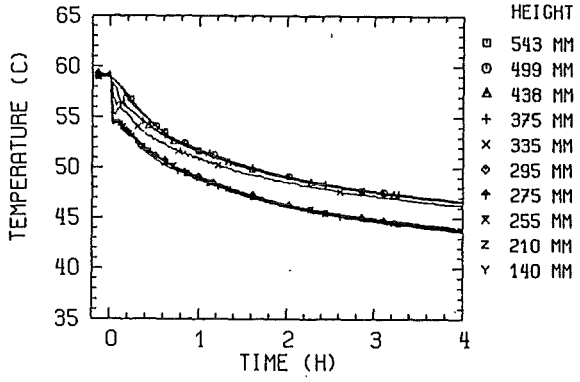

c) upper plenum temperatures

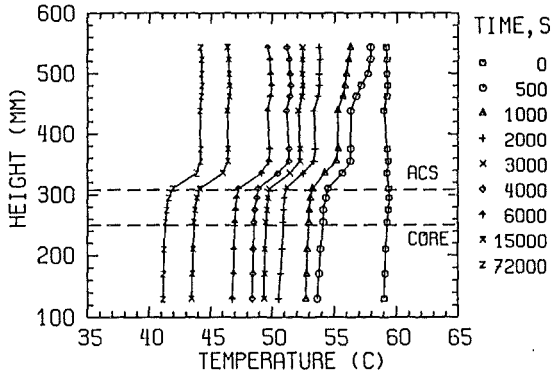

d) vertical temperature distributions in the upper plenum

Fig. 58 Influence of the core power before scram on the transition from forced to natural convection (P_t = 75 kW; τ_{IHX} = 15 s; ACS impermeable)

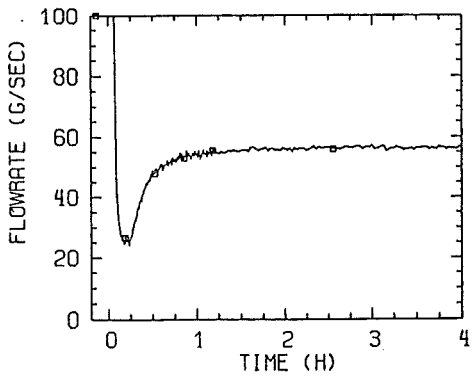

a) core mass flow rate

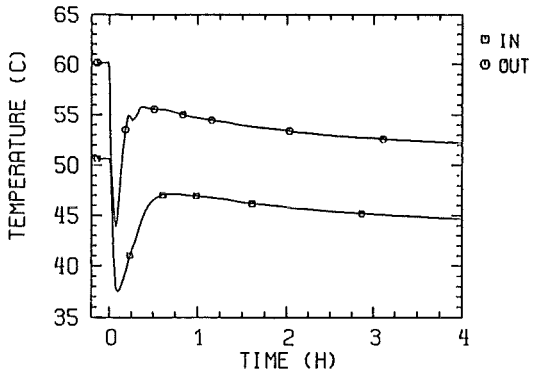

b) core inlet and outlet temperatures

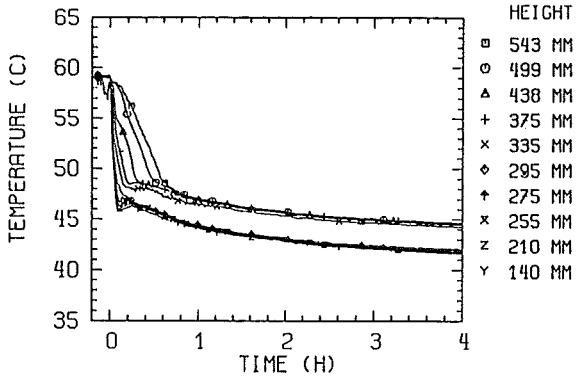

c) upper plenum temperatures

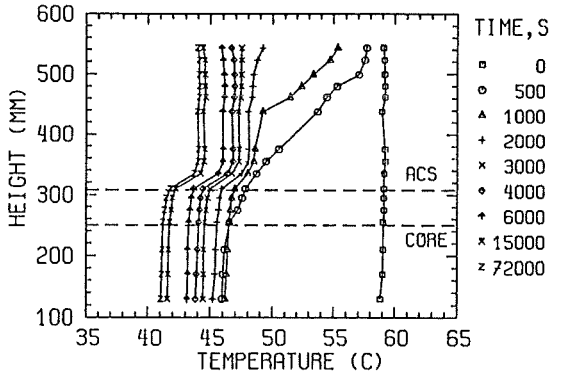

d) vertical temperature distributions in the upper plenum

Fig. 59 Influence of the IHXs secondary-side pump run-down on the transition from forced to natural convection (P_t = 75 kW; τ_{IHX} = 240 s; ACS impermeable)

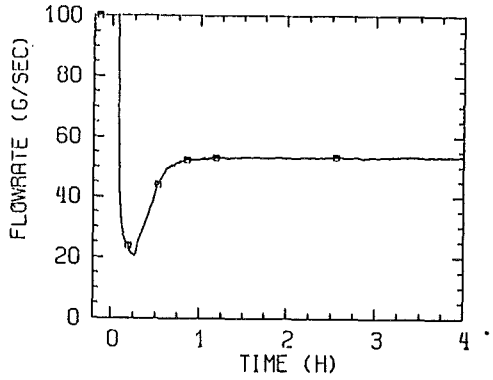

a) core mass flow rate

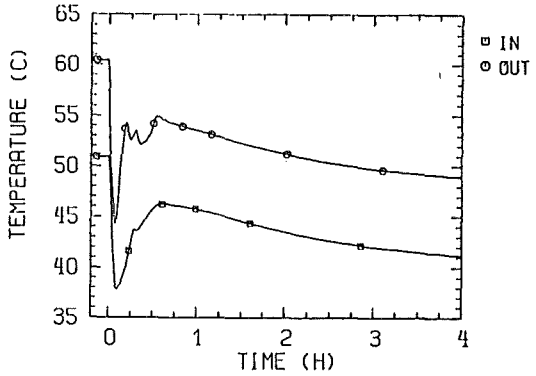

b) core inlet and outlet temperatures

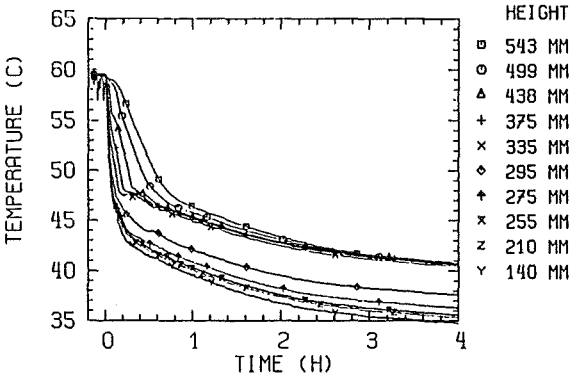

c) upper plenum temperatures

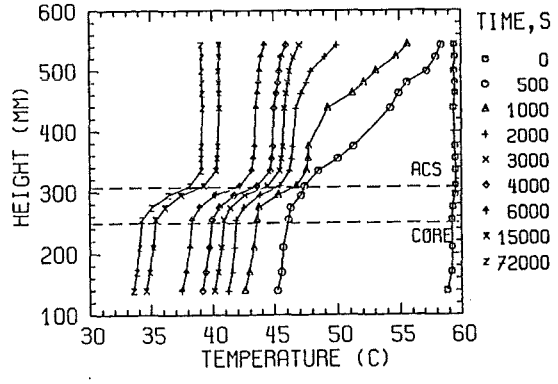

d) vertical temperature distributions in the upper plenum

Fig. 60 Influence of the increase of the DHXs immersion depth on the transition from forced to natural convection (P_t = 75 kW; τ_{IHX} = 240 s; ACS impermeable)

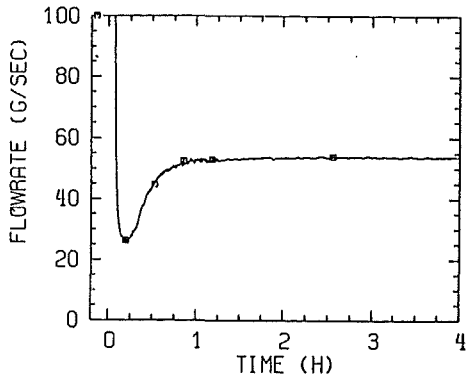

a) core mass flow rate

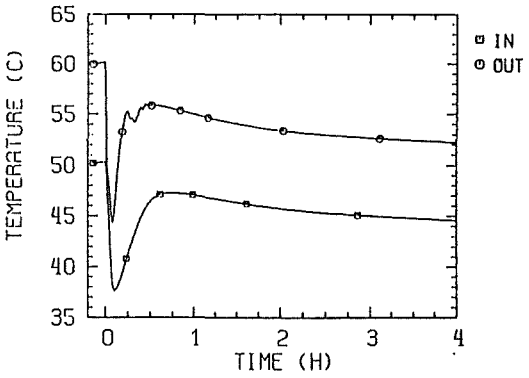

b) core inlet and outlet temperatures

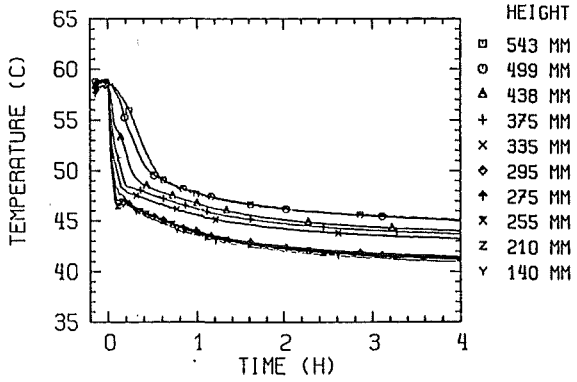

c) upper plenum temperatures

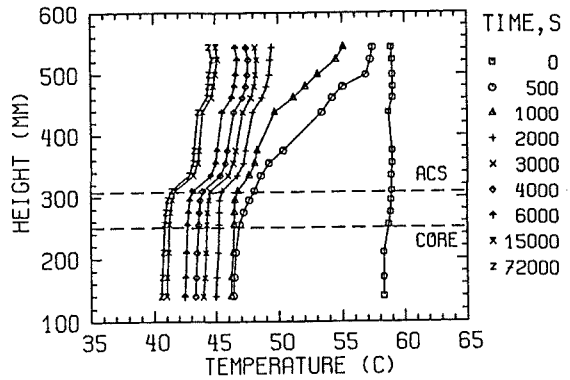

d) vertical temperature distributions in the upper plenum

Fig. 61 Influence of the ACS design on the transition from forced to natural convection (P_t = 75 kW; τ_{IHX} = 240 s; ACS permeable)

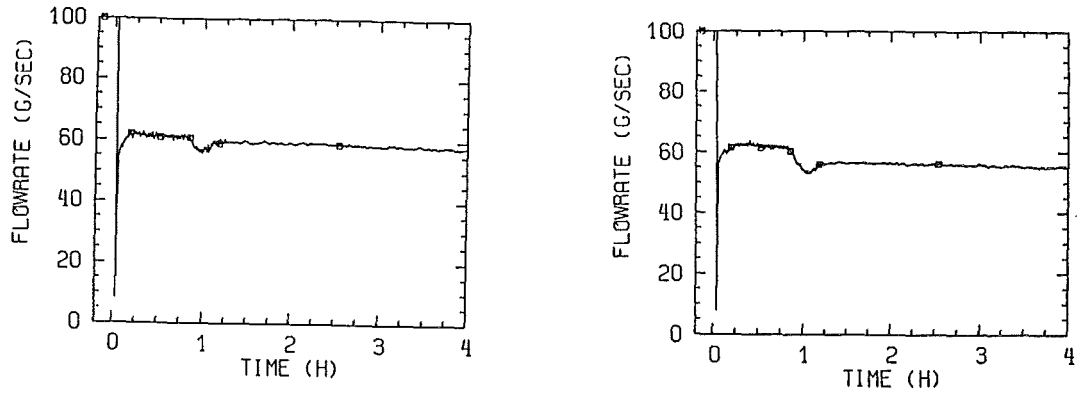

a) core mass flow rate

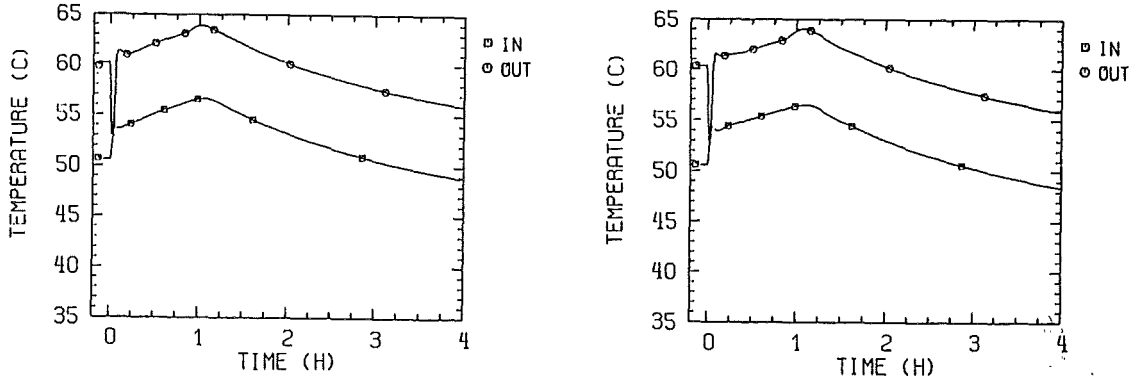

b) core inlet and outlet temperatures

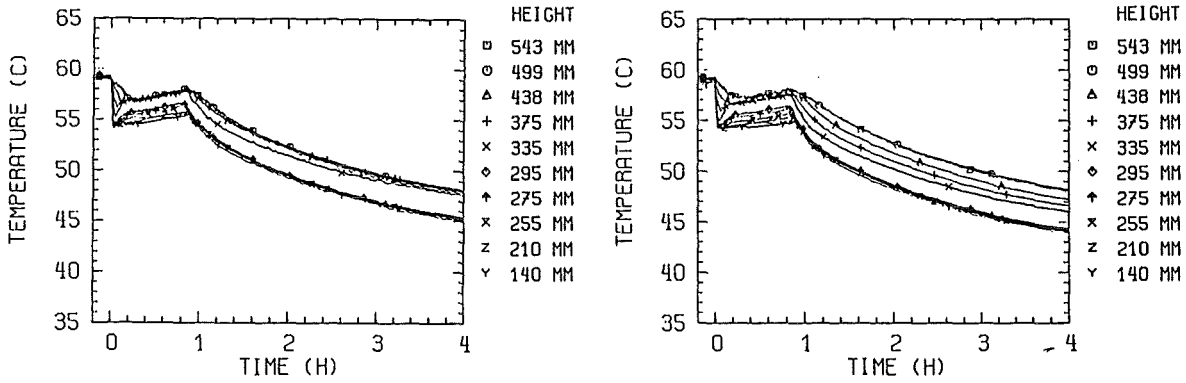

c) upper plenum temperatures

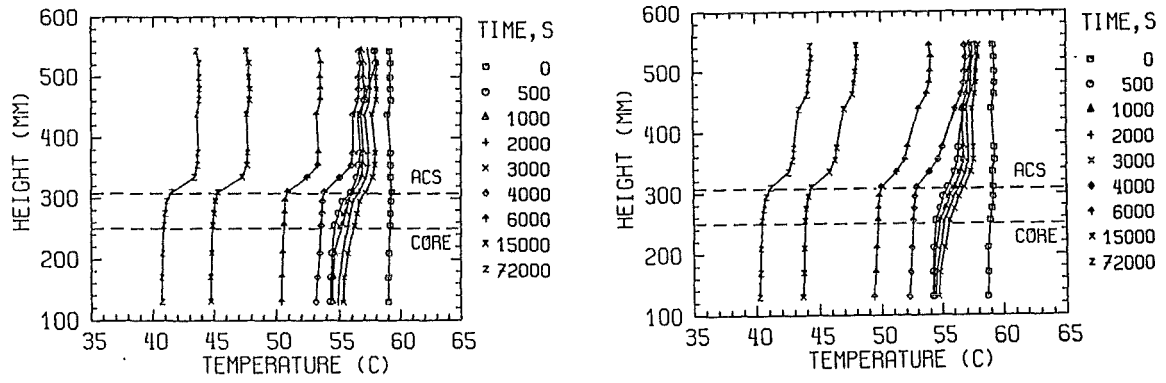

d) vertical temperature distributions in the upper plenum

impermeable ACS

permeable ACS

Fig. 62 Influence of the ACS design on the transition from forced to natural convection for a 3000 s delayed DHX startup (P_t = 75 kW; τ_{IHX} = 15 s)

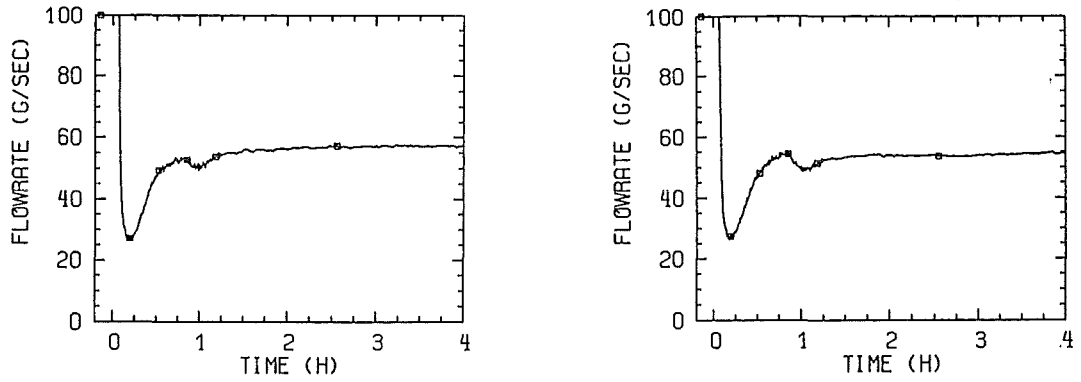

a) core mass flow rate

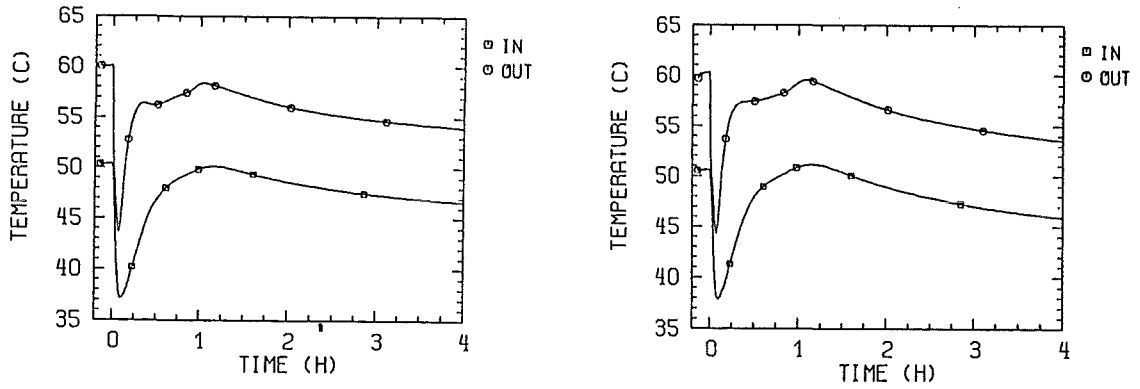

b) core inlet and outlet temperatures

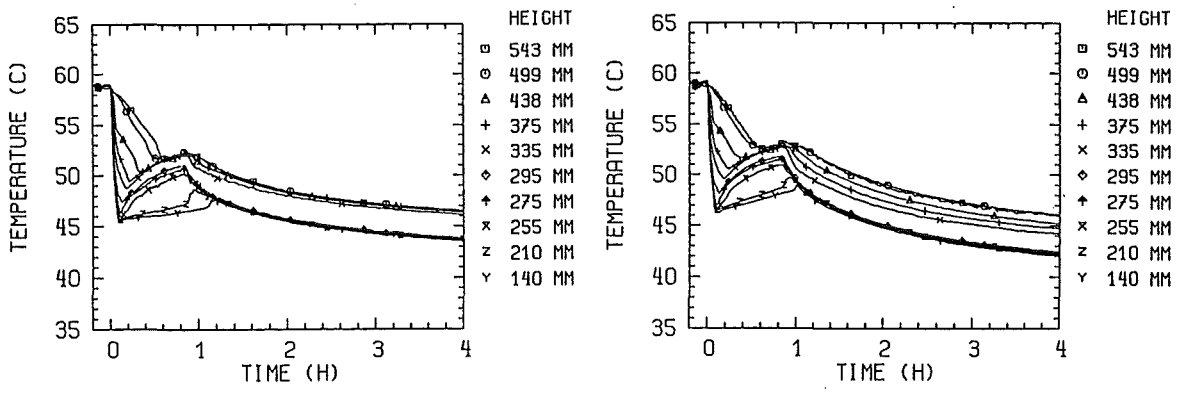

c) upper plenum temperatures

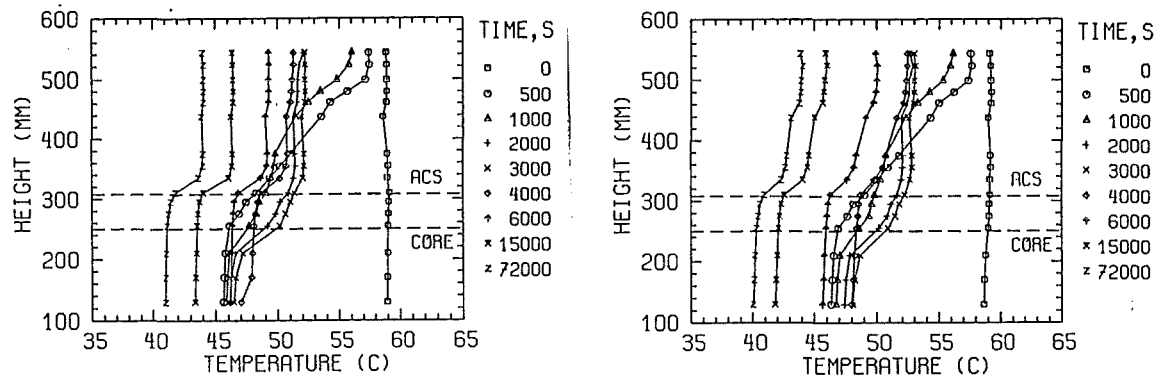

d) vertical temperature distributions in the upper plenum

impermeable ACS permeable ACS

Fig. 63 Influence of the ACS design on the transition from forced to natural convection for a 3000 s delayed DHX startup (P_t = 75 kW; τ_{IHX} = 240 s)

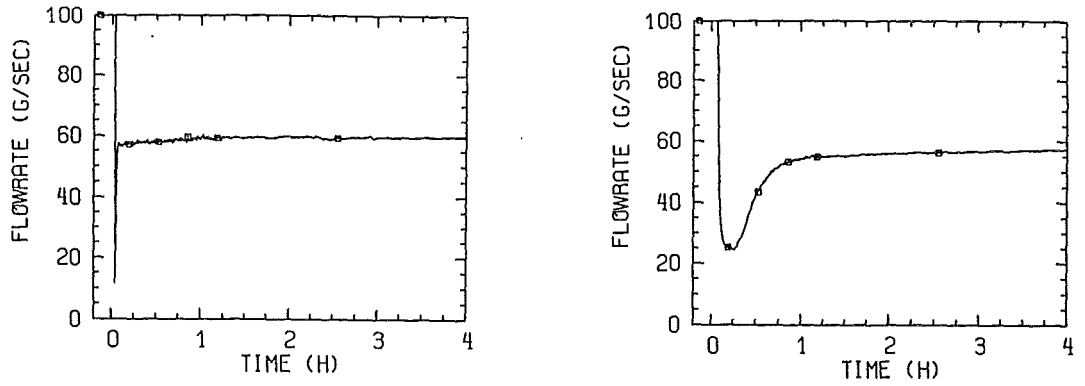

a) core mass flow rate

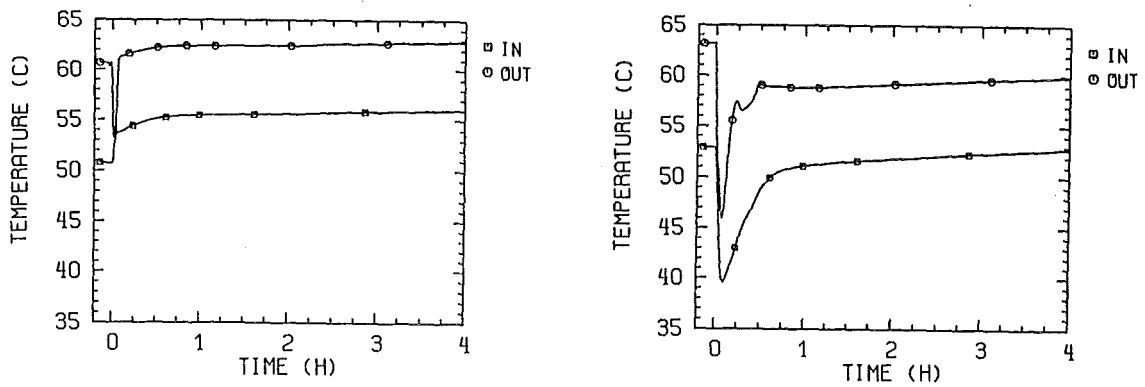

b) core inlet and outlet temperatures

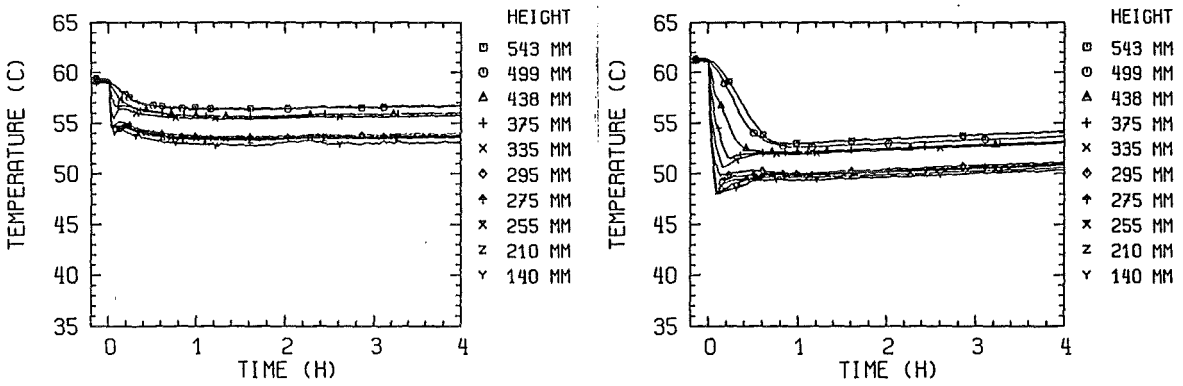

c) upper plenum temperatures

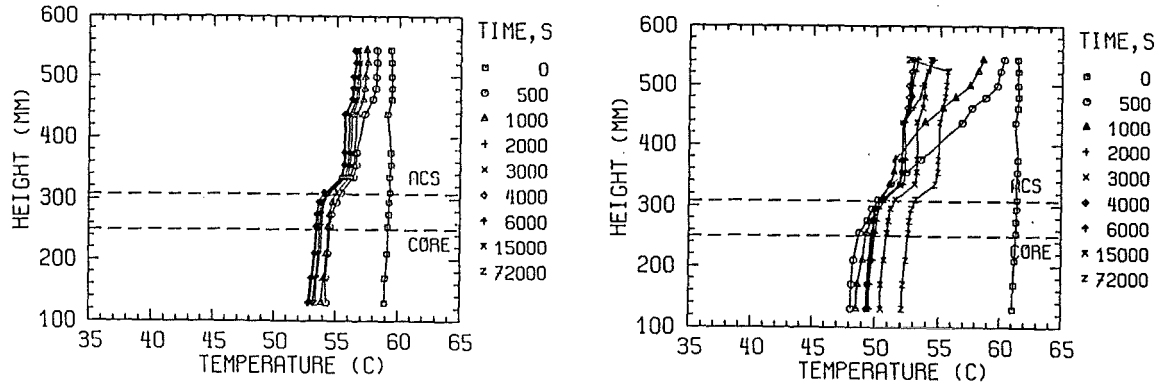

d) vertical temperature distributions in the upper plenum

$\tau_{IHX} = 15$ s

$\tau_{IHX} = 240$ s

Fig. 64 Influence of the IHXs secondary-side pump run-down on the transition from forced to natural convection for an assymmetric cooling mode of the primary system ($P_t = 75$ kW; ACS permeable)